MODELING OF THE MECHANICAL BEHAVIOR OF COMPOSITES SHOWING NONLINEAR MATERIAL BEHAVIOR USING THE EMBEDDED ELEMENT METHOD

GÖMÜLÜ ELEMAN YÖNTEMİ İLE DOĞRUSAL OLMAYAN MALZEME DAVRANIŞI GÖSTEREN KOMPOZİT MALZEMELERİN MEKANİK DAVRANIŞININ MODELLENMESİ

ALP ŞIK

ASSOC. PROF. DR BARIŞ SABUNCUOĞLU
Supervisor

Submitted to
Graduate School of Science and Engineering of Hacettepe University
as a Partial Fulfillment to the Requirements
for the Award of the Degree of Master of Science
in Mechanical Engineering

2020

Aileme…

ETHICS

In this thesis study, prepared in accordance with the spelling rules of Institute of Graduate School of Science and Engineering of Hacettepe University,

I declare that

- all the information and documents have been obtained in the base of the academic rules
- all audio-visual and written information and results have been presented according to the rules of scientific ethics
- in case of using others works, related studies have been cited in accordance with the scientific standards
- all cited studies have been fully referenced
- I did not do any distortion in the data set
- and any part of this thesis has not been presented as another thesis study at this or any other university.

24 / 06 / 2020

ALP ŞIK

YAYINLANMA VE FİKRİ MÜLKİYET HAKLARI BEYANI

Enstitü tarafından onaylanan lisansüstü tezimin/raporumun tamamını veya herhangi bir kısmını, basılı (kağıt) ve elektronik formatta arşivleme ve aşağıda verilen koşullarla kullanıma açma iznini Hacettepe Üniversitesi'ne verdiğimi bildiririm. Bu izinle Üniversiteye verilen kullanım hakları dışındaki tüm fikri mülkiyet haklarım bende kalacak, tezimin tamamının ya da bir bölümünün gelecekteki çalışmalarda (makale, kitap, lisans ve patent vb.) kullanım hakları bana ait olacaktır.

Tezin kendi orijinal çalışmam olduğunu, başkalarının haklarını ihlal etmediğimi ve tezimin tek yetkili sahibi olduğumu beyan ve taahhüt ederim. Tezimde yer alan telif hakkı bulunan ve sahiplerinden yazılı izin alınarak kullanması zorunlu metinlerin yazılı izin alarak kullandığımı ve istenildiğinde suretlerini Üniversiteye teslim etmeyi taahhüt ederim.

Yükseköğretim Kurulu tarafından yayınlanan "***Lisansüstü Tezlerin Elektronik Ortamda Toplanması, Düzenlenmesi ve Erişime Açılmasına İlişkin Yönerge***" kapsamında tezim aşağıda belirtilen koşullar haricince YÖK Ulusal Tez Merkezi / H. Ü. Kütüphaneleri Açık Erişim Sisteminde erişime açılır.

□ Enstitü / Fakülte yönetim kurulu kararı ile tezimin erişime açılması mezuniyet tarihimden itibaren 2 yıl ertelenmiştir.

□ Enstitü / Fakülte yönetim kurulu gerekçeli kararı ile tezimin erişime açılması mezuniyet tarihimden itibaren .... ay ertelenmiştir.

□ Tezim ile ilgili gizlilik kararı verilmiştir.

21 / 06 / 2020

ALP ŞIK

ABSTRACT

MODELING OF THE MECHANICAL BEHAVIOR OF COMPOSITES SHOWING NONLINEAR MATERIAL BEHAVIOR USING THE EMBEDDED ELEMENT METHOD

Alp ŞIK

Master of Science, Department of Mechanical Engineering
Supervisor: Assoc. Prof. Dr. Barış SABUNCUOĞLU
June 2020, 79 pages

Composite materials are heterogeneous materials that are composed of two or more different materials. They are used in numerous applications, such as, automotive, aerospace, biomechanics application. Accurate and realistic modeling of these materials are important to ensure a high-quality production and obtaining a durable material. Finite element method is the most common choice to model these types of materials. Usual approach in modeling composites is the homogenization of the material properties. However, this approach is only valid under many assumptions. Apart from this limitation, this approach does not allow evaluation of stresses and strains in component materials. In order to achieve more realistic modeling, components should be modeled separately. This approach also has problems with meshing, since continuity between meshes of components should be provided. On the other hand, if component materials have complex shapes, many elements come to existence, which makes the analysis difficult.

In order to resolve these issues, embedded element method was developed. In this method, component materials are meshed separately, as embedded and host regions. Constraint equations are defined between these regions such that they behave as a unified material. Continuity of meshes is not needed in this method, hence proper and fewer

elements can be used. Besides, modeling of mechanical behavior is not limited to assumptions, and stresses and strains on the components can be investigated. However, in order to achieve realistic results, relative size of embedded regions should be smaller than host region, and host materials should show linear-elastic material behavior. In addition to these limitations, the host material in the embedded region still exists in this method and this redundant volume affects the mechanical behavior. Most common composite host (matrix) materials are thermo-elastic and thermo-plastic materials, and also muscles and tissues show non-linear mechanical behavior. When the embedded region ratio increases, this non-linearity and effect of the redundant volume should be taken into consideration.

The aim of this study is to develop a method to use embedded element method for elasto-plastic and inelastic materials. This aim is achieved by developing a custom user subroutine that can be used to define proper material behavior, such that the effect of the redundant volume is eliminated. A single fiber model with single element and multiple elements and a randomly distributed fibers model with a volume fraction of 0.6 is used to test the proposed approach. Obtained results are compared with a continuously meshed version of this model. As it comes out, the proposed model can provide reliable results on S11 and S12 components of stress on a two-dimensional model. Accuracy of these results improves as expected, when the fiber volume fraction decreases from 0.6 to 0.4.

Keywords: Composite materials, finite element method, embedded element method, volume redundancy, constituent properties, multiscale modeling

ÖZET

GÖMÜLÜ ELEMAN YÖNTEMİ İLE DOĞRUSAL OLMAYAN MALZEME DAVRANIŞI GÖSTEREN KOMPOZİT MALZEMELERİN MEKANİK DAVRANIŞININ MODELLENMESİ

Alp ŞIK

Yüksek Lisans, Makine Mühendisliği Bölümü
Tez Danışmanı: Doç. Dr. Barış SABUNCUOĞLU
Haziran 2020, 79 sayfa

Kompozit malzemeler, birden fazla malzemenin bir araya getirilmesiyle oluşturulan heterojen malzemelerdir. Birçok malzemede olduğu gibi bu tip malzemelerin modellenmesinde de sonlu eleman yöntemi sıkça kullanılır. Model oluşturulurken malzemelerin homojenize edilerek ortak bir malzeme özelliği değeri kullanılması bilinen bir yaklaşımdır. Ancak bu yaklaşım birçok varsayım altında geçerlidir. Bunun yanında kompozit malzemeyi oluşturan bileşen malzemelerin her biri üzerindeki gerilme ve gerinimlerin ayrı ayrı incelenmesine olanak sağlamazlar. Gerçekçi modelleme için malzemelerin ayrı ayrı modellenmesi gerekir. Ancak özellikle bu bileşen malzemelerin şekillerinin karmaşık olması, sonlu eleman modelinin oluşturulması kısmında eleman sürekliliğini sağlamak için oldukça soruna yol açacak veya modelde çok fazla eleman kullanılması nedeniyle çözüm süresi uzayacaktır. Bu soruna çözüm için gömülü eleman yöntemi geliştirilmiştir. Bu yöntemde kompozit malzemeyi oluşturan bileşen malzemeler gömülü bölge ve ana bölge olarak birbirlerinden bağımsız ağ yapıları oluşturulur. Malzemeler arasında bağlantı sınırlandırmaları koşulları belirlenerek malzemelerin tek bir malzeme gibi davranması sağlanır. Bu yöntem sayesinde hem bileşenler arası eleman sürekliliği gerekmediğinden göreceli olarak daha düzgün ve daha az elemanlı ağ yapılı modeller oluşturulabilir hem de çoğunlukla ampirik olan yaklaşımlar yerine direkt

malzemeler modellendiği için bileşke malzemenin mekanik davranışı daha gerçekçi elde edilebilir. Bunun yanında bileşen malzemelerin üzerindeki gerilme ve gerinimler incelenebilir. Ancak bu yöntemin de gerçekçi sonuçlar verebilmesi için gömülü hacmin ana hacme göre oranının çok düşük olmasının yanı sıra ana elemanın doğrusal elastik malzeme davranışı göstermesi gerekmektedir. Çünkü gömülü malzemenin olduğu yerdeki ana malzeme halihazırda modelde yer aldığından (artık hacim) malzemenin mekanik davranışını etkileyecektir. Kompozit malzemelerde en sık kullanılan ana malzeme (matris) termoelastik veya termoplastik polimerlerdir. Bu malzemelerin de dış yükler altında doğrusal olmayan mekanik davranış gösterdikleri bilinmektedir. Buna ilaveten kas ve doku yapılarının malzemeleri de yüksek derecede inelastik malzeme davranışı içeririr. Gömülü hacim (fiber) oranı yükseldiğinde matristeki bu davranışının dahil edilmesi daha da önem kazanmaktadır.

Bu projedeki amaç, modellemelerde oldukça kolaylık sağlayan ve sadece doğrusal malzeme davranışı için kullanılabilen bu gömülü eleman yönteminin elasto-plastik ve inelastik malzeme davranışı için de kullanılmasına olanak sağlayan bir yöntem geliştirmektir. Bu amaçla, uygun malzeme özelliğini tanımlayacak oldukça uzun ve karmaşık kullanıcı döngüleri geliştirilmiş ve bu yöntem ile elde edilen sonuçlar klasik sürekli eleman yöntemi uygulanan modellerle kıyaslanmıştır. Tek fiberli tek ve çok elemanlı modellerle birlikte rastgele dağıtılmış çok fiberli bir modelin 0.6 ve 0.4 olmak üzere iki farklı fiber hacimsel oranındaki çeşidinde geliştirilen yöntem test edilmiştir. Sonuçlar göstermektedir ki, geliştirilen yöntem iki boyutlu bir modelin S11 ve S12 gerilme bileşenlerinde gerçekçi sonuçlar vermektedir. Beklendiği üzere, fiber hacimsel oranı 0.4'e düştüğünde sonuçların gerçekçiliği artmaktadır.

Anahtar Kelimeler: Kompozit malzemeler, sonlu eleman yöntemi, gömülü eleman yöntemi, artık hacim, bileşen malzeme özellikleri, çok ölçekli modelleme

ACKNOWLEDGEMENTS

I would like to express my thanks to my supervisor Assoc. Prof. Dr. Barış SABUNCUOĞLU for his invaluable support and responding my all questions tirelessly during this project.

I would also like to thank The Scientific and Technological Research Council of Turkey for supporting this study in the framework of 3001 - Starting R&D Projects Funding Program, project number 217M994.

Finally, I would like to thank my precious family, Emine ŞIK and Mehmet ŞIK for their support and endless love throughout my whole life, but especially for this master's thesis. I would not be writing these sentences if not for their encouragement.

ALP ŞIK

TABLE OF CONTENTS

ABSTRACT i

ÖZET iii

ACKNOWLEDGEMENTS v

TABLE OF CONTENTS vi

LIST OF TABLES ix

LIST OF FIGURES x

LIST OF SYMBOLS AND ABBREVIATIONS xii

1. INTRODUCTION 1

1.1. Aim of the Study 1

1.2. Research Methodology 2

1.3. Outline of the Study 2

2. COMPOSITE MATERIALS AND THEIR ANALYSIS METHODS 4

2.1. Definition of Composite Materials 4

2.2. Finite Element Method 4

2.3. Analysis of Composite Materials 6

2.3.1. Homogenization Methods 6

2.3.2. Separate Modeling of Constituent Materials 7

2.3.3. Embedded Element Method 10

2.3.4. Elimination of the Redundant Volume 13

3. DEVELOPMENT OF EMBEDDED ELEMENT METHOD FOR NON-LINEAR MATERIAL PROPERTY CONDITIONS 15

3.1. Introduction 15

3.2. Preliminary Study to Calculate the Stiffness According to the Nodal Results (not employed in this study) 16

3.3. Determination of Equivalent Stiffness Based on the Integration Point Results (employed in this study) 18
3.4. Working Principle of the Custom Subroutine 18
3.4.1. Matrix UMAT 22
3.4.2. Fiber UMAT 23
3.4.3. URDFIL 25
3.5. Summary 25
4. MODELS AND ANALYSIS 26
4.1. General Overview of Models 26
4.2. Inspected Parameters 29
4.2.1. Fiber Volume Fraction 30
4.2.2. Implementation of Variations of the Proposed Method and von Mises Plasticity 30
4.2.3. Comparison of Plane Strain and Generalized Plane Strain 30
4.2.4. Mesh Study 31
4.2.5. Effect of IP_{cons} Value on Processing Time and Results 32
4.2.6. Performance of the Proposed Method Under Shear Loading 32
4.3. Summary 33
5. RESULTS 34
5.1. Validation of the Stated Problems on Single Fiber Model (SFM) 34
5.2. Results of the Proposed Solution Method on Randomly Distributed Fibers Model (RDFM) 37
5.3. Results of Parametric Studies 44
5.3.1. Mesh Study 44
5.3.2. Effect of Element Type (CPE4 vs. CPEG4) 47
5.3.3. Effect of Fiber Volume Fraction 51
5.3.4. Effect of von Mises Plasticity 53
5.3.5. Effect of IP_{cons} 55

5.3.6. Performance of the Proposed Solution Under Shear Loading 57
6. CONCLUSION 61
6.1. Summary of the Study 61
6.2. Outcomes of the Study 61
6.3. Future Studies 62
7. REFERENCES 64
APPENDIX 67
A. Introduction to the Plasticity Models 67
a. Original DP Approach 67
b. Extended DP Approach 68
B. Drucker-Prager Plasticity Model Formulations 69
C. Von-Mises Plasticity Model Formulations 75
a. Elastic Volumetric Modulus 76
b. Consistent Tangent Modulus 76

LIST OF TABLES

Table 3.1. An example of the output file. 17
Table 4.1. Elastic and Drucker-Prager properties for materials 29
Table 4.2. Element numbers, node numbers, element sizes for each mesh structure..... 31

LIST OF FIGURES

Figure 2.1. Finite element method working scheme 6
Figure 2.2. An example of continuously meshed modeling where meshes are refined between matrix (yellow) and fiber (blue). (Sabuncuoglu et al. 2015) 8
Figure 2.3. a) Woven composite with a complex yarn structure (Lomov et al. 2007); b) Usage of triangular meshing on a textile composite (Grail et al. 2013).....9
Figure 2.4. EE method and CNT (Romanov 2015).....11
Figure 2.5. A schematic of how embedded element method works. An embedded element model is an equivalent of (a). A real composite model should be represented as in (b).....13
Figure 3.1. a) Single element trial model. Matrix is shown in green and fiber is shown in beige. b) Representation of distances between an embedded node and host element nodes surrounding it. The purple dot shows the embedded node and red dots show surrounding host element nodes. 17
Figure 3.2. Flowchart of subroutine employment in finite element analysis. (Systèmes 2012).....20
Figure 3.3. Flowchart of user custom subroutine.....21
Figure 3.4. Matrix UMAT Flowchart.....22
Figure 3.5. Fiber UMAT Flowchart.....24
Figure 3.6. A figure that represents the working principle of IP distance measuring process. Yellow circle represents the maximum distance for IP searching distance, yellow dots represent the selected host (matrix) IPs, purple dots represent unselected host IPs and the red dot represent the subjected embedded node. 24
Figure 4.1. a) SFM geometry; b) RDFM geometry for vf = 0.6 26
Figure 4.2. Mesh structure of a) embedded element-based models; b) continuously meshed models 27
Figure 4.3. Boundary conditions of a) SFM; b) RDFM; c) an example of successful application of PBC (the opposite edges of the model move together). 28
Figure 4.4. Hardening behavior data of matrix stress vs. strain (%).....29
Figure 4.5. Model geometry of RDFM for a) vf=0.4; b) vf = 0.6.....30

Figure 4.6. Mesh structures of a) Coarse-1 and b) Dense-1 setups 31
Figure 4.7. Boundary conditions of shear loading for a) model without PBC; b) model with PBC. 32
Figure 4.8. Superimposed images of deformed and undeformed versions of a) model without PBC; b) model with PBC. 33
Figure 5.1. SFM fiber length. L represents the total fiber length. y/L represents the position on the fiber. 35
Figure 5.2. Stresses in the loading direction (σ11) vs normalized fiber length in SFM for the applied displacement of a) 0.15; b) 0.50; c) 1.00. 36
Figure 5.3. Selected fibers are shown with red on the model. Fiber numbers are given near fibers. 37
Figure 5.4. RDFM Results. a-b-c) represent S11 values, d-e-f) represent S22 values and g-h-i) represent S12 values. a-d-f) for Fiber 1, b-f-h) for Fiber 2 and c-f-i) shows results for Fiber 3, respectively. 42
Figure 5.5. Strain distributions on 11-direction on matrices of a) Classical; b) UMAT; c) EE Equivalent models 42
Figure 5.6. Distribution of strains in the X-direction on fiber 1 of a) Classical; b) UMAT; c) EE Equivalent models 43
Figure 5.7. Variation of S11 along Fiber 1 centerline: a) Coarse Mesh 1; b) Coarse Mesh 2; c) Coarse Mesh 3; d) Default Mesh; e) Dense Mesh 47
Figure 5.8. Comparison of models with CPE4 and CPEG4 element types. a) S11; b) S22 and c) S12 stress component results. 49
Figure 5.9. RDFM results for vf=0.4. a-b-c) represent S11 values for Fiber 1, Fiber 2 and Fiber 3, respectively. 52
Figure 5.10. RDFM Results for von Mises plasticity. a-b-c) represent S11 values, for Fiber 1, Fiber 2 and Fiber 3, respectively. 54
Figure 5.11. Effect of IPcons on processing time 55
Figure 5.12. Effect of IPcons on stress values 56
Figure 5.13. S12 results for the case without PBC application. Figures a, b and c represent Fiber 1, Fiber 2 and Fiber 3, respectively. 58
Figure 5.14. S12 results for the case with PBC application. Figures a, b and c represent Fiber 1, Fiber 2 and Fiber 3, respectively. 60

LIST OF SYMBOLS AND ABBREVIATIONS

Symbols

K_*	stiffness matrix (general formulas)
w_i	weight factor
ε_x	correct strain fields
σ_x	correct stress fields
C_i^m	stiffness matrix of matrix material
$C_i^{eq.m}$	equivalent stiffness matrix of matrix material acting on the redundant volume
C_i^f	stiffness matrix of fiber material
$C_i^{corrected}$	corrected stiffness matrix acting on the redundant volume
V^*	volume fraction
E^*	Young's modulus
θ	friction angle
α_v	dilation angle
K	flow-stress ratio

Abbreviations

SFM	single fiber model
RDFM	randomly distributed fibers model
EVM	elastic volumetric moduli
CTM	consistent tangent moduli
vM	von Mises plasticity
DP	Drucker-Prager plasticity

1. INTRODUCTION

1.1. Aim of the Study

In order to produce high quality fiber-reinforced composites, and increase their usage life, modeling of the mechanical behavior of these materials is important. Finite element method is the most widely used method of modeling for fiber-reinforced composites. Since fiber-reinforced composites are heterogeneous materials, implementing their mechanical behavior into a modeling scheme needs extra processes. One of them is homogenization, where constituent material properties are homogenized under some assumptions and obtained material properties are input into the modeling interface as a single material. This approach does not let constituent properties, such as, strains and stresses, to be investigated independently. These issues can cause some problems, hence for more detailed analysis, separate modeling of the constituents is needed. There are various studies in the literature, where this approach is used. In this approach, in the case of usage of complex material shapes, excessive numbers of elements may be needed. Also, providing a continuous mesh structure becomes harder. Hence, a new method called "Embedded Element Method" is developed and presented in the ABAQUS software.

In this method, constituent materials are meshed independently from each other and fiber is overlapped onto matrix. This process eliminates the need of providing a mesh continuity, thus making mesh creation easier. On the other hand, superposition of fiber mesh onto matrix, creates a redundant volume of matrix material beneath the fiber. This redundant volume has negative effects on the analysis, where the fiber volume fraction is high or fiber stiffness is close to the matrix stiffness. In order to perform an accurate analysis, effect of this redundant volume needs to be corrected.

The aim of this study is to develop an approach to eliminate the redundant volume issue for cases, where non-linear material properties are used. Because of the non-linear material behavior, material properties of the redundant volume changes in every step according to the position of nodes. In every step, stiffness and other properties of the redundant volume from the previous step is used and manipulated to determine the stiffness of the redundant volume in the current step. These processes are realized with a

custom user subroutine, which is explained in detail in later chapters. Results from the proposed solution is compared with a conventional continuous meshing method.

1.2. Research Methodology

This study makes a brief introduction to composite materials and finite element method. After that, finite element analysis applications of composite materials are investigated. Examples and applications from the literature are explained in detail in these sections. Studies on embedded element method are also investigated in detail. Following these, studies for a proposed solution is started. A custom user subroutine is developed. This proposed subroutine is tested in every small change to ensure its capability and reliability. After managing to obtain a working solution, different case studies for testing the subroutine are determined, such as, different volume fractions, different plasticity models, some variations upon the proposed solution. After all these test cases are finalized, analyses are performed under these conditions and some results are obtained. These results are proposed and discussed upon in detail. At last, conclusions upon this study are given.

1.3. Outline of the Study

There are 6 chapters in this thesis. A short explanation of all chapters can be found below:

Chapter 1: Introduction

Brief introduction about the scope of the study is given.

Chapter 2: Composite Materials and Their Analysis Methods

Basic information on composite materials and finite element method is given as a first step into the study. After that, the embedded element method, the main subject of this study, is explained in detail and its working principles are given. Finally, a previous study from the literature, the basis of this study's calculations, is investigated. Its achievements and shortcomings are explained in detail. An extensive literature review about the study is also given in this chapter.

Chapter 3: Development of Embedded Element Method for Non-Linear Material Property Conditions

In this chapter, proposed method for the given problem is explained step-by-step in detail.

Chapter 4: Models and Analysis

Composite models and test cases for the testing of the proposed model are represented in this chapter. Key properties belonging to models and test cases are given in tables and figures.

Chapter 5: Results

Obtained results from each test case are represented and discussed in this chapter.

Chapter 6: Conclusion

A summary of the study and key outcomes are given in this chapter.

Appendix

Detailed explanation about plasticity models and developed variations of proposed model are given.

2. COMPOSITE MATERIALS AND THEIR ANALYSIS METHODS

2.1. Definition of Composite Materials

Composite materials are materials that are being created by the combination of two or more different materials, in order to obtain a more suitable material for users' needs. In general, one constituent is the *reinforcement*, which contributes to the increase of overall material stiffness. The second constituent is the *matrix*, in which the reinforcement material lies. These kinds of materials are being used since ancient times, starting with the infusion of clays and straws, which provided stronger and more durable bricks for house making. More sorts of composites have been used in numerous work fields, such as, civil engineering applications, aerospace applications or biomechanics (Bonfield 1988; Holzapfel 2001). However, composite materials have some limitations in terms of manufacturing. Manufacturing a composite material can be costly because of the need for complex production tools, such as injection molds. Moreover, composites have complex mechanical behavior in comparison to monolithic materials such as steel or aluminum. Therefore, analyzing the mechanical behavior of a composite material before manufacturing becomes important. Analysis of fiber-reinforced composites is also vital for achieving high-quality designs, so that possible flaws in manufacturing can be eliminated beforehand.

2.2. Finite Element Method

In order to examine the mechanical behavior of materials under certain loads and conditions, a lot of partial differential equations should be solved. Solving these equations analytically can be practically impossible; hence a variety of numerical methods are developed to achieve this aim. The finite element method (FEM) is the most widely used numerical method, which can be employed for both monolithic and composite materials. The main objective of this method is to divide a model into finite number of representative elements and perform a solution on these elements to analyze the material. The finite element method can be inspected step by step which are explained and represented in a flowchart in Figure 2.1 (Barbero 2007; Stolarski et al. 2018):

Mathematical Model (Idealization): First of all, desired geometry that is subjected to analysis is modeled mathematically. This process simplifies the geometry and approximates the displacement field and other material properties.

Discretization: Idealized model is divided into finite number of elements. This process is also called meshing. Size and number of elements affect the accuracy of the analysis. Hence, this process should be performed with caution.

Selection of Element Type: This process determines which interpolation function is going to be used. The number of nodes per element and element shape also affects the accuracy of the analysis. As elements have more nodes per element, accuracy will increase, but solution time will be longer.

Derivation of Element Properties: In this step, stiffness matrices of elements are derived from forces and displacement applied upon elements. Governing equation can be given as:

$$[K^e]\{u^e\} = \{F^e\} \tag{2.1}$$

where e denotes the subjected element, F is the element force vector, u are displacements on nodes, and K is the stiffness matrix of the subjected element.

Assembly of Elemental Stiffness Matrices: Nodes of discretized geometries have the same displacement value for neighboring elements. Turning this principle into compatibility and equilibrium equations, provides a global stiffness matrix which can be used for the whole model.

Application of Boundary Conditions and Solving the Equations: Applying the boundary conditions and loads affect the global stiffness matrix in each and every step.

Derivation of Unknown Displacements: Solution of the equation (2.2) provides the deformation applied to the geometry.

$$\{u^e\} = [K^e]^{-1}\{F^e\} \tag{2.2}$$

Calculation of Strains and Stresses: Once the displacements are obtained, strains and stresses can be calculated by employing constitutive equations between displacements, strains and stresses.

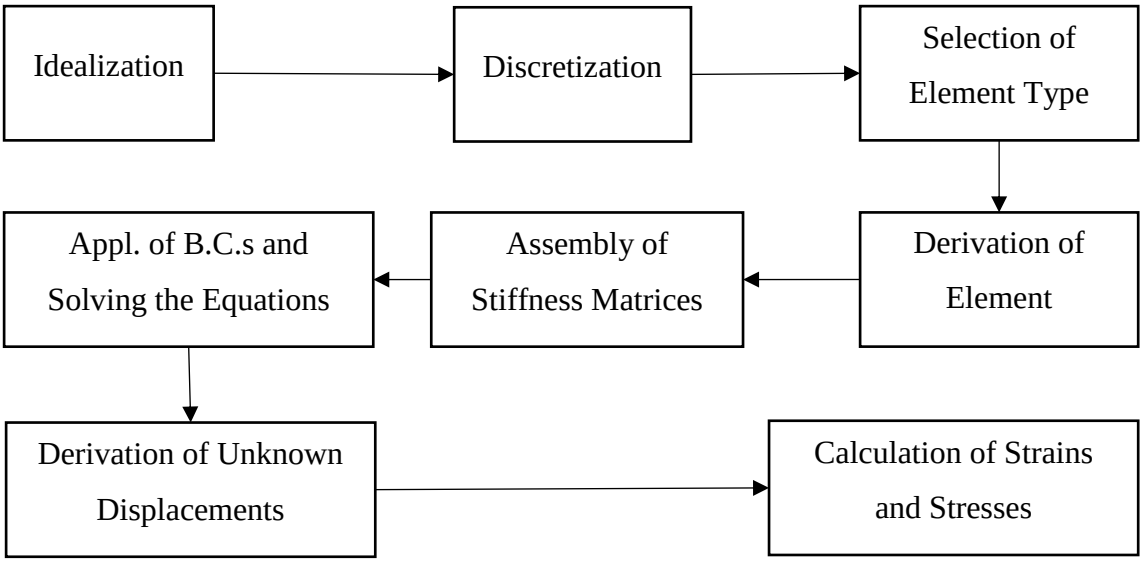

Figure 2.1. Finite element method working scheme

2.3. Analysis of Composite Materials

In the finite element modeling of composite materials, there are two main approaches used for defining the material behavior. In the first approach, constituent material properties are combined together in various mathematical constraints and obtained material properties represent a single, monolithic material. These methods are called "homogenization methods". In the second approach, constituent materials are defined independently from each other, which is called "separate modeling method". In the following subsections, these approaches will be explained alongside the "embedded element method", which builds the base of this study.

2.3.1. Homogenization Methods

Homogenization methods are one of these approaches, where the properties of constituent materials are homogenized by some calculations and treated as if it is a monolithic material. Most extensively used theory is the rule of mixtures, given in equation (2.3) which is a weighted mean of a material property according to the material volume fractions. c, f and m denote composite, fiber and matrix, respectively. This theory provides realistic results on the longitudinal direction, but is not useful on the transverse direction, since fiber distribution is not considered.

$$E^c = E^f V^f + E^m V^m \tag{2.3}$$

where E^f and E^m are the Young's moduli of fiber and matrix, respectively. V^f and V^m are the volume fractions of fiber and matrix. Resulting value of E^c is equal to the composites overall Young's modulus.

Halpin-Tsai Model (Affdl and Kardos 1976) is a development over classical rule of mixtures, which can provide more realistic results on the transverse direction, but only valid for some certain fiber volume fractions. Nielsen Model (Nielsen and Landel 1994) adds parameters to determine the boundaries of the validity of the previous model. Chamis formulation (Chamis 1989) uses square root of fiber volume fraction for the calculation of shear and transverse elastic properties. For the geometries containing different shapes other than straight fibers, inclusion-based models are being used (Eshelby 1957; Hill 1965; Mori and Tanaka 1973). All of these models provide approximate results for strains and stresses inside the material, but cannot provide properties for each constituent material. Because of that, non-linear material properties, fiber-matrix separation or damage modeling cannot be inspected with these methods. Furthermore, these models are mostly empirical and valid under certain assumptions. As an example, when applying homogenization on woven composites, waviness caused by the woven structure is neglected.

2.3.2. Separate Modeling of Constituent Materials

When homogenization methods cannot be applied or properties of fiber and matrix needed to be inspected, constituent materials should be separately modeled. The mechanical behavior of materials can be modeled without the restrictions of homogenization methods. In order to accurately model the interaction between constituents, continuity between discretized elements should be provided. If simple shaped materials are used, providing the continuity does not become an issue. A representative figure of mesh continuity is given in Figure 2.2.

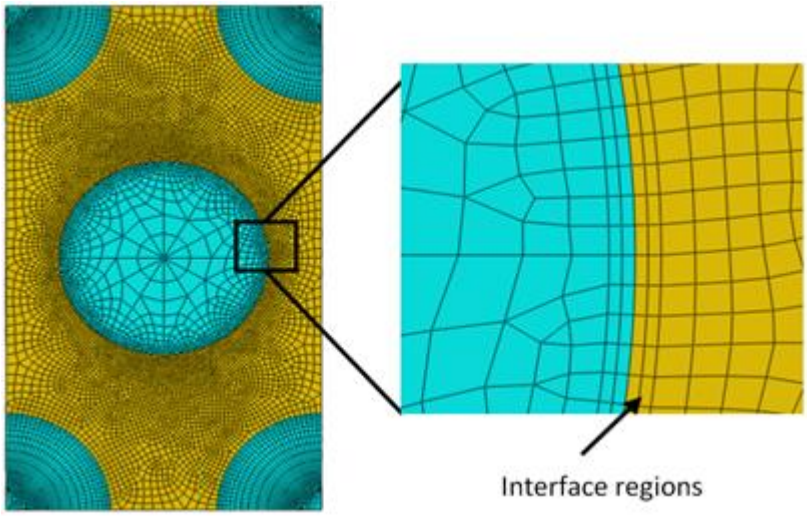

Figure 2.2. An example of continuously meshed modeling where meshes are refined between matrix (yellow) and fiber (blue). (Sabuncuoglu et al. 2015)

Separate modeling approach has two important issues that should be considered. First of all, because of the modeling of constituents separately, macroscopic scale finite element models may consist of too many elements. This causes the need to prepare smaller representative volumes of the main geometry. Desired material properties are gathered through these smaller volumes. These properties are the equivalent of homogenized properties and they are applied onto macroscopic scale model. The second issue is that when the constituent materials have complex geometries, maintaining the mesh continuity becomes harder. Modeling of textile composites can be given as examples regarding this difficulty (Bedogni et al. 2012; Fagiano et al. 2014; Lomov et al. 2007). In these kinds of models, yarns made of fibers are modeled instead of fibers themselves. These woven yarns have wavy structures inside the material. Thus, when they are combined with the matrix, interface regions between matrix and fiber becomes degenerated and generating a continuous mesh at these regions is generally quite tricky (Lomov et al. 2007). Sometimes a lot of triangular meshes should be used to provide continuity, but these types of meshes have lower accuracy than quadratic meshes. Examples of complex yarn structures and usage of triangular meshes are given in Figure 2.3.

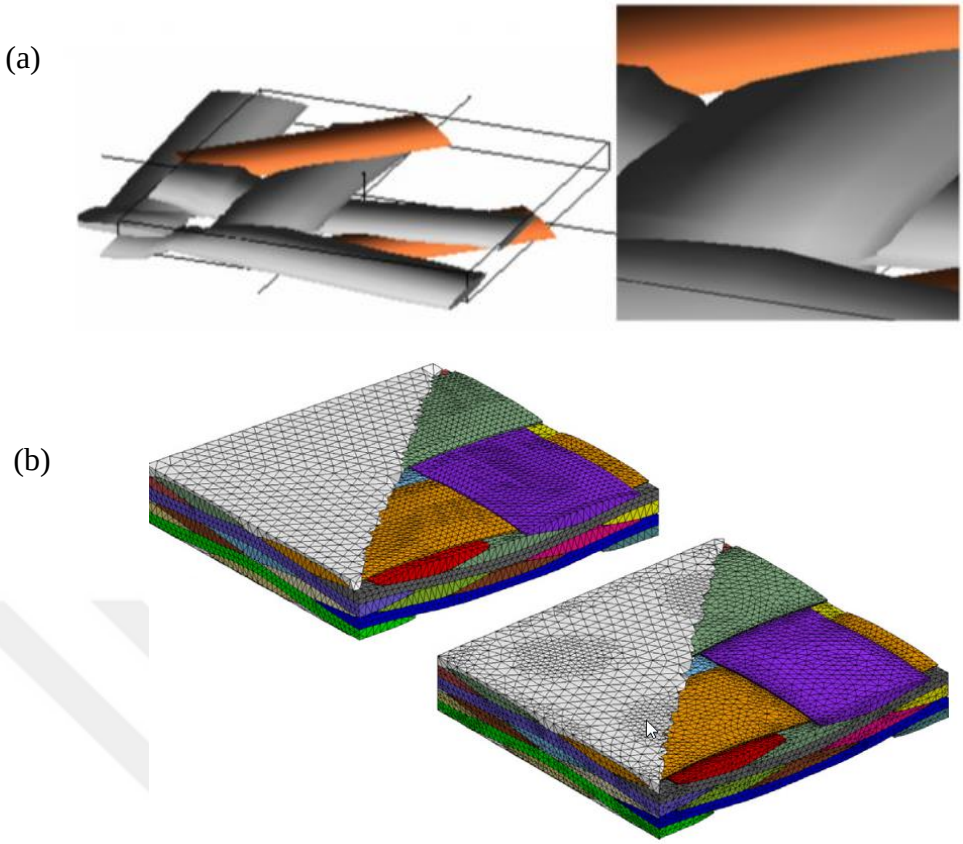

Figure 2.3. a) Woven composite with a complex yarn structure (Lomov et al. 2007); b) Usage of triangular meshing on a textile composite (Grail et al. 2013).

In an attempt to solve these issues on mesh structure, numerous approaches are developed. Fish (1992) created mesh structures on top of each other with the superposition method and defined a discontinuous material behavior for each constituent. This method is applied on textile composites. Zako et al. (2005) have developed M^3 method. In this method, models are created in three different scales as macro, meso and micro scales. Every scale is modeled separately and stiffness matrices obtained from each model are superposed into another scale. Kurashiki et al. (2007), Honda et al. (2008), Ohyama et al. (2011) used this method for different types of composites and damage studies. Jiang et al. (2008) used domain superposition technique in order to define constraints between constituents and applied the technique to woven composites. All of these methods are usually valid for novel types of composites and cannot be directly employed on every type of composites.

Apart from the previously mentioned problems about woven composites, if fibers are too small relative to the matrix, other problems may arise. A typical example is the modeling of nano-reinforced composites, where homogenized material properties are used in the literature (Chatzigeorgiou et al. 2011; Kundalwal and Ray 2012; Ren et al. 2015; Sabuncuoglu et al. 2018). However, if separate modeling for this kind of composites is needed, creating a mesh structure will be problematic. Since the reinforcements are too small, in order to provide mesh continuity, fine meshes containing an excessive number of elements should be used. An example of this condition is presented in the study of Li and Chou (2008). In this study, the effect of carbon nanotubes (CNT) distributed inside a glass-fiber composite is analyzed. Since these CNT's are too small, excessively fine meshes are used in interface regions. This caused the usage 350000 discretized elements and limiting the model into a two-dimensional model. Similar problems have occurred in the modeling of short-fiber composites, thus homogenized material properties are preferred in these applications (Abdin et al. 2016; Jain et al. 2015).

2.3.3. Embedded Element Method

For the purpose of eliminating these issues, embedded element method is developed, which can be found as a standard tool inside the ABAQUS software. As the name suggests, in this method, regions of discretized elements are embedded into another region. The first region is called the "embedded" region and the second one is called the "host" region. In this method, embedded region is created inside the host region. In the conventional continuous meshing method, there should be a gap inside the host region in the shape of embedded region. This gap can cause degenerated surfaces in the host region when the embedded region geometry is complex as mentioned earlier. On the other hand, with the embedded element method, this problem is averted, since there is no need to create a gap inside the host region. In Figure 2.4, a representative figure of CNT's inside a matrix, where CNT's are the embedded region and matrix is the host region. Separate and superposed mesh structures can clearly be seen in the figure.

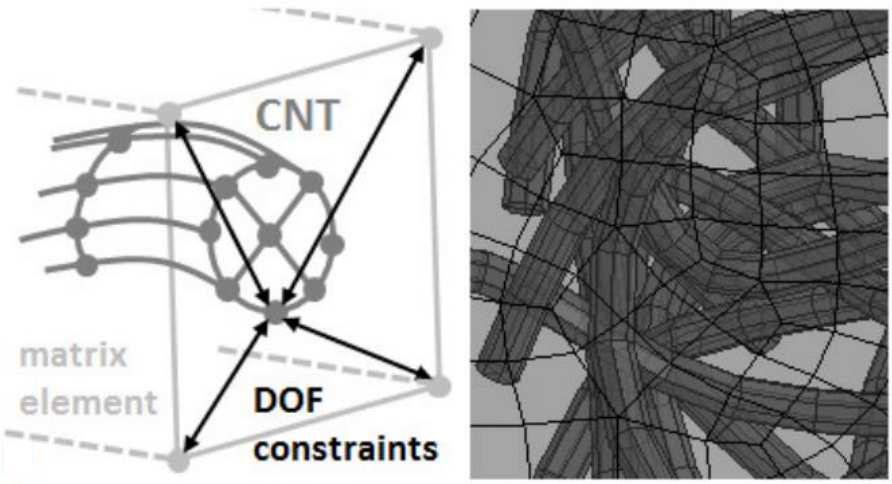

Figure 2.4. EE method and CNT (Romanov 2015)

In ABAQUS software, embedded element condition is defined as “contact condition”. The software scans for embedded CNT nodes lying inside host elements, and matches each embedded node with a host element. Degrees of freedom of embedded nodes are constrained with the host elements’ degrees of freedom. These constraints are calculated according to the relative position of an embedded node to the host nodes surrounding it. Equations employed for these constraints are given below in equations (2.4) and (2.5):

$$D^{x,y,z} = \sum_{i}^{N} d_i^{x,y,z} w_i \tag{2.4}$$

where N denotes the number of nodes belonging to a host element, $d_i^{x,y,z}$ denotes the displacement of i th host element and w_i denotes the weight factor of each host node on the encircled embedded node. It is predicted that w_i is calculated as in the equation below:

$$w_i = \frac{1}{l_i} \Big/ \sum_{i}^{N} \frac{1}{l_i} \tag{2.5}$$

There are numerous studies that employed embedded element method. Savvas et al. (2012) applied this method to inspect the effect of interfacial shear strength on the mechanical and damping properties of CNT reinforced composites. CNTs are modeled as beam elements in this study. Tabatabaei et al. (2014) applied this method to the woven composites and modeled different weave types with embedded element model. Obtained results were compared with the continuously meshed models and embedded element

method is proven to be realistic. Matveeva et al. (2014) applied the method for wavy and straight fibers and compared the effects of beam, shell or three-dimensional element usage. Romanov (2015) used this method and modeled both fibers and matrix in three-dimensional elements. Abdin et al. (2016) used Mori-Tanaka model for short wavy fibers and compared the results with models created with embedded element method. Muñoz et al. (2015) inspected the mechanical performance of hybrid three-dimensional woven composites under ballistic impact. X-ray tomography results are compared with the numerical model where embedded element method is used as the model. Liu et al. (2016) developed a model with this method to predict the effective elastic constants of discontinuous fiber composites. Joosten et al. (2016) employed cohesive elements into the matrix domain, and used them to investigate matrix cracking with embedded element method. Vorobiov et al. (2017) compared embedded element method with another mesh superposition method and a continuously meshed model. A unidirectional single fiber model and a complex weave three-dimensional composite are used for base models in this study. Liu et al. (2019) combined cohesive elements and embedded element method to investigate damage development in fibrous composites. All of these studies have proved that embedded element method is a reliable tool for separate modeling of constituents in composites.

When this method is applied, model behavior is given in Figure 2.5a. It can be clearly seen that there occurs an extra volume of matrix under the volume of fibers. However, to model the true material behavior, it should be as shown in the Figure 2.5b. This redundant volume does not affect the analysis when the embedded volume is really small compared to the host (matrix) domain. Also, the high stiffness of embedded volume compared to the host domain also reduces the effects of the redundant volume. On the other hand, in case where high fiber volume fractions or low stiffness fibers exist, such as natural fibers, effects of the redundant volume should be eliminated.

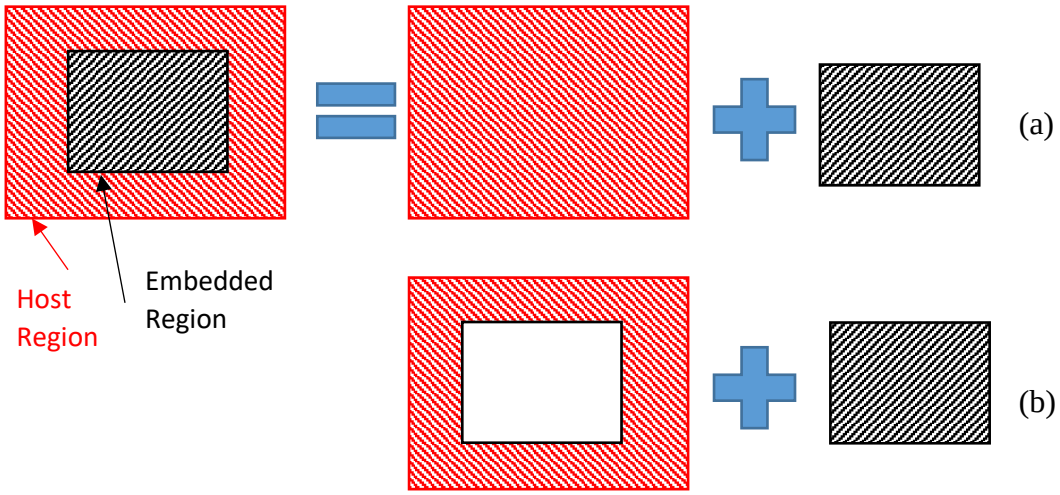

Figure 2.5. A schematic of how embedded element method works. An embedded element model is an equivalent of (a). A real composite model should be represented as in (b).

Different studies have attempted to solve this issue by either eliminating the degrees of freedom of the redundant volume (Fish 1992), or eliminating the shape functions of the elements corresponding to the redundant volume (Iarve et al. 2009). Another study of Tabatabaei and Lomov (2015) subtracted host element stiffness matrices from embedded element stiffness matrices on the redundant volume. This last approach is the preferred way of solution for the current study and a detailed investigation is given in the following subsection.

2.3.4. Elimination of the Redundant Volume

The study of Tabatabaei and Lomov (2015) provides an approach for the elimination of the redundant volume, which is easy to implement inside ABAQUS. As it is explained in the study, the stiffnesses of the continuously meshed model in Figure 2.5b (K_{cont}) and embedded element model in Figure 2.5a (K_{emb}) are given in equations (2.6) and (2.7)

$$K_{cont} = K_f V_f + K_m V_m \tag{2.6}$$

$$K_{emb} = K_f V_f + K_m V_m + K_r V_r \tag{2.7}$$

where K denotes stiffness, V denotes volume and subscripts of f, m and r denote fiber, matrix and the redundant volume, respectively. In this case, K_r actually equals to K_m and

V_r equals to V_f. It is offered to replace K_f with a K_f' that is equal to $K_f - K_m$. Now if the equation of K_{emb} is rewritten it comes out as:

$$K_{emb} = (K_f - K_m)V_f + K_m V_m + K_m V_f = K_f V_f + K_m V_m = K_{cont} \qquad (2.8)$$

Equation (2.8) indicates that substituting matrix stiffness from the fiber stiffness provides a corrected stiffness on the redundant volume. On the other hand, this process leads to the outcome of wrong stress values because of the changed stiffness value. Hence, stresses should be recalculated with the strains obtained via the corrected stiffness (ε_x) and the original stiffness value. This relation can be shown in an equation:

$$K_f \varepsilon_x = \sigma_x \qquad (2.9)$$

This process is chosen in the current thesis, since it is more straightforward to implement it over setting $K_r = 0$ as it is done in Iarve et al. (2009)'s study. Contrary to the approach in this thesis, in Iarve et al. (2009)'s approach, the user should find which embedded nodes are lying inside each host element. Apart from that, it requires user to thoroughly know how ABAQUS handles the embedding process, which is not explained in detail in the documentation of the software. This information that is hard to gather is not necessary in the current approach used in this thesis.

However, this method is only valid while both host and embedded elements have elastic material behavior. Hence, embedded element method needed to be developed to eliminate this redundant volume issue when using non-linear material properties. In the next chapter, a proposed solution is explained step-by-step in detail.

3. DEVELOPMENT OF EMBEDDED ELEMENT METHOD FOR NON-LINEAR MATERIAL PROPERTY CONDITIONS

3.1. Introduction

In this chapter, all of the processes and methods that are developed for achieving the modeling of non-linear material properties with the embedded element method are explained in detail. To start with, the very first trials for obtaining the node connectivity information are explained in section 3.2. After discussing its advantages and disadvantages, a second attempt, which is the proposed solution is explained in detail in section 3.4. Flowcharts and working principles about the developed subroutines are given in this section.

In order to provide a solution for non-linear material property cases, there some issues to be considered. First, stiffness of the redundant volume changes in each analysis step and at each position. Because of that, elastic stiffness of host elements cannot be subtracted directly from the embedded element as the stiffness of this redundant volume would be changing due to the inelastic behavior. Another problem is that, the host element would have a distribution of plastic strain. In such a case the redundant volume would also have a distribution of stiffness, which prevents to enter the modified stiffness matrix for the embedded element at the beginning of the analysis. These problems should be taken into consideration while preparing an approach. As a solution, in every step, the stiffness of embedded elements is calculated based on the results obtained from the host element results of the previous step. These equivalent stiffness values are subtracted from the embedded elements' stiffness values. Since these values are different for each embedded element, new stiffness matrices should be applied per each element. This process is handled by a custom developed user subroutine. In the sections below, these processes are explained in detail.

At the start of this code development procedure, there seemed to be two options to calculate the equivalent stiffness of the embedded element according to the results of the host element from the previous elements. The calculations could be performed according to the nodal or integration point results. At first, we considered performing calculations according to nodal results. Due to the problems encountered in this procedure, it was

decided to perform calculations according to the integration points. Nevertheless, our preliminary study based on modifying the stiffness according to the nodal is explained below to be used as a reference in the future.

3.2. Preliminary Study to Calculate the Stiffness According to the Nodal Results (not employed in this study)

Initially, determination of the equivalent stiffness according to the nodal results, requires to obtain information of which embedded node is lying in which host element. ABAQUS software obtains this information automatically, but the process is not explained clearly in the documentation. The software also gives this information, after running the analysis, as a result file, which cannot be extracted. Hence, a custom method should be developed to gather and process this information before running the analysis.

At first, a custom python code is written to achieve this objective. This code gathers coordinates of every node and classifies them according to the user input, which is the selection of elements as matrix (host) or fiber (embedded). ABAQUS' default node numbering system starts both instances nodes from number 1. In order to sort them better and prevent complications, local node numbers are changed with custom global numbers. For host elements, the first element is numbered 20000 (HEN) and the first node is numbered 2000 (HN1-2-3-4). For embedded elements, these numbers are 30000 (EEN) and 3000 (ENN), respectively. As an approach to process this information, a function that checks whether a two-dimensional coordinate is inside a two-dimensional polygon, is implemented into the code. After that, the code runs through the embedded and host elements, and checks every embedded node until it finds the host element it lies within. If a match between an embedded node and a host element is found, the code calculates the distance between each of the host element nodes (HEN) and the embedded node (ENN). The code prints the output to an external text file as shown in Table 3.1.

An example of the very first model used for this job is given in Figure 3.1a and a representative figure showing the node finding process is given in Figure 3.1b

Distance between a host node (HN1-2-3-4) and an embedded node is given by d1, d2, d3 and d4 notations, which are determined by the code itself. The code starts building a

polygon starting from the smallest numbered node and follows the other nodes of the elements in counterclockwise.

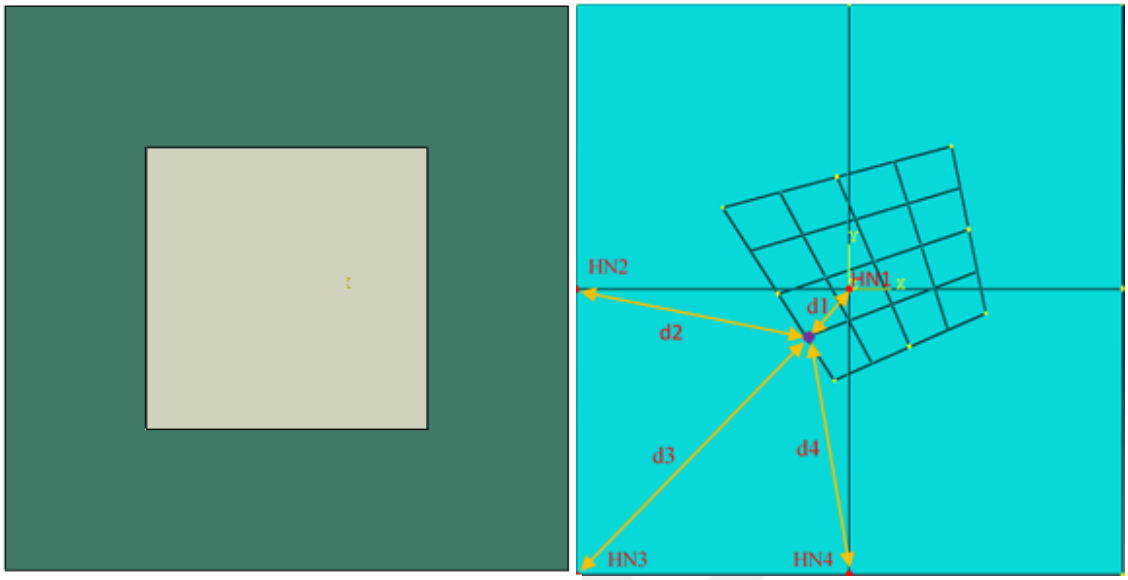

a) b)

Figure 3.1. a) Single element trial model. Matrix is shown in green and fiber is shown in beige. b) Representation of distances between an embedded node and host element nodes surrounding it. The purple dot shows the embedded node and red dots show surrounding host element nodes.

Table 3.1. An example of the output file.

EEN	**ENN**	**HEN**	**HN1**	**d1**	**HN2**	**d2**	**HN3**	**d3**	**HN4**	**d4**
30000	3000	20002	2003	5.07	2004	5.07	2007	10.42	2006	10.42
30000	3001	20000	2000	10.78	2001	10.49	2004	4.72	2003	5.34

This approach seems to be working at first glance, but it runs into some issues. First of all, when the number of host elements is over 1000, element numbering should be changed manually to match node labels to the nodes correctly. This causes information files to be inconsistent over different sized models. Apart from that, reading the

information file in the custom subroutine, becomes problematic. In order to match the read node numbers to the subjected IPs, a command named “GETPARTINFO” inside the subroutine should be called. That command did not work consistently every time, thus failing the analysis. Also, this approach obtained results that are extrapolated from IPs onto the nodes. Because of these issues, a new approach is developed, which is based on the results at the integration points.

3.3. Determination of Equivalent Stiffness Based on the Integration Point Results (employed in this study)

The key difference in this approach is the usage of integration points (IP) instead of nodes for the calculation of equivalent material properties. This change is needed since gathering and sorting IP information is more straightforward than obtaining node information in the subroutine. In addition to that, results are directly obtained from IPs, which increased the accuracy of the analysis results. Combining these processes into a subroutine eliminates the inconsistencies caused by the compilation of code and provides a more efficient solution. Elimination of the effects of the redundant volume on material stiffnesses is achieved with a different custom subroutine. Working principles of this custom subroutine is explained in detail in the next section.

3.4. Working Principle of the Custom Subroutine

A user subroutine is a tool to increase the functionality of the finite element software, by allowing users to adapt the software to the particular requirements. ABAQUS provides numerous user subroutines for various cases, such as, non-linear fluid flow, heat transfer problems and defining non-linear material properties. In the developed subroutine, UMAT and URDFIL subroutines were used together. These subroutines are employed in different stages of analysis according to the characteristics of the subroutine. Employment of these subroutines is represented as a flowchart in Figure 3.2. In every step an IP is chosen by ABAQUS and if the material property of the element it belongs is assigned as “used defined”, the calculation related to the material stiffness for this IP is performed with UMAT. After the calculation is finished, the next IP is handled, similarly. After all the calculations are performed, URDFIL subroutine is used to store the results as in the next step, all the information is normally lost.

In this study, developed user subroutine consists of two main UMAT subroutines to calculate the material properties, and one URDFIL subroutine for transferring values from the previous step to the current step. The analysis is run for each IP. The element to be analyzed is chosen randomly by the software. So above these two UMAT subroutines, there is a main UMAT subroutine that transfers the calculations for that element IP depending on the material of the element it belongs - Matrix UMAT or Fiber UMAT. Matrix UMAT subroutine calculates the stiffness matrix of matrix material (C_i^m) in every increment and stores it to be used by fiber IP in the next step. Fiber UMAT uses the stiffness values calculated by UMAT in the previous step to calculate the corrected stiffness matrix for embedded material ($C_i^{corrrected}$) for each fiber IP. $C_i^{corrrected}$ is substituted for original embedded material stiffness matrix (C_i^f), to eliminate the effect of the redundant volume. The transfer of C_i^mcalculated by Matrix UMAT in the i'th step to the Fiber UMAT subroutine for the calculation of $C_i^{corrrected}$ in the (i+1) th step is satisfied by URDFIL subroutine. The general flowchart of the subroutines is given in Figure 3.3. Details of Matrix UMAT, Fiber UMAT and URDFIL are explained in the following subsections.

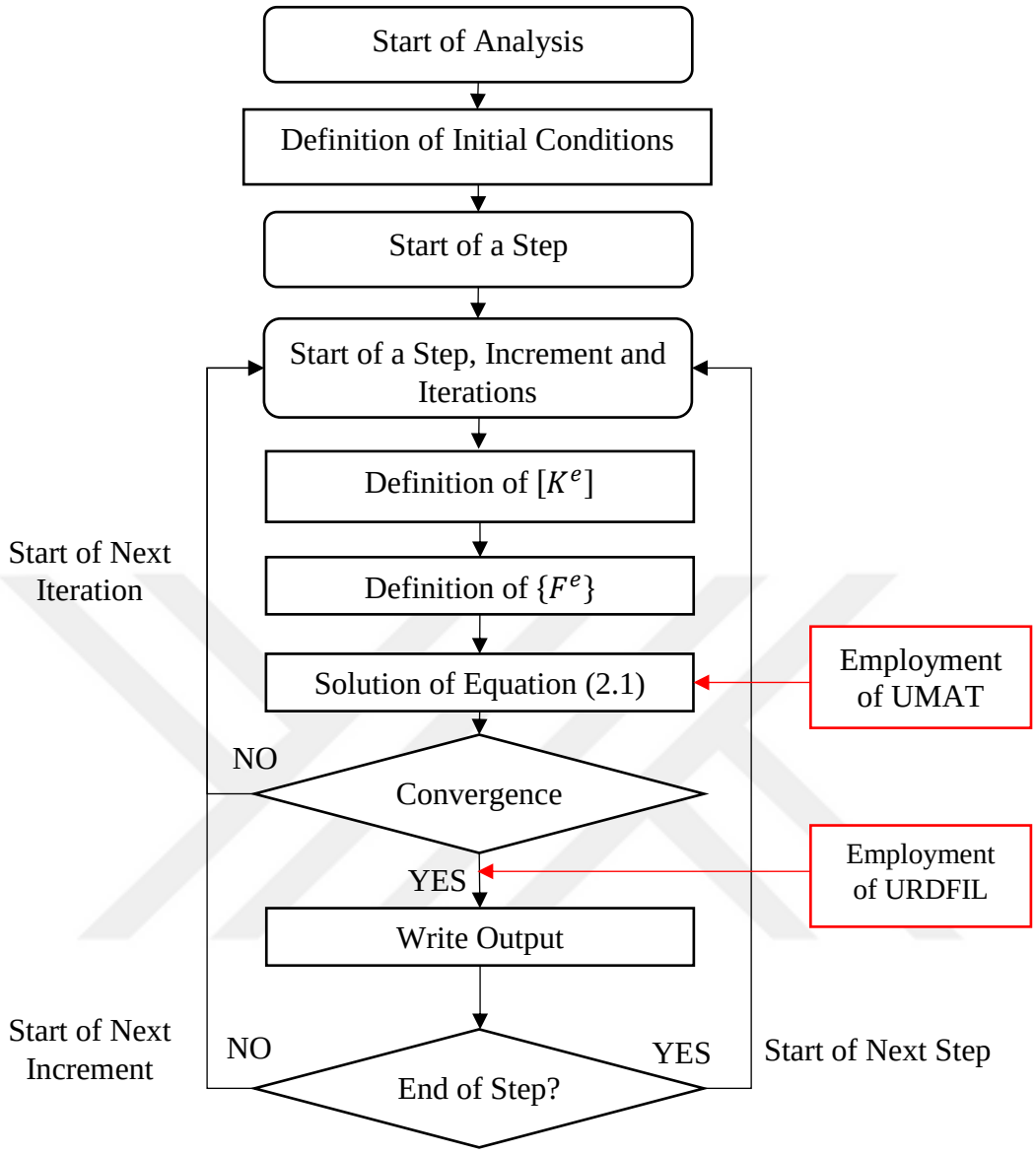

Figure 3.2. Flowchart of subroutine employment in finite element analysis. (Systèmes 2012)

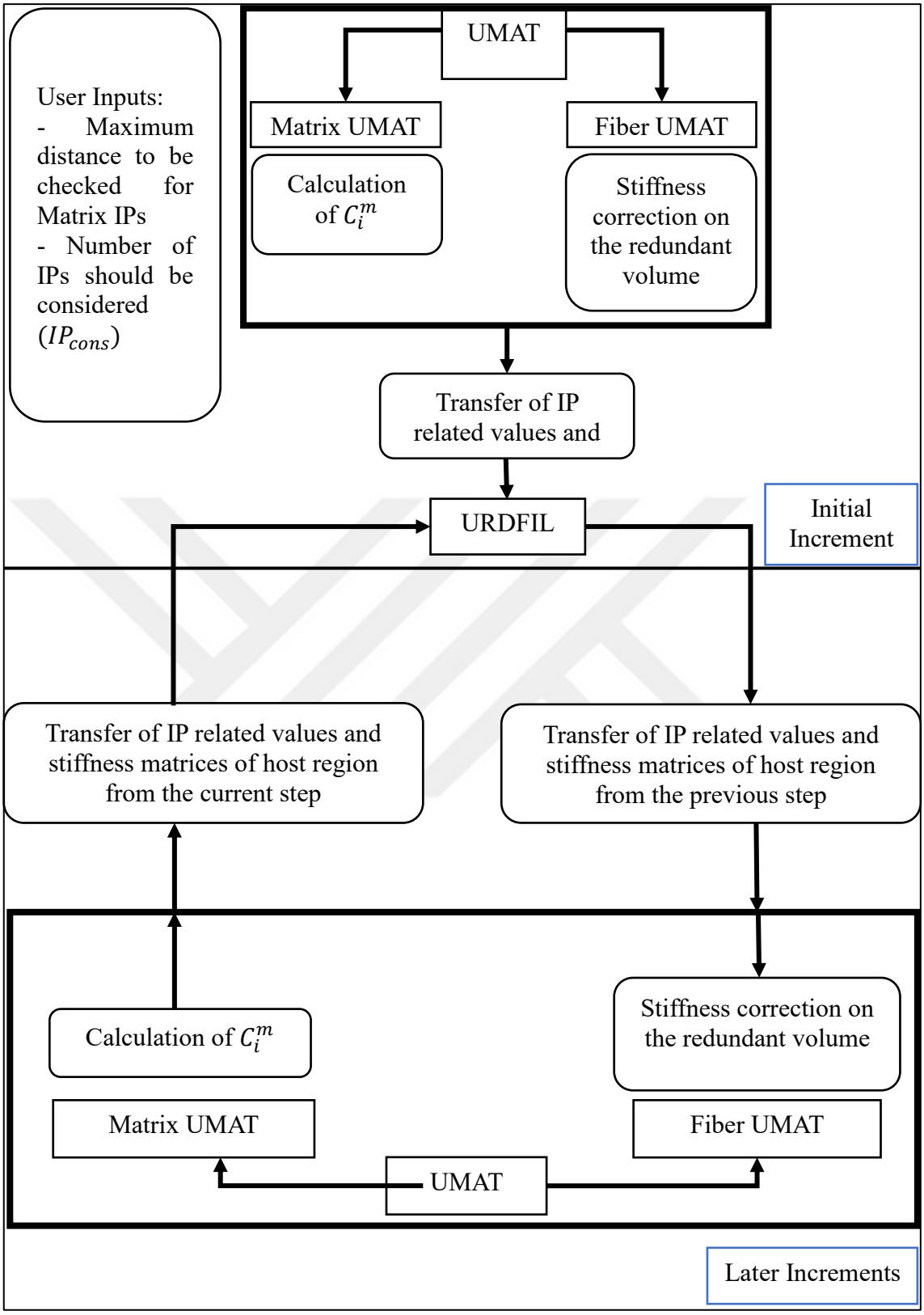

Figure 3.3. Flowchart of user custom subroutine

3.4.1. Matrix UMAT

When the IP that belongs to a matrix element is handled, it enters to the matrix UMAT section of the subroutine. The aim of this section is to calculate the stiffness matrix of the IP (C_i^m) in each step and store this to be used in the next step to modify the stiffness matrix of the embedded elements. The elastoplastic tangent stiffness matrix (C_i^m) of each IP is calculated by using the formulations of this inelastic behavior. Drucker-Prager plasticity model (DP) is used, which is an accepted model for various types of epoxies (De Morais et al. 2007; Hua et al. 2007; Zhang et al. 2017). The detailed information and formulations for this model are explained in the 69. Then the stiffness matrix is assigned to a new variable for the stiffness correction process. The variable is converted to column format for easier processing. The integration point number, element number and coordinates of the IP are also stored into different arrays to be able to identify in the next step. As this information is lost for the next IP, these arrays are transferred to the URDFIL subroutine which allows using these values in the next step. The entire flowchart of this matrix UMAT is shown in Figure 3.4.

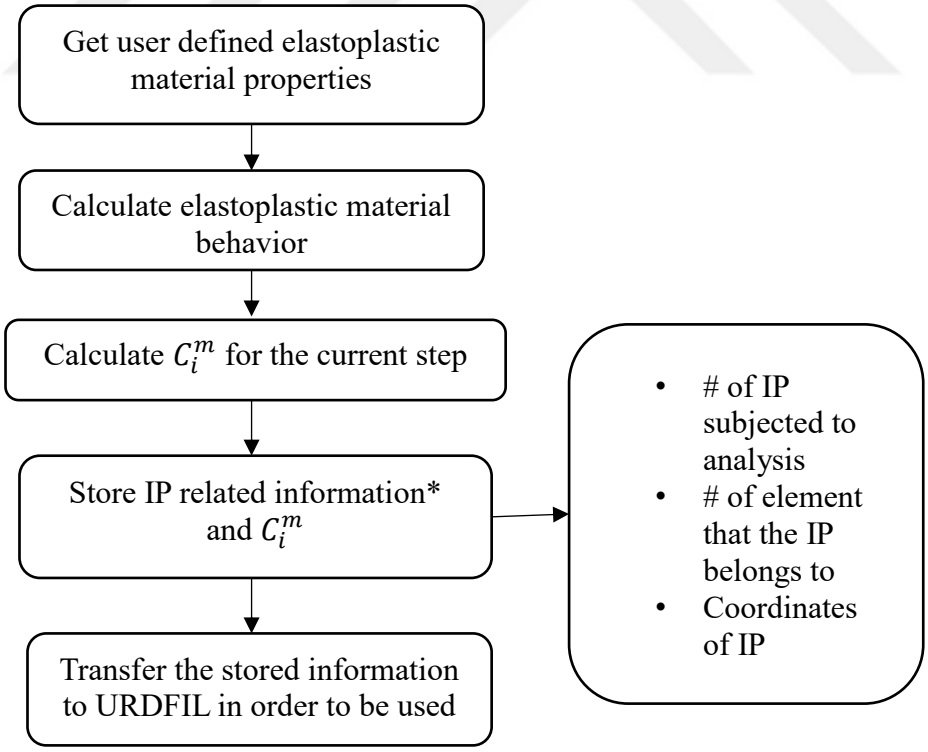

Figure 3.4. Matrix UMAT Flowchart

3.4.2. Fiber UMAT

When the calculation is performed for the IP of fiber, the code enters this section of the subroutine. The aim of this section is to modify the C_i^f according to the C_i^m, in the vicinity of the considered fiber IP, calculated in the previous step. The flowchart of this section is given in Figure 3.5. This section starts with transferring the arrays stored by URDFIL which contain the information related to the matrix IPs (C_i^m) from the previous step. C_i^f of the fiber IP is modified by the weighted average of the C_i^ms of matrix IPs to this IP in the later stage of this part. Thus first, the distance of each matrix IP in the model to the considered fiber IP is calculated by using the coordinate information array of the matrix IPs transferred from URDFIL and the coordinates of the fiber IP. In order to save computational time, the stiffness of matrix IPs farther away than a defined threshold distance value to the considered fiber IP is eliminated. In that distance, only a certain number of IPs are considered (IP_{cons}) for the calculation of an equivalent stiffness matrix of host elements on the subjected fiber IP ($C_i^{eq.m}$). A representative image of this process is given in Figure 3.6. Purple dots represent matrix IPs and the red dot represents the fiber IP. The yellow circle represents the maximum distance barrier and the yellow-purple dots are the matrix IPs that should be considered. Red arrows indicate the closest matrix IPs to the considered fiber IP.

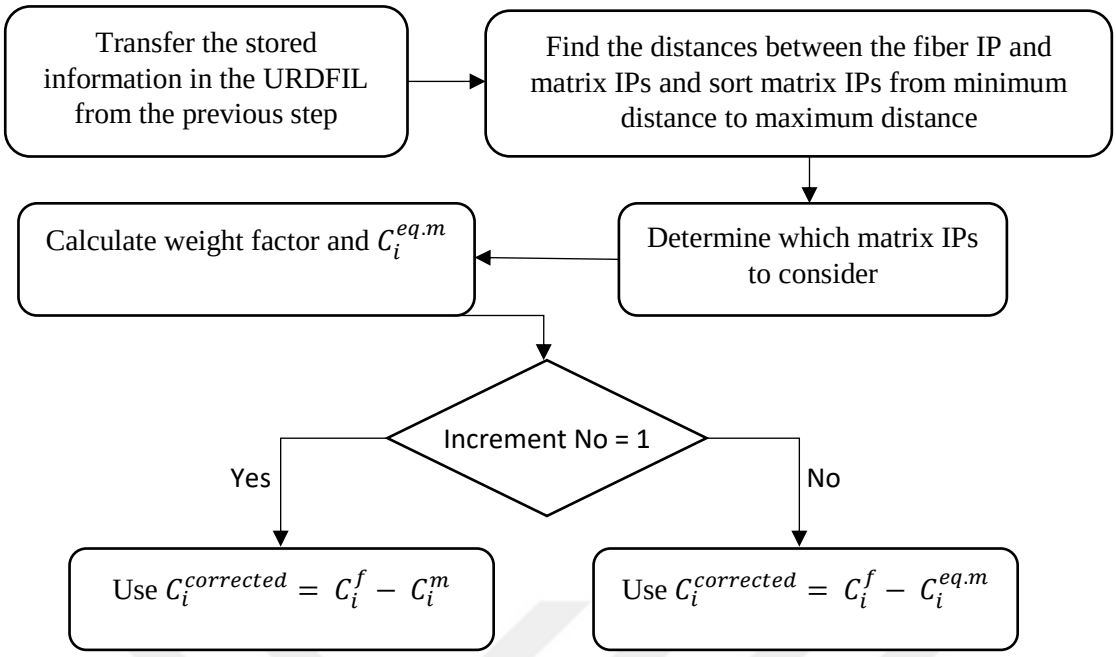

Figure 3.5. Fiber UMAT Flowchart

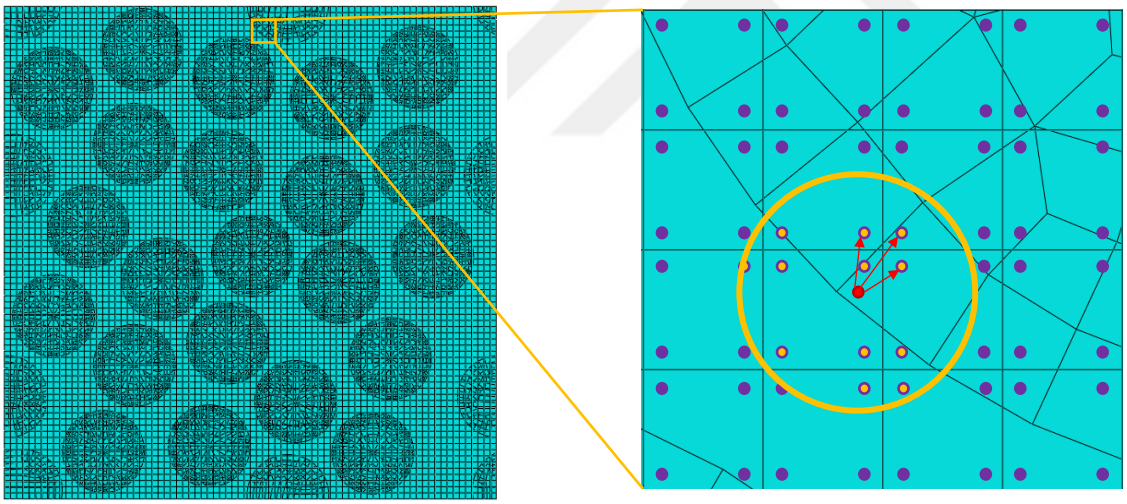

Figure 3.6. A figure that represents the working principle of IP distance measuring process. Yellow circle represents the maximum distance for IP searching distance, yellow dots represent the selected host (matrix) IPs, purple dots represent unselected host IPs and the red dot represent the subjected embedded node.

Then, new arrays are generated with the reduced size, and the rest of the matrix IPs are sorted from minimum distance to maximum distance to the current fiber IP. Then,

according to the defined IP_{cons} in the subtraction process, $C_i^{eq.m}$ is calculated. First, the weight factor of each matrix IP (w_i) is calculated via equation (2.5). Then $C_i^{eq.m}$ is calculated via equation (3.1). The stiffness matrix of the fiber IP is then calculated by equation (3.2). In the initial step, there is no information on the previous step. Thus $C_i^{eq.m} = C_i^m$ is used for the first step, where *i* denotes the considered fiber IP. Strain and stress fields, $\varepsilon(x)$, $\sigma(x)$ are calculated and stored by the software for both matrix and fiber separately. The stress field calculated by the software is not correct as the stiffness matrix of the embedded fibers is modified. The stress field of these fibers is calculated using the original fiber stiffness matrix. Correct stress fields on the embedded region are calculated according to the equation (3.3).

$$C_i^{eq.m} = \sum_i^N C_i^m w_i \tag{3.1}$$

$$C_i^{corrected} = C_i^f - C_i^{eq.m} \tag{3.2}$$

$$\sigma(x) = C_i^f \, \varepsilon(x) \tag{3.3}$$

3.4.3. URDFIL

The arrays calculated in Matrix UMAT are stored in this part to be used. This last subroutine is used to store the matrix integration point data coming from the matrix UMAT, in order to be used by fiber UMAT in the next step.

3.5. Summary

In this chapter, studies for the development of a solution to the stated problem in the thesis are explained. First, the approach of calculating the stiffnesses through nodal output, which is not employed, is discussed and its properties and shortcomings are mentioned. Then, another approach that calculates the stiffnesses through IP values, which is employed in this thesis is discussed and its principles are explained. Finally, the implementation of the latter approach through the user subroutines of UMAT and URDFIL are explained in detail.

In the following chapter, the proposed approach to the stated problem is explained in detail. In the following chapter, test models, their properties and inspected parameters are explained.

4. MODELS AND ANALYSIS

4.1. General Overview of Models

Two different models are used to test the developed approach to the embedded element method. A single fiber model (SFM) and a randomly distributed fiber model (RDFM). The SFM is used for troubleshooting and calibrating the user subroutines. SFM consists of a 20 µm ^{X} 20 µm matrix and a circular fiber with an 8 µm radius. The subroutine is applied to RDFM for a more realistic representation of a two-dimensional composite. RDFM model was previously generated with the algorithm of Melro et al. (2008). This model generates fibers randomly according to the user-defined fiber-volume ratio. It also generates these fibers by considering the periodical structure. Model geometries are given in Figure 4.1.

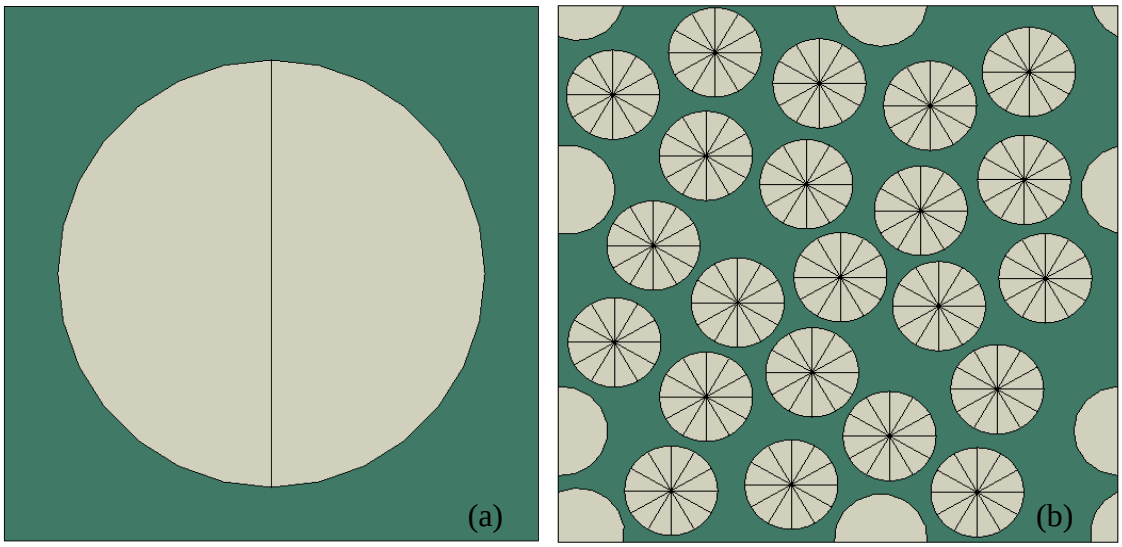

Figure 4.1. a) SFM geometry; b) RDFM geometry for vf = 0.6

In order to validate the developed method of embedded element, a reference model is needed. Thus, models with continuous meshing approach for both configurations are created. This model is called as “Classical” model. In addition to these, three models meshed with the embedded element method are created. The first one has original fiber

material properties with no stiffness correction application, called “EE Standard”. The second model is defined to replicate the method used in the study of Tabatabaei and Lomov (2015). It represents the elastic stiffness correction process, where non-linear material property cases are expected to fail under as explained in Section 2.3.4. This model is called “EE Equivalent”. The third configuration is the proposed method of this study, called “UMAT” model. Mesh structures of Classical and embedded element-based models are given in Figure 4.2. Mesh structure of a) embedded element-based models; b) continuously meshed models. Mesh configurations are adjusted to have a similar mesh size in both configurations. In all models, generalized plane strain elements (CPEG4) with full integration (4 IP/element) are used.

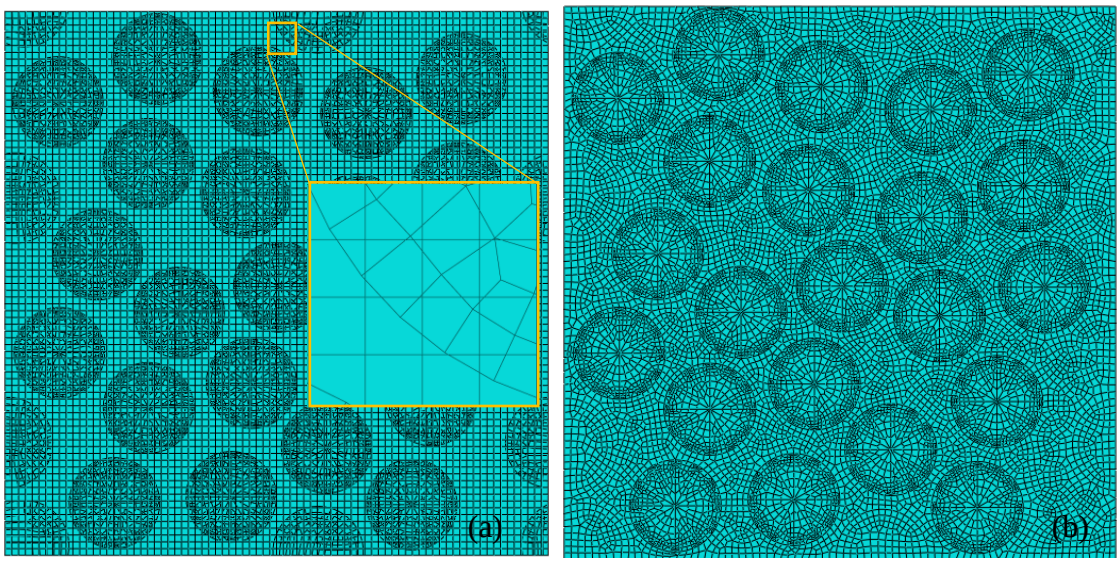

Figure 4.2. Mesh structure of a) embedded element-based models; b) continuously meshed models

The boundary conditions for both models are shown in Figure 4.3. In SFM configuration, the model is fixed in the left edge and uniaxial displacement is applied to the right side, where u_1 is equal to 0.15, 0.35 and 1.00 displacements and $u_2 = 0$. These displacements are defined to observe the fully elastic and elasto-plastic deformation in the matrix, clearly. RDFM model is a representative region of periodic unit cell. Thus, periodic boundary conditions (PBC) were applied by introducing constraint equations representing periodicity. Uniaxial displacement, $u_1 = 0.08$ and are applied in the x-direction and

displacement was applied in y-direction to simulate the poisson contraction, $u_2 = 0.024$ which was calculated by the rule of mixtures.

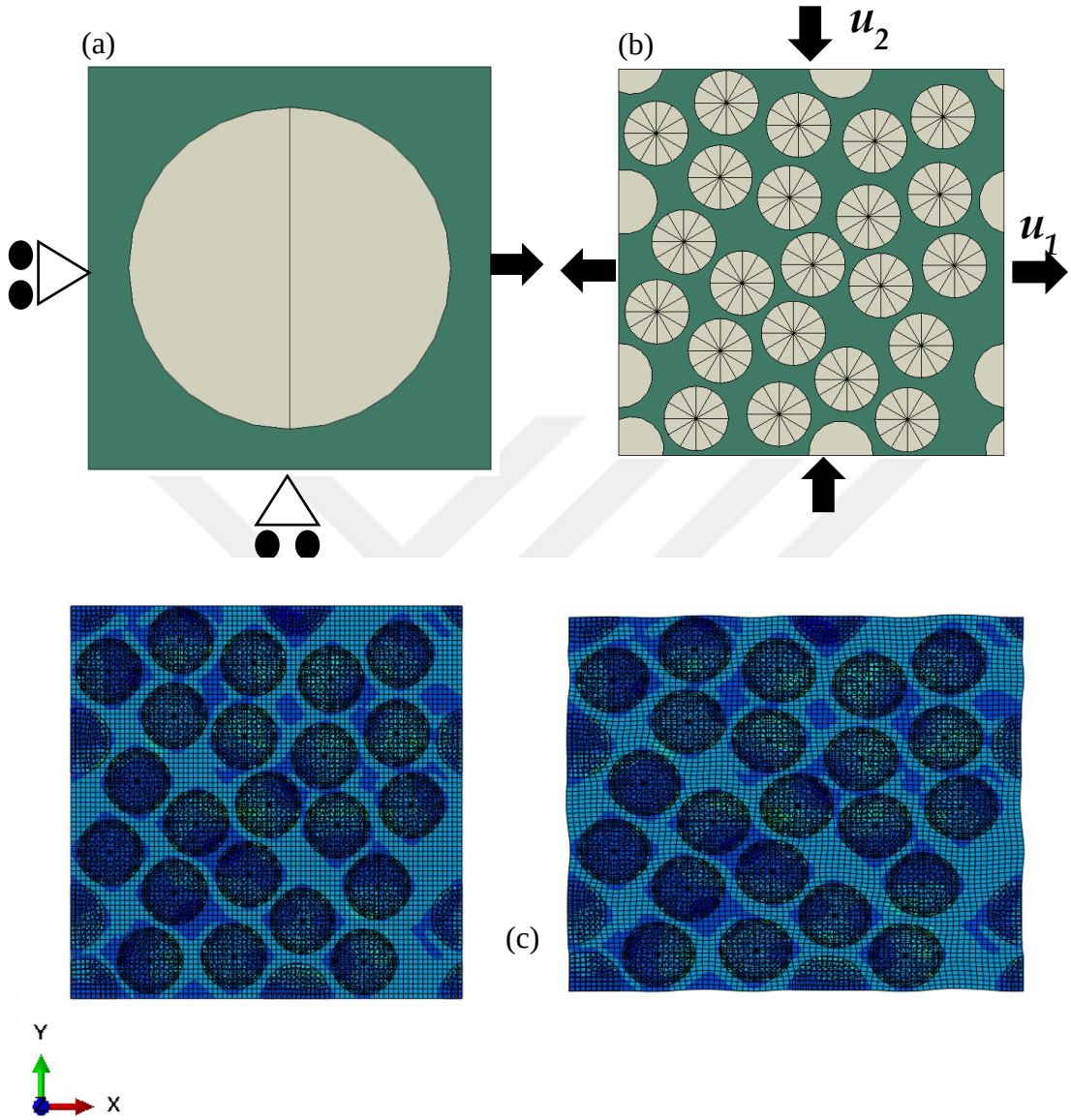

Figure 4.3. Boundary conditions of a) SFM; b) RDFM; c) an example of successful application of PBC (the opposite edges of the model move together).

As mentioned, the stiffness of the redundant region is effective in case the fiber stiffness is not very high compared to the matrix. Natural fibers are generally much softer compared to the conventional carbon and glass fibers. In the transverse direction, they are even much softer. Thus, a natural fiber, flax is used as the fiber material, whereas epoxy

is used as the matrix material, which is the most commonly used thermoset matrix type. Elastic properties of the flax are taken from (Baley et al. 2006) and (Sabuncuoglu 2014), respectively and the plastic hardening data of epoxy is taken from (Okabe et al. 2010). Properties required for the definition of Drucker-Prager model are determined from examples in the literature (Allen 2002). Elastic and Drucker-Prager properties are given in Table 4.1 and hardening data is given in Figure 4.4.

Table 4.1. Elastic and Drucker-Prager properties for materials

	Elastic Properties		**Drucker-Prager Properties**		
	Young's Modulus (MPa)	Poisson's Ratio	Friction Angle (rad)	Flow-Stress Ratio	Dilation Angle (rad)
Epoxy	3000	.3	0.0635	1	0.024
Flax Fiber	4000	.3			

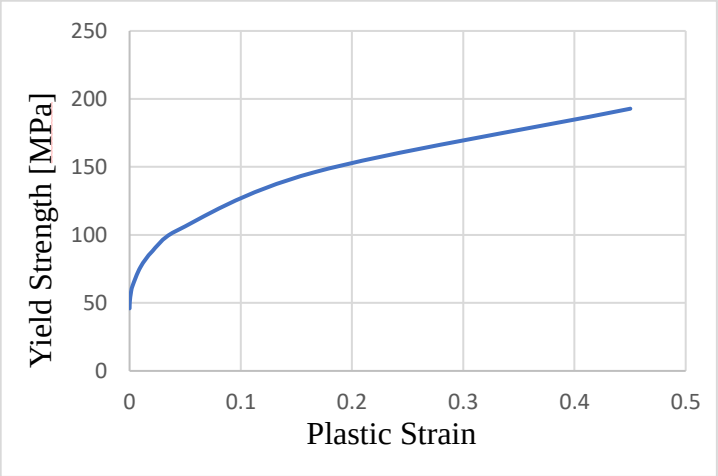

Figure 4.4. Hardening behavior data of matrix stress vs. strain (%)

4.2. Inspected Parameters

In order to ensure the accuracy of the proposed method, some parametric studies are performed. Details about these parameters are given in the following subsections.

4.2.1. Fiber Volume Fraction

In addition to the 0.6 volume fraction (vf) in the RDFM, a model with 0.4 volume fraction is used for comparison. Model geometries are given in Figure 4.5.

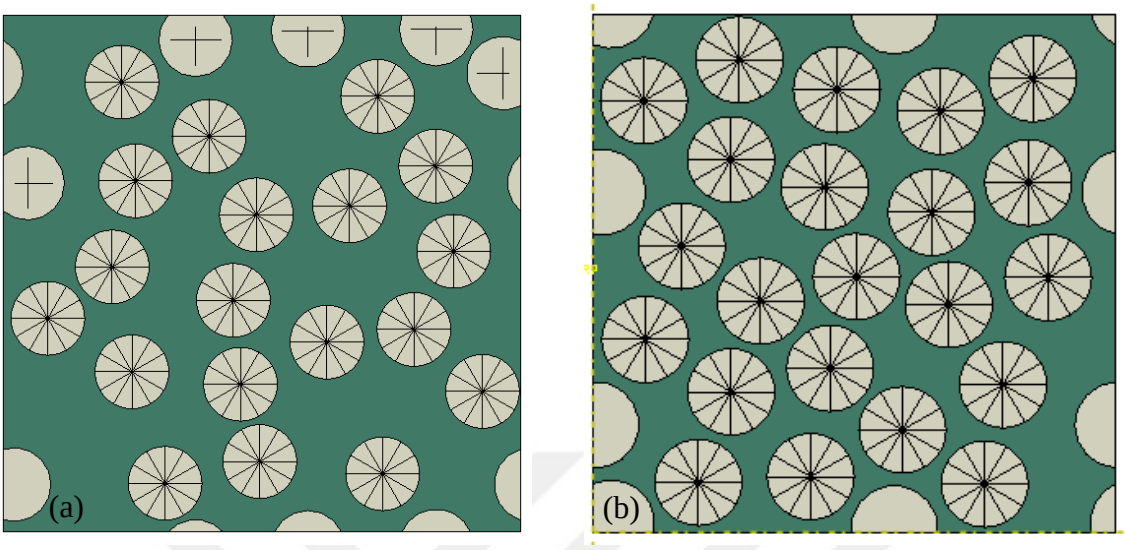

Figure 4.5. Model geometry of RDFM for a) vf=0.4; b) vf = 0.6

4.2.2. Implementation of Variations of the Proposed Method and von Mises Plasticity

As the development of proposed method (UMAT) went on, some variations are also developed and tested, in an attempt to model the elasto-plastic behavior better. The first variation is the subtraction of elastic volumetric moduli (EVM), and the second one is the subtraction of consistent tangent moduli (CTM). Details about these variations are given in Appendix C. These variations are only valid and tested under von Mises plasticity, since governing equations may differ under the case of Drucker-Prager plasticity.

4.2.3. Comparison of Plane Strain and Generalized Plane Strain

When composite micro-structure is represented with planar elements, the correct element formulation to be used is the generalized plane strain (GPS) elements, which assumes that the model dimension is very high in z-direction compared to the other two dimensions. This is actually the case as the fibers are long along the z-direction. In the plane strain (PS) condition, the model is long in z-direction but is fixed from the end. Our proposed model is tested for both element types and results are compared. The element types used

for GPS and PS are CPEG4 and CPE4 in ABAQUS, so these abbreviations are used to represent these models.

4.2.4. Mesh Study

In order to improve the reliability of the model, the subroutine is validated by applying various mesh sizes in the model. To achieve this, 5 different mesh densities are tested with our model, where 3 coarser and 1 denser mesh structures relative to the used mesh in the comparison. Representative figures for coarse and dense meshes are given in Figure 4.6. Corresponding element and node numbers and element sizes for each setup are given in Table 4.2.

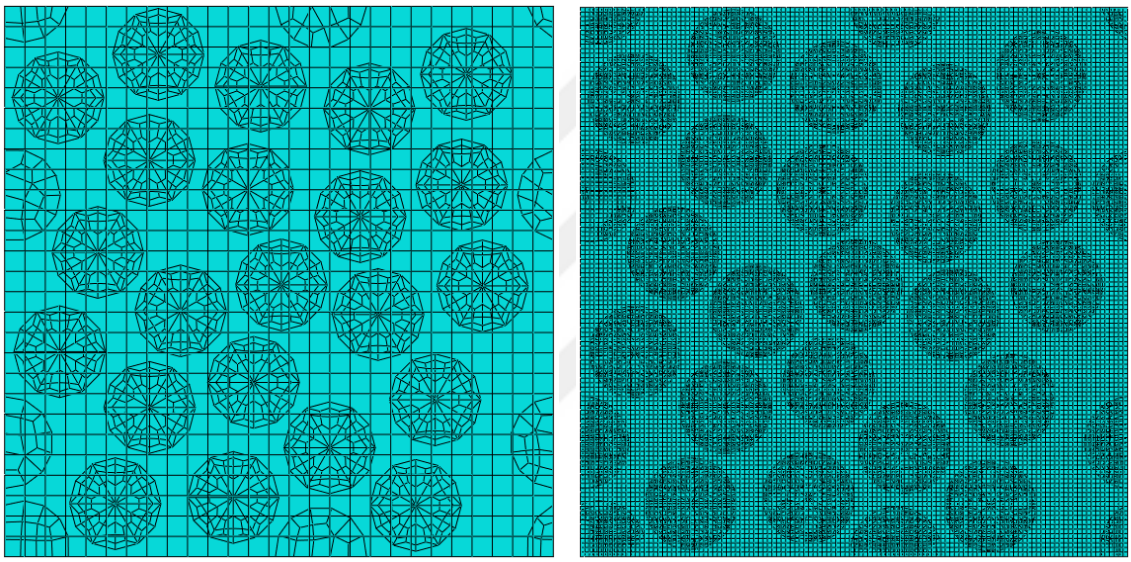

(a) (b)

Figure 4.6. Mesh structures of a) Coarse-1 and b) Dense-1 setups

Table 4.2. Element numbers, node numbers, element sizes for each mesh structure

	Total Element No.	Total Node No	Element Size
COARSE-1	2081	2135	5.625
COARSE-2	4256	4712	3.75
COARSE-3	9351	10015	2.5
DEFAULT	15581	16455	1.875
DENSE-1	31303	32991	1.25

4.2.5. Effect of IP_{cons} Value on Processing Time and Results

As mentioned before, IP_{cons} value represents the maximum number of host IPs that are considered for the calculation $C_i^{eq.m}$ value. This parameter is applied to limit the number of IPs taken into consideration, thus saving processing time. Higher numbers are expected to cause more processing time, hence IP_{cons} of 4, 16 and 64 are compared. In addition to that, IP_{cons} values of 1,2,4,8,16 and 32 are compared to investigate if this value has any significant effect on the analysis results.

4.2.6. Performance of the Proposed Method Under Shear Loading

In order to improve the reliability of the proposed method, it is tested against a different loading type, shear loading. For a more extensive testing, shear load is applied in two different configurations, with PBC and without PBC. Representative figures of applied boundary conditions are given in Figure 4.7. A comparison of deformed and undeformed versions of each model is given in Figure 4.8. Model geometries and applied load are the same in both cases to ensure obtaining more comparable results. For the models, RDFM with vf=0.6 is used and a strain of $u_1 = 0.08$ and $u_2 = 0$ are applied to create a shear force. Since it is a shear load, a comparison of models is examined upon the S12 results of the analyses.

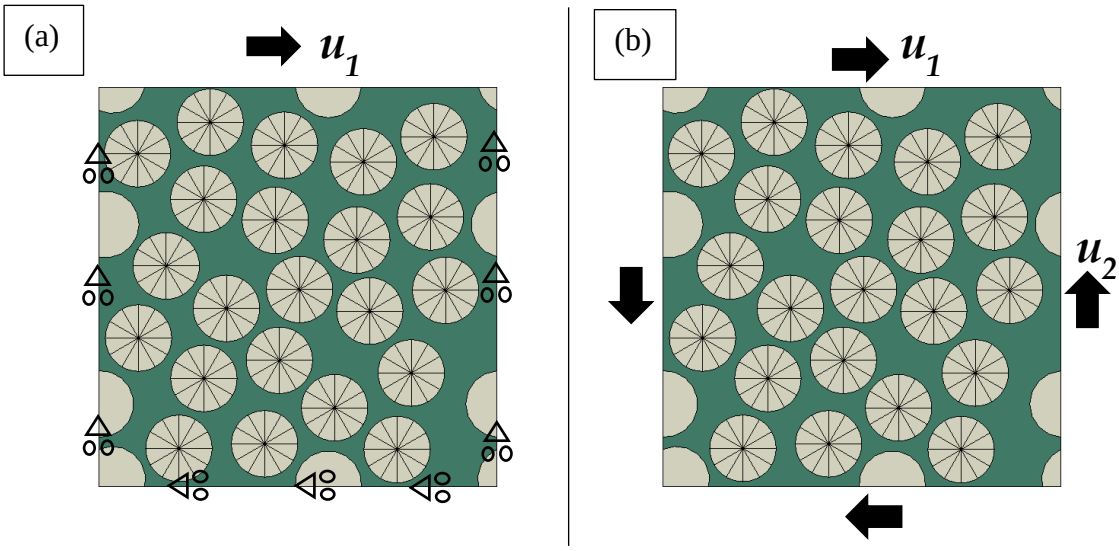

Figure 4.7. Boundary conditions of shear loading for a) model without PBC; b) model with PBC.

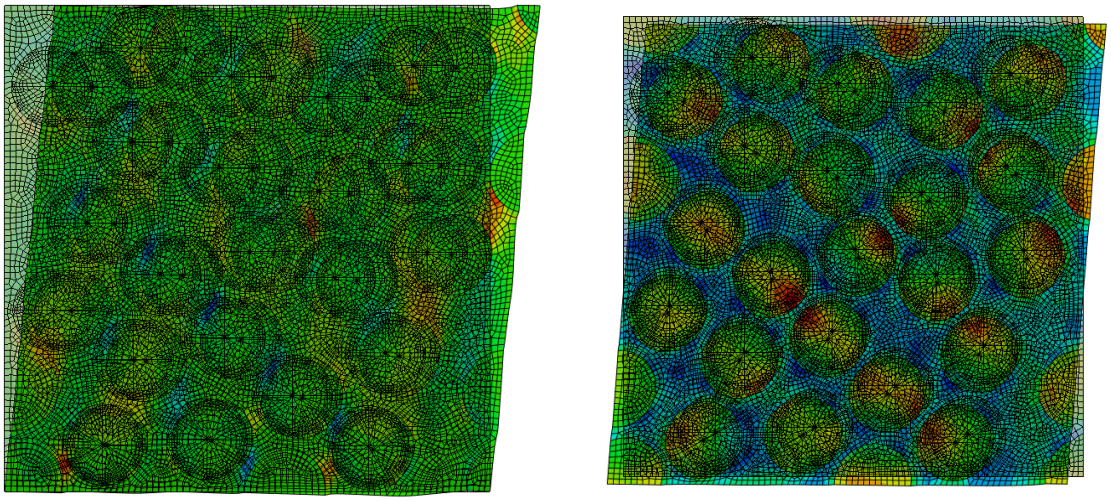

(a) (b)

Figure 4.8. Superimposed images of deformed and undeformed versions of a) model without PBC; b) model with PBC.

4.3. Summary

In this chapter, models that are used to test the proposed method are defined extensively. First, the single-fiber model is explained, which is used for preliminary validation of an example study (Tabatabaei and Lomov 2015). After that, the multi-fiber model (RDFM) that is used for the employment of the proposed method in a more realistic case, is defined. The material behavior of matrix and fibers are given for each test case. Finally, parameters that are subject to the testing of the proposed method are explained. Geometries of different fiber volume fractions, properties of different plasticity models, IP_{cons} value and its meaning, different loading types, properties about different mesh structures and implementation of other variations of the proposed solution are given.

In the following chapter, the results of the proposed model under each stated case are given and discussed upon.

5. RESULTS

5.1. Validation of the Stated Problems on Single Fiber Model (SFM)

In order to safely develop a model for the stated problem, previous cases from the literature are used as a reference point. In the study of Tabatabaei and Lomov (2015), a stiffness correction was performed for a glass-fiber/epoxy composite, where the stiffness of glass-fiber is higher than matrix. For this study, the fiber type is changed to flax to be able to compare with the present model. It is expected that the method used in (Tabatabaei and Lomov 2015) will reveal similar results under elastic loads, but will start to fail under plastic loads.

In order to compare the results, stresses on the loading direction (11-direction) are obtained along the fiber length. A representative figure that shows this fiber length is given in Figure 5.1. Three loads of different magnitudes to represent elastic and plastic loadings are applied. Corresponding results are given in Figure 5.2. In that figure and the following result plots in this chapter, “Classical” represent the continuously meshed model, “EE Standard” represents the embedded element method without any changes, “EE Equivalent” represents the method of (Tabatabaei and Lomov 2015), “UMAT” represents the proposed method in this study and “EVM” represents the variation of “UMAT”, which is explained in Appendix C.

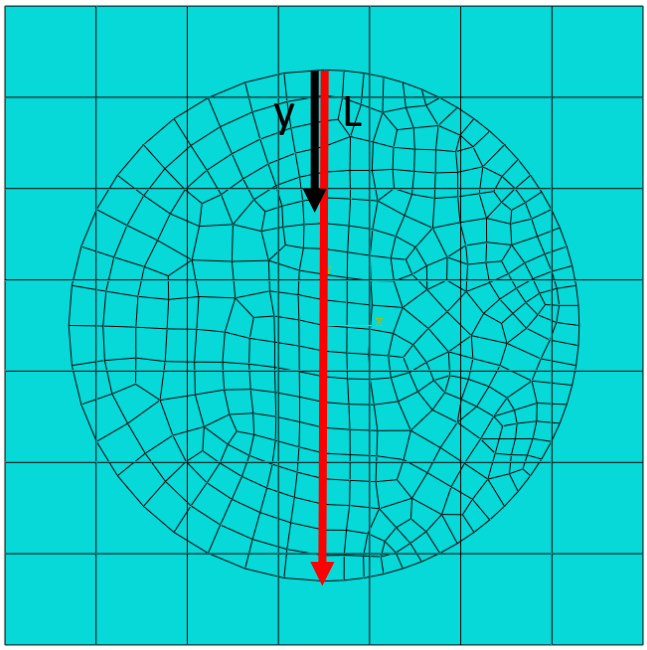

Figure 5.1. SFM fiber length. L represents the total fiber length. y/L represents the position on the fiber.

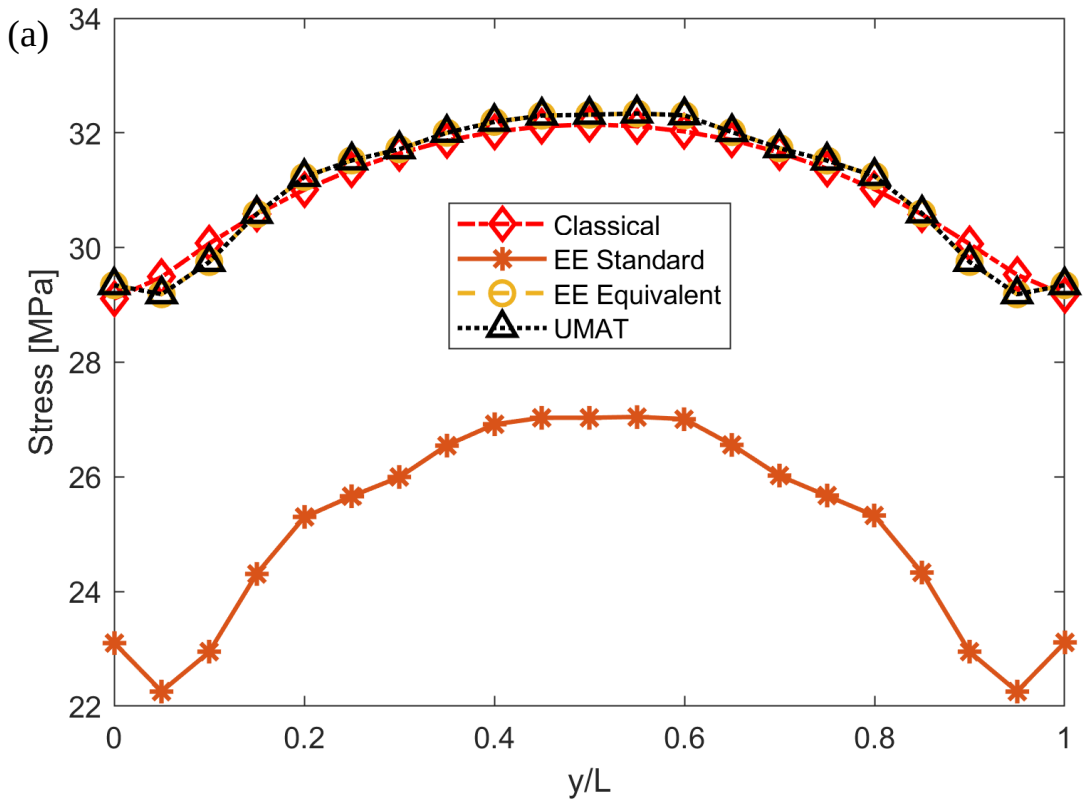

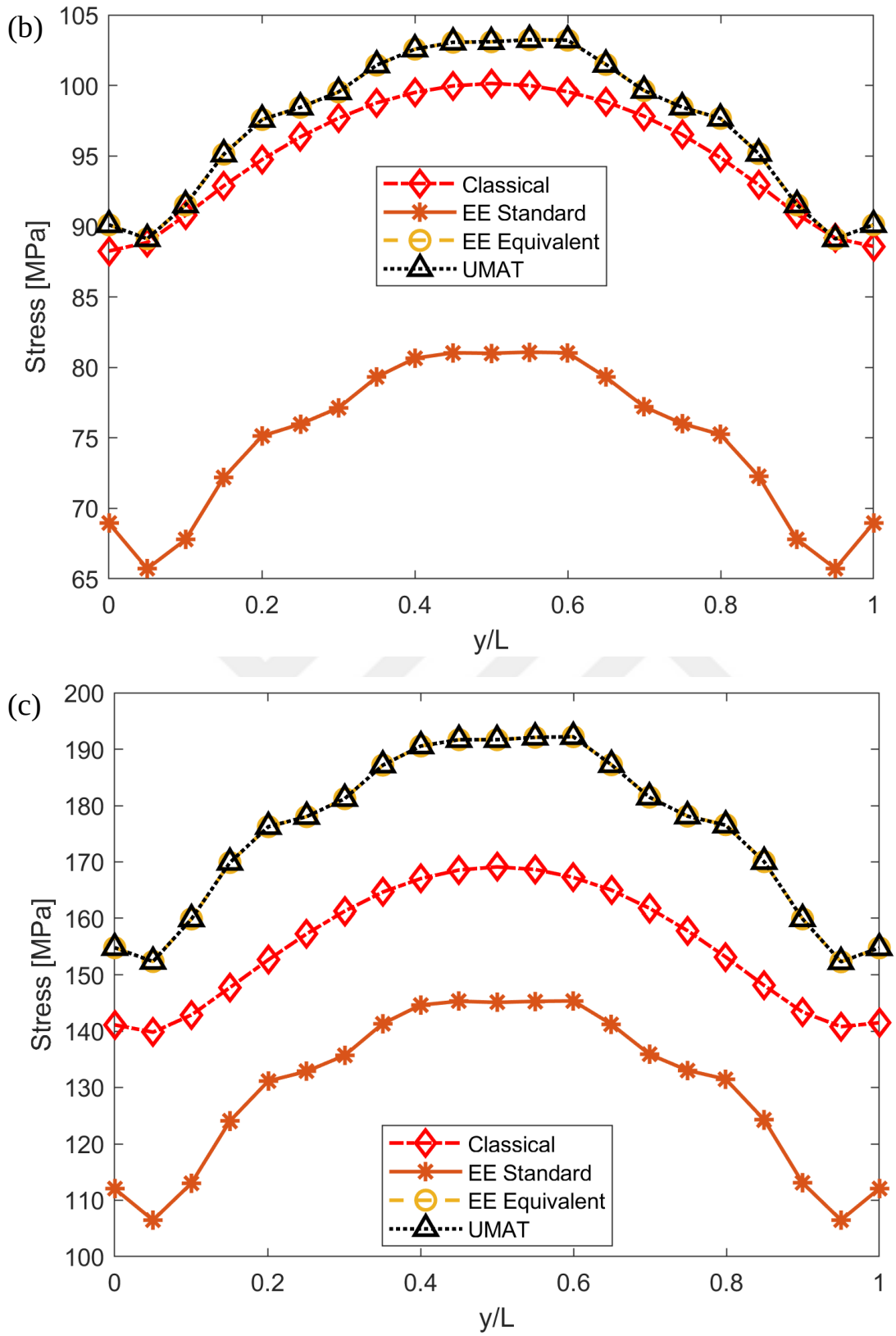

Figure 5.2. Stresses in the loading direction (σ11) vs normalized fiber length in SFM for the applied displacement of a) 0.15; b) 0.50; c) 1.00.

It is clearly seen that previously proposed study of Tabatabaei and Lomov (2015) only work under elastic loading (Figure 5.2a), where Classical model and EE Equivalent models are almost identical to each other. In these analyses UMAT model replicates the EE Equivalent in a subroutine, which is helpful for understanding the working principles of a user subroutine. As the load increases and causes more and more plastic deformation, Classical model and EE Equivalent models diverge from each other, which indicates the failing of this subjected approach. Convergence of EE Standard and Classical models does not mean that EE Standard is providing realistic results under highly plastic loads, since they continue to diverge from each other as loading continues to increase after a certain level of displacement (about 5.00 displacement).

5.2. Results of the Proposed Solution Method on Randomly Distributed Fibers Model (RDFM)

In these models, measurements are taken from 3 different arbitrarily picked fibers. These fibers are shown in Figure 5.3. Detailed results are given in Figure 5.4, Figure 5.5 and Figure 5.6. In these figures, the results are presented for the applied transverse strain of 0.08.

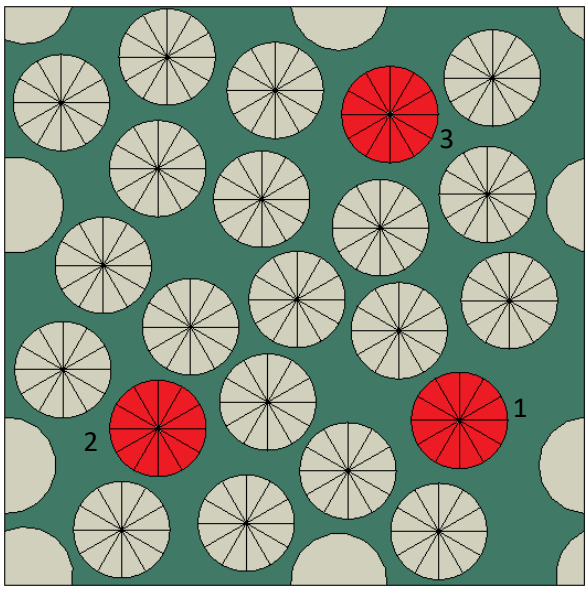

Figure 5.3. Selected fibers are shown with red on the model. Fiber numbers are given near fibers.

(a)

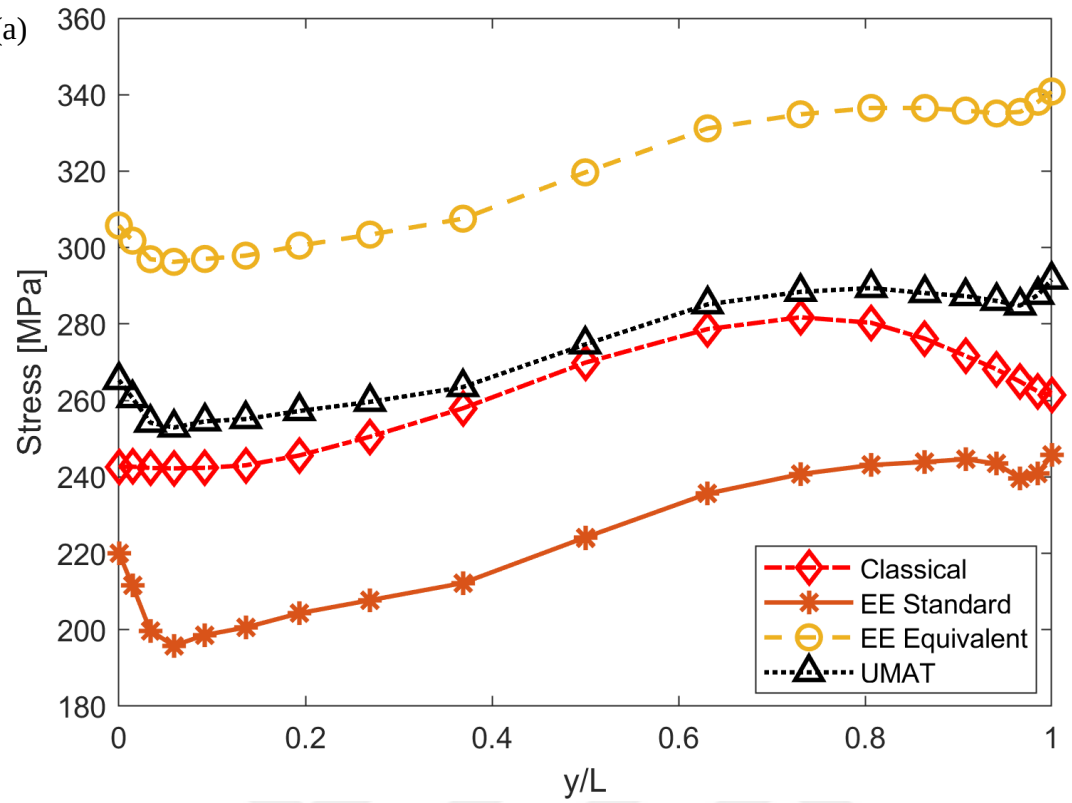
360
340
320
300
280
260
240
220
200
180
Stress [MPa]
0
0.2
0.4
0.6
0.8
1
y/L
Classical
EE Standard
EE Equivalent
UMAT

(b)

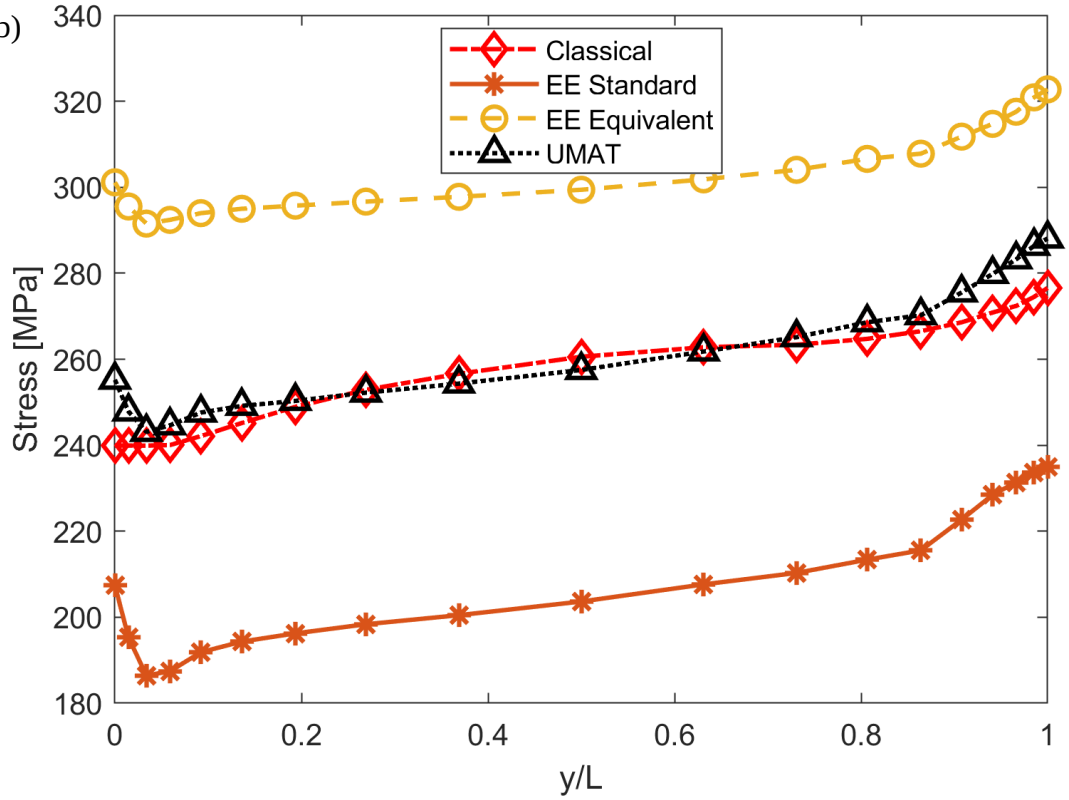
340
320
300
280
260
240
220
200
180
Stress [MPa]
0
0.2
0.4
0.6
0.8
1
y/L
Classical
EE Standard
EE Equivalent
UMAT

(c)

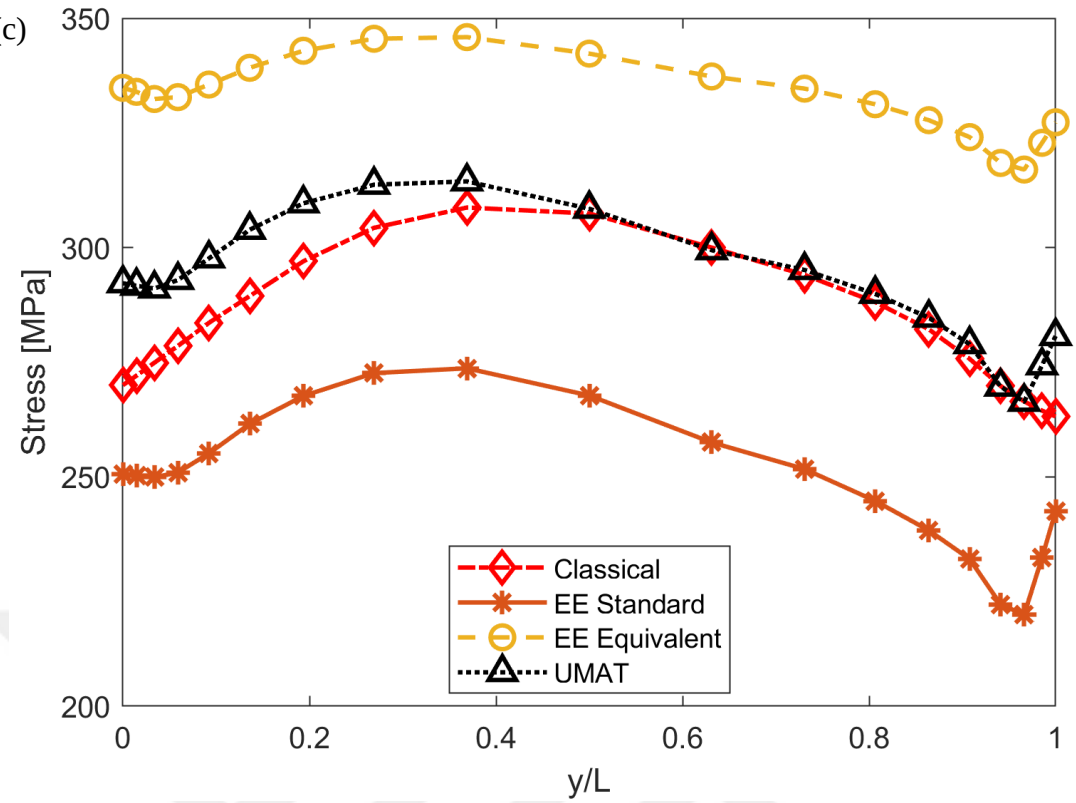
350
300
250
200
Stress [MPa]
0
0.2
0.4
0.6
0.8
1
y/L
Classical
EE Standard
EE Equivalent
UMAT

(d)

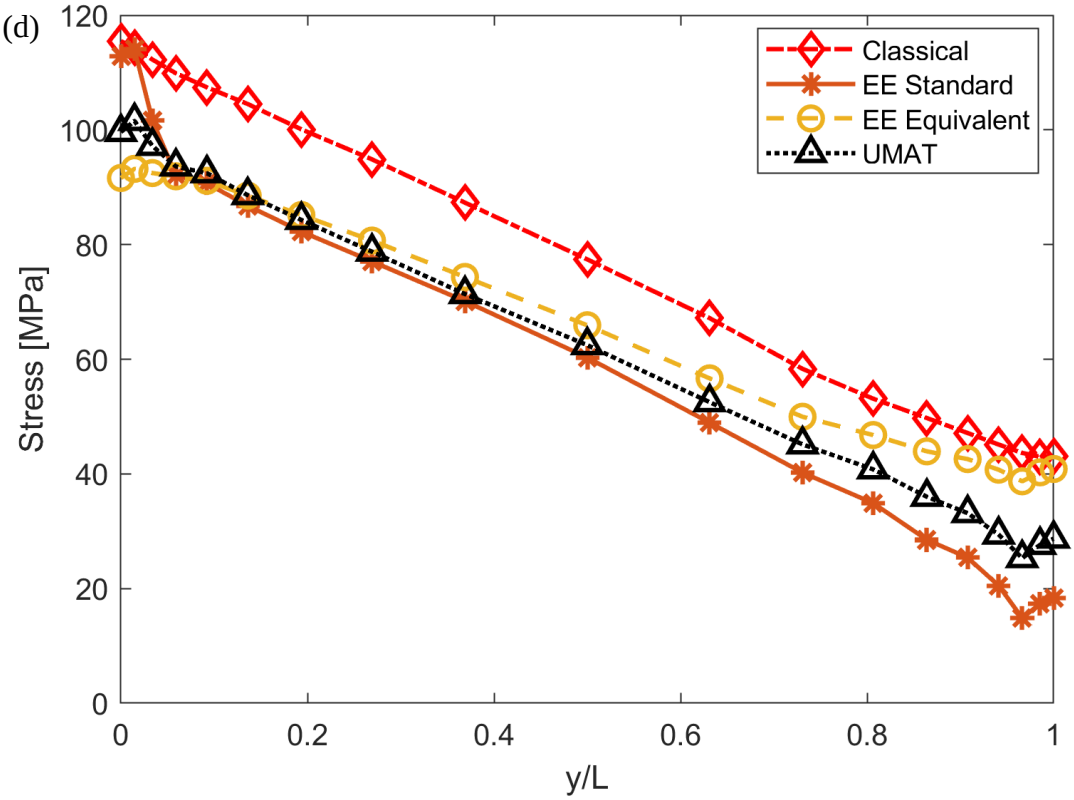
120
100
80
60
40
20
0
Stress [MPa]
0
0.2
0.4
0.6
0.8
1
y/L
Classical
EE Standard
EE Equivalent
UMAT

(e)

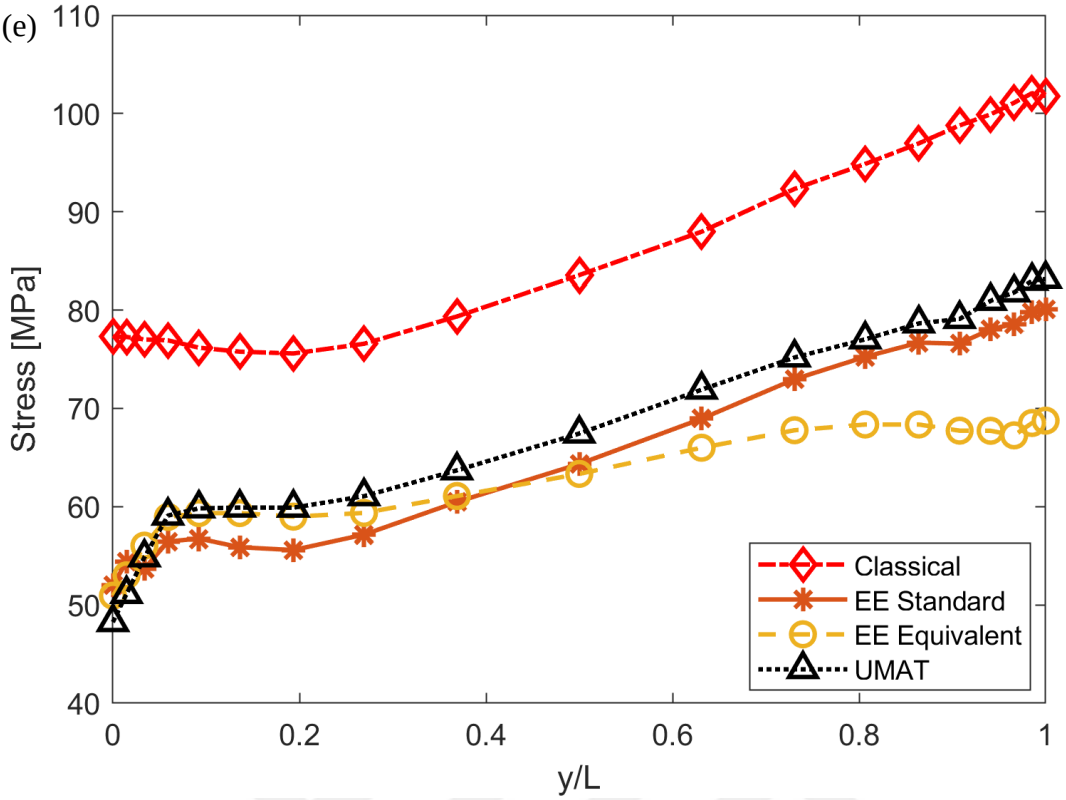
110
100
90
80
70
60
50
40
Stress [MPa]
0
0.2
0.4
0.6
0.8
1
y/L
Classical
EE Standard
EE Equivalent
UMAT

(f)

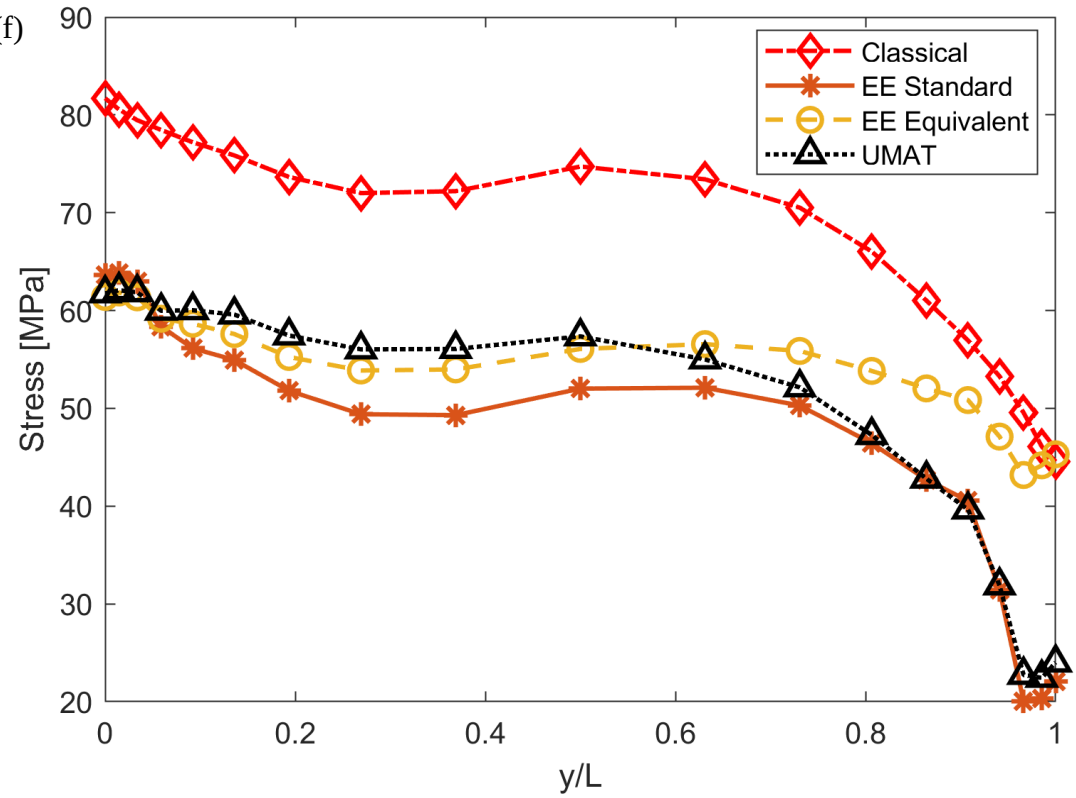
90
80
70
60
50
40
30
20
Stress [MPa]
0
0.2
0.4
0.6
0.8
1
y/L
Classical
EE Standard
EE Equivalent
UMAT

(g)

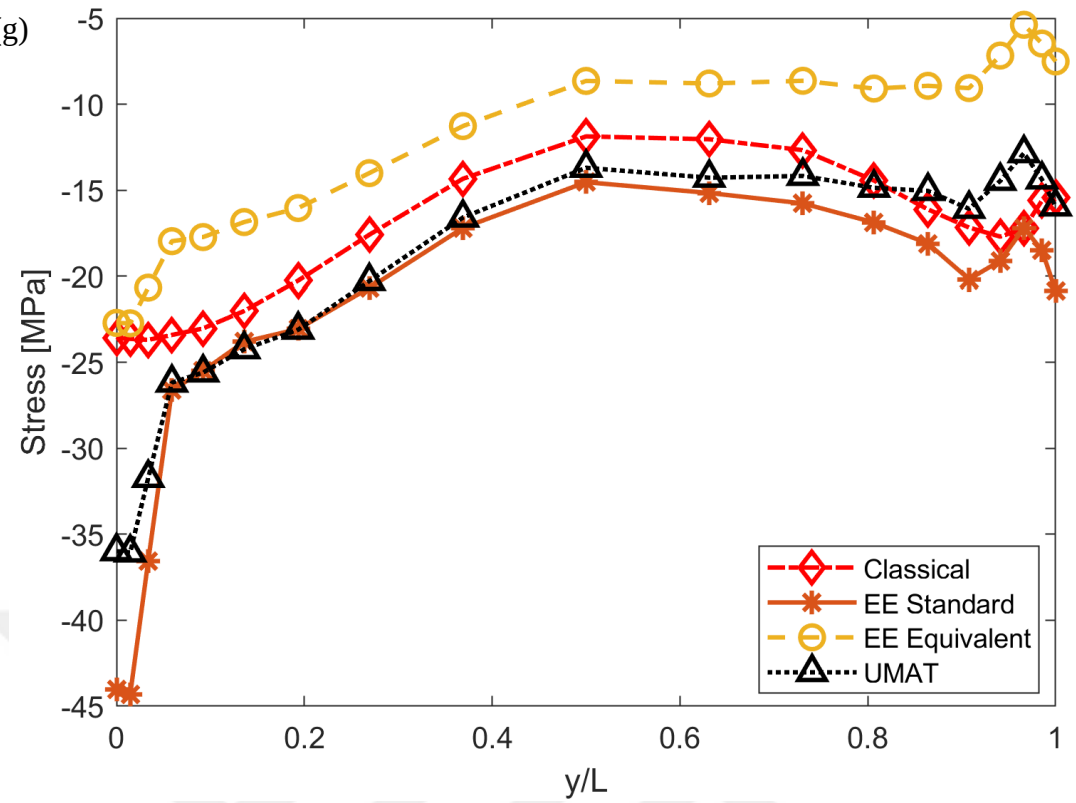
-5
-10
-15
-20
-25
-30
-35
-40
-45
Stress [MPa]
0
0.2
0.4
0.6
0.8
1
y/L
Classical
EE Standard
EE Equivalent
UMAT

(h)

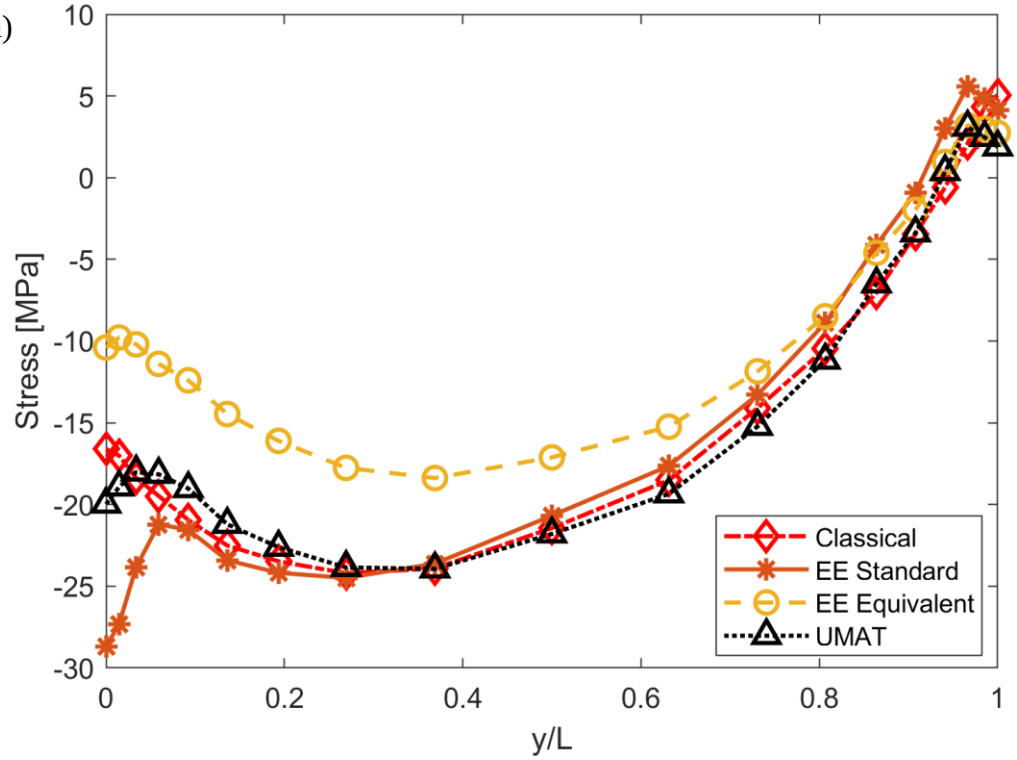
10
5
0
-5
-10
-15
-20
-25
-30
Stress [MPa]
0
0.2
0.4
0.6
0.8
1
y/L
Classical
EE Standard
EE Equivalent
UMAT

(i)

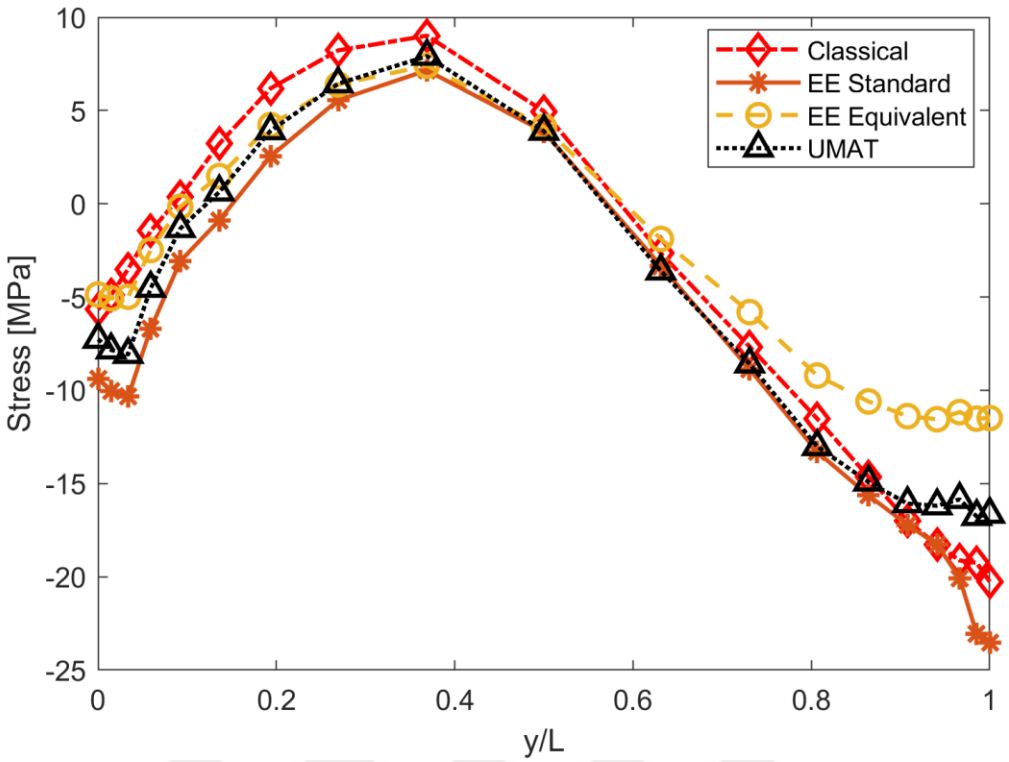

Figure 5.4. RDFM Results. a-b-c) represent S11 values, d-e-f) represent S22 values and g-h-i) represent S12 values. a-d-f) for Fiber 1, b-f-h) for Fiber 2 and c-f-i) shows results for Fiber 3, respectively.

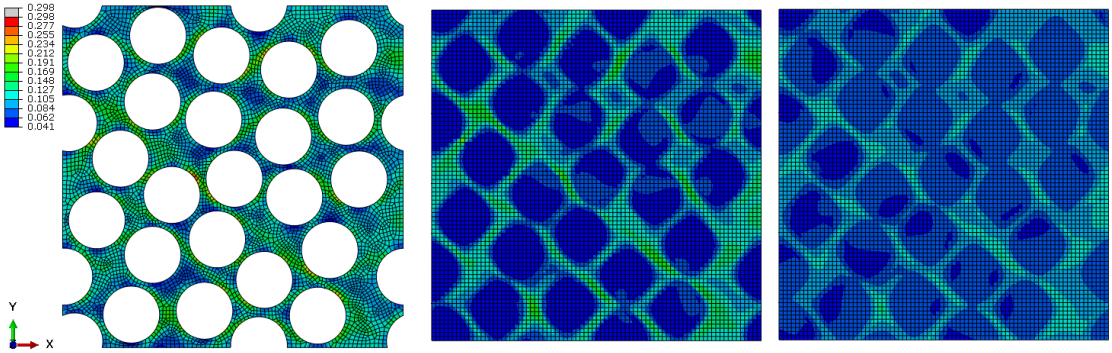

(a) (b) (c)

Figure 5.5. Strain distributions on 11-direction on matrices of a) Classical; b) UMAT; c) EE Equivalent models

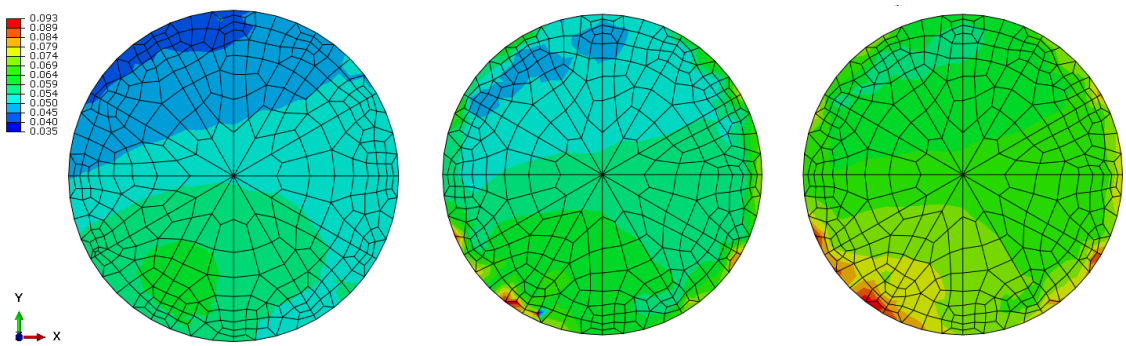

(a) (b) (c)

Figure 5.6. Distribution of strains in the X-direction on fiber 1 of a) Classical; b) UMAT; c) EE Equivalent models

The results that are given in Figure 5.4a, b and c clearly show that the proposed method of stiffness correction provides significantly closer results to the Classical model than EE Equivalent for the stresses in the loading direction. Figure 5.4d, e and f show that Classical model yields higher values for the S22 component, hence proving that none of these models perform as desired for the S22 component. Figure 5.4g, h and i also show that proposed approach yields closer results to the Classical model for the S12 component.

According to the strain distribution in the matrix given in Figure 5.5, it is apparent that the colors between the fibers are similar in Classical and UMAT models whereas they are quite different for the EE Equivalent model. Similarly, the distribution of strains in the fibers given in Figure 5.6 also indicate that UMAT and Classical model results are similar and the EE Equivalent model is quite different. There is still a slight difference between UMAT and Classical models for the fibers close to the fiber edge. At the edges, the Classical model has direct nodal connectivity with the matrix elements. Thus, the calculated strains at the matrix nodes are interpolated to the nodes of the fiber element. As this is not the case for the embedded element models, this difference is expected.

It can be concluded that proposed model of this study, UMAT, provides a significant development over EE Equivalent even under highly plastic loads. Under this material behavior and boundary conditions, proposed approach can be used to obtain reliable results. In transverse and shear directions, the results are different. In these directions

none of the other formulations are accurate as well. The stress values in the directions other than the load application direction are low. Hence, a small difference in the results for such low stresses seem to be very high when scaled to the figures. When in a certain direction where the stresses are low, parameters such as mesh structure, element connectivity etc. can be more effective. As UMAT model shows good results in the load application direction, that is enough to be considered a reliable model.

5.3. Results of Parametric Studies

5.3.1. Mesh Study

The results for various mesh sizes indicated in Chapter 4 are shown in Figure 5.7 for fiber 1. In the Figure 5.7a and Figure 5.7b, it is clear that UMAT and Classical models are diverged from each other, because of the inadequate mesh sizes. In Figure 5.7c, the results seem to get closer to the results obtained with the default mesh, but still a deviation, which also shows that this mesh structure is also inadequate, exists. However, in Figure 5.7e, it is clear that the obtained results are the same as with the default mesh model. Hence, using more elements than it is used in default mesh is unnecessary. Apparently, the results do not deviate too much, apart from small changes, according to the mesh size. This proves our default mesh structure is appropriate.

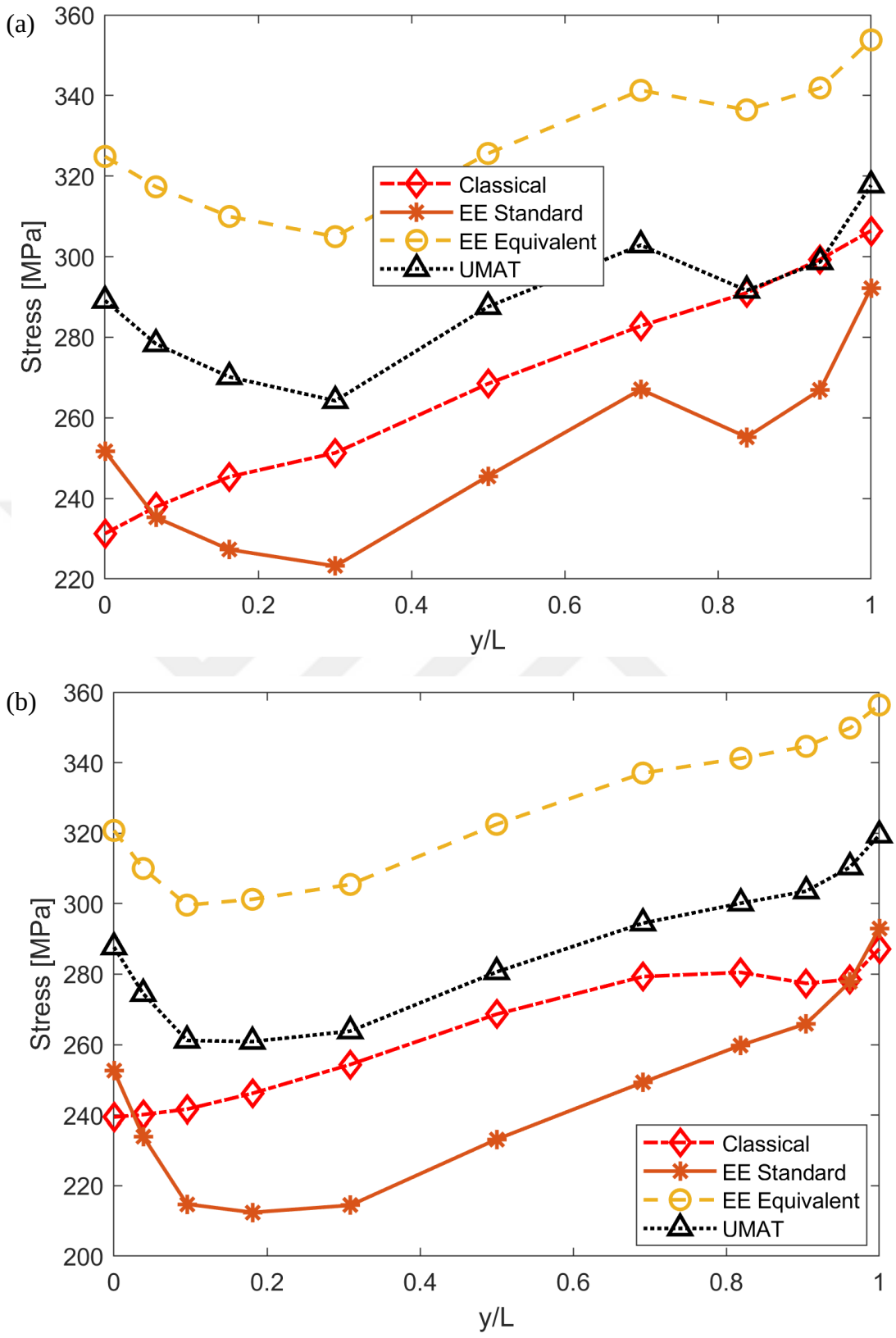
(a)
360
340
320
300
280
260
240
220
Stress [MPa]
0
0.2
0.4
0.6
0.8
1
y/L
Classical
EE Standard
EE Equivalent
UMAT
(b)
360
340
320
300
280
260
240
220
200
Stress [MPa]
0
0.2
0.4
0.6
0.8
1
y/L
Classical
EE Standard
EE Equivalent
UMAT

(c)

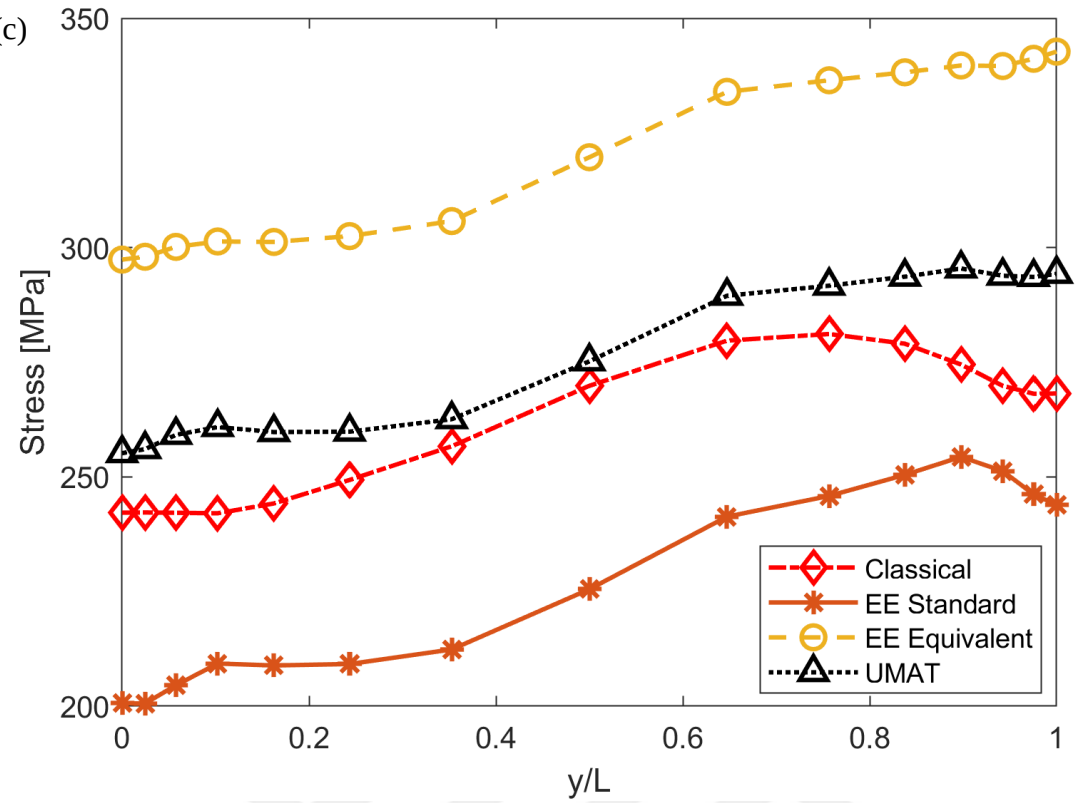
350
300
250
200
Stress [MPa]
0
0.2
0.4
0.6
0.8
1
y/L
Classical
EE Standard
EE Equivalent
UMAT

(d)

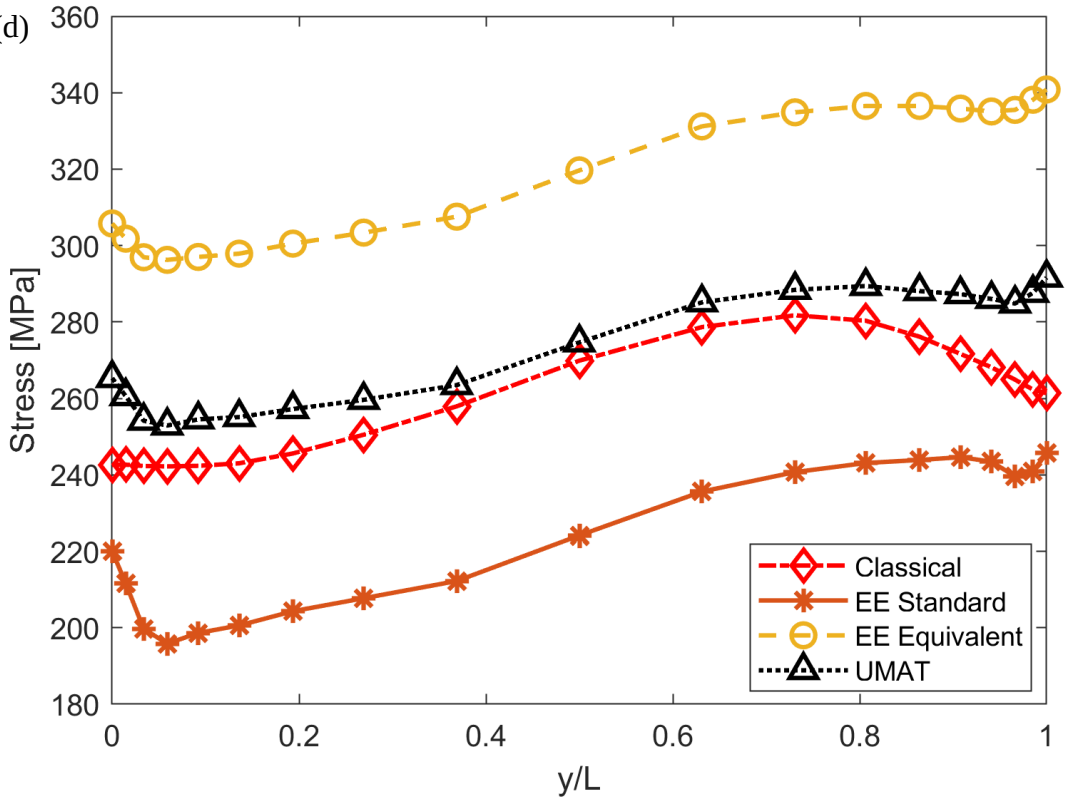
360
340
320
300
280
260
240
220
200
180
Stress [MPa]
0
0.2
0.4
0.6
0.8
1
y/L
Classical
EE Standard
EE Equivalent
UMAT

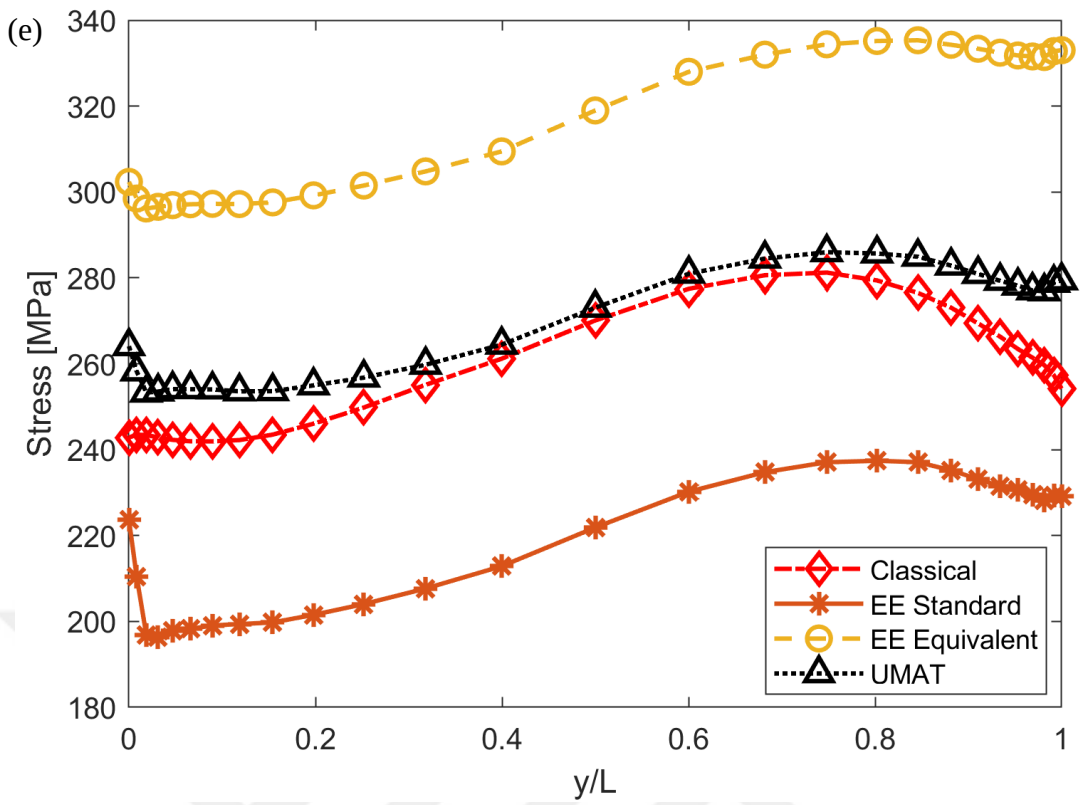

Figure 5.7. Variation of S11 along Fiber 1 centerline: a) Coarse Mesh 1; b) Coarse Mesh 2; c) Coarse Mesh 3; d) Default Mesh; e) Dense Mesh

5.3.2. Effect of Element Type

Generalized plane strain (CPEG4) is the default element type for the mesh structure. In an attempt to provide an extensive study on parameters, standard plane strain (CPE4) elements are used for the mesh structure and results are compared with the default results on Fiber 1, for three stress components. Result plots are given in Figure 5.8. Apart from that comparison, same analyses are performed with quadratic elements (CPEG8), to demonstrate the effect of quadratic elements on the results. Result plots are only given for S11 results on Fiber 1, since there is no difference in elemental equations. It is expected that the increase in the number of total nodes should improve the accuracy of the results.

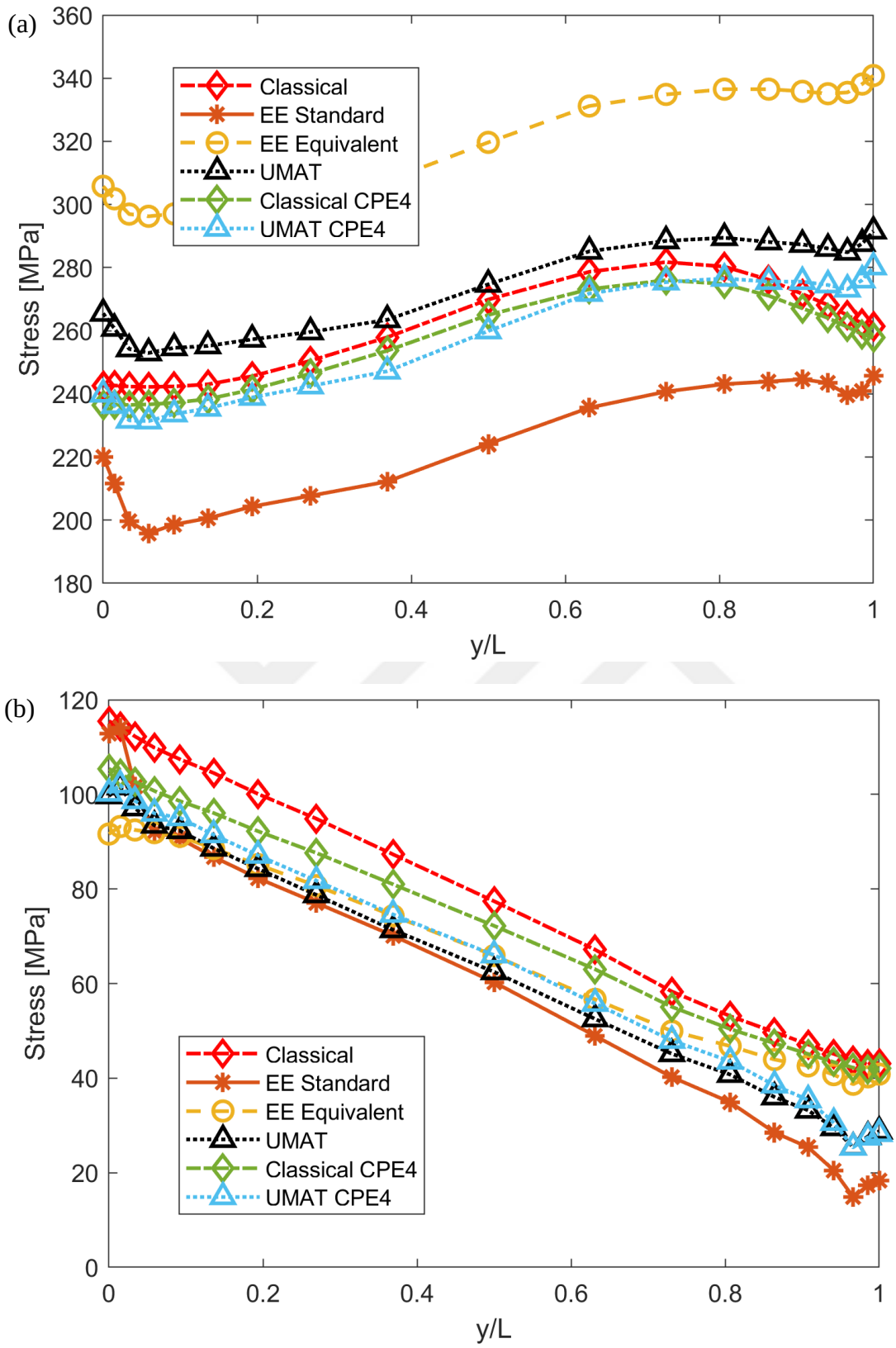
(a)
Stress [MPa]
y/L
Classical
EE Standard
EE Equivalent
UMAT
Classical CPE4
UMAT CPE4
(b)
Stress [MPa]
y/L
Classical
EE Standard
EE Equivalent
UMAT
Classical CPE4
UMAT CPE4

(c)

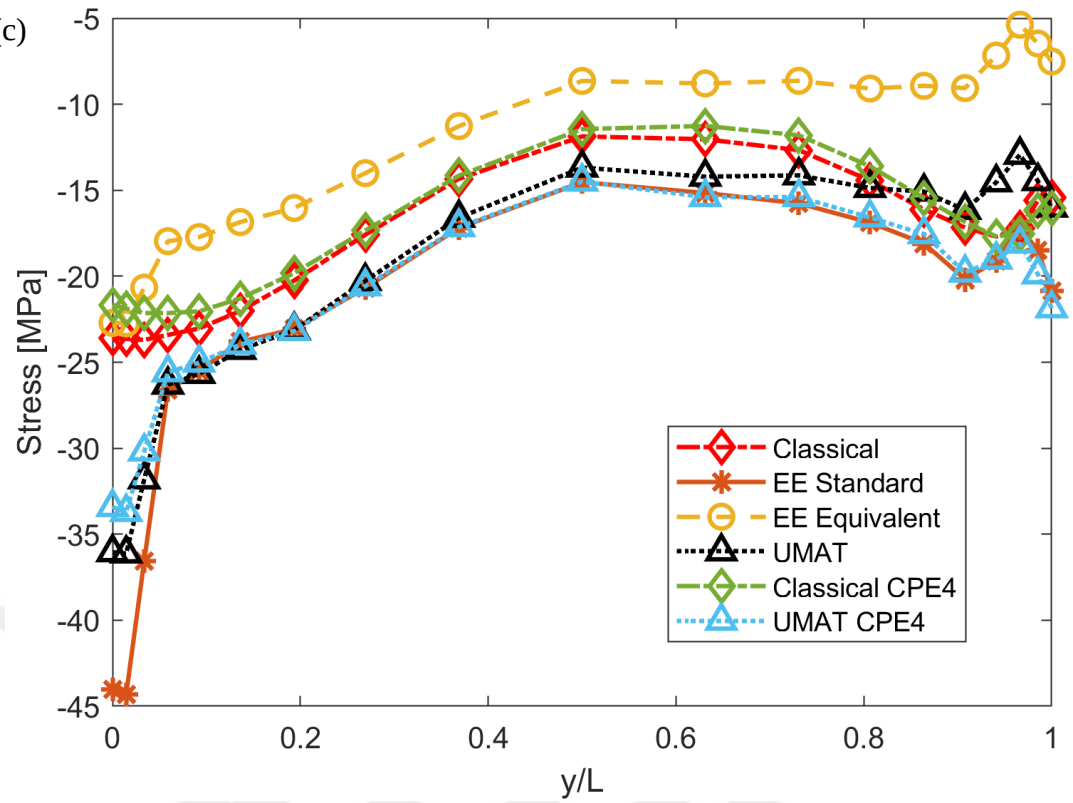

Figure 5.8. Comparison of models with CPE4 and CPEG4 element types. a) S11; b) S22 and c) S12 stress component results.

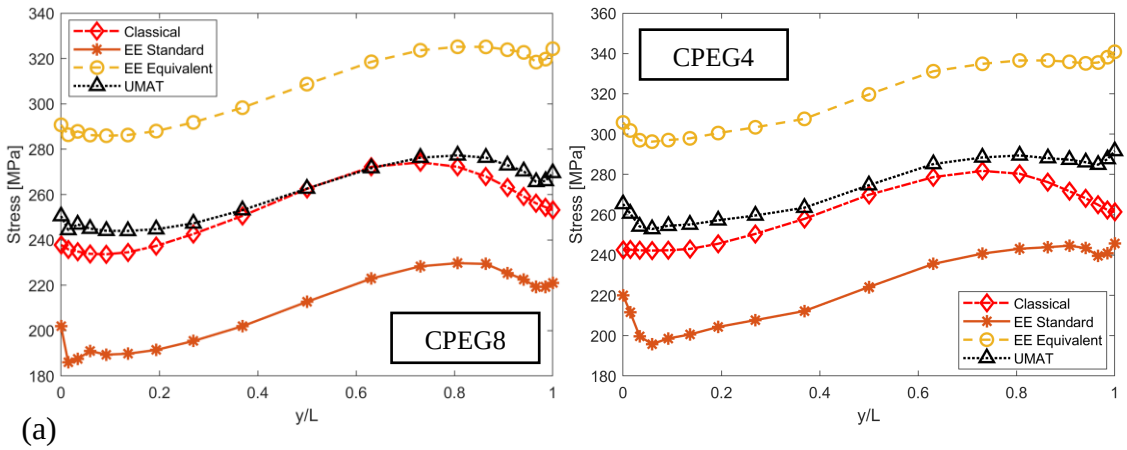

(a)

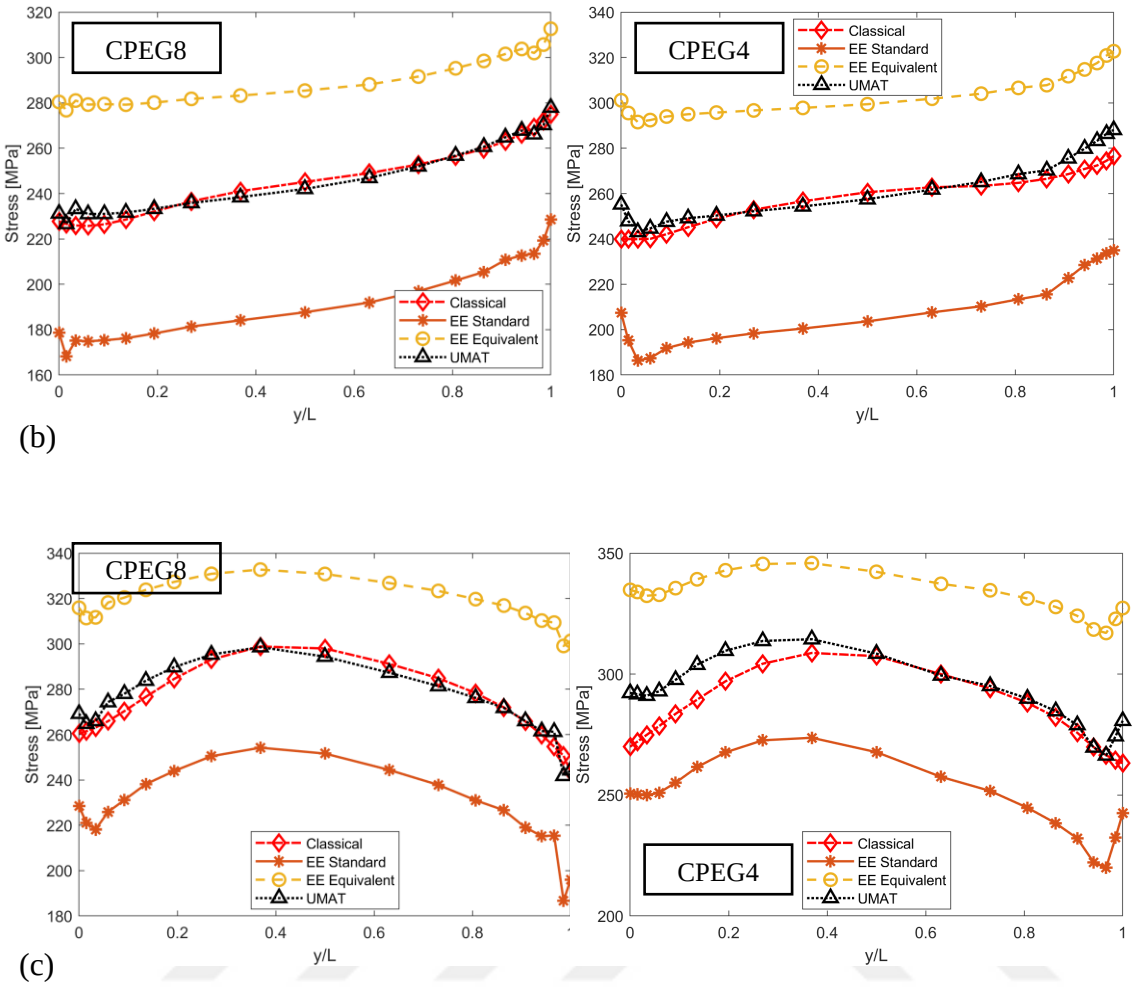

Figure 5.9. Comparison of models with CPEG8 and CPEG4 element types. S11 results given for a) Fiber 1; b) Fiber 2 and c) Fiber 3.

As Figure 5.8a indicates that, Classical and UMAT models are still close to the each other, while both models provide a less stiff solution. That same phenomenon is valid for both S22 and S12 cases. Hence, it can be said that there are negligible changes in the stress results due to these element types. Figure 5.9 provides results as expected, such that more nodes for each element improved the results even more, especially on interface regions. This option may increase computational time on more complex models, hence it presents a tradeoff between computational time and result accuracy. Using quadratic elements can be a viable option.

5.3.3. Effect of Fiber Volume Fraction

Same analyses are performed for a fiber volume fraction of 0.4. It is expected that results from this configuration should be better because of the smaller fiber size as mentioned before. Results are given in Figure 5.10.

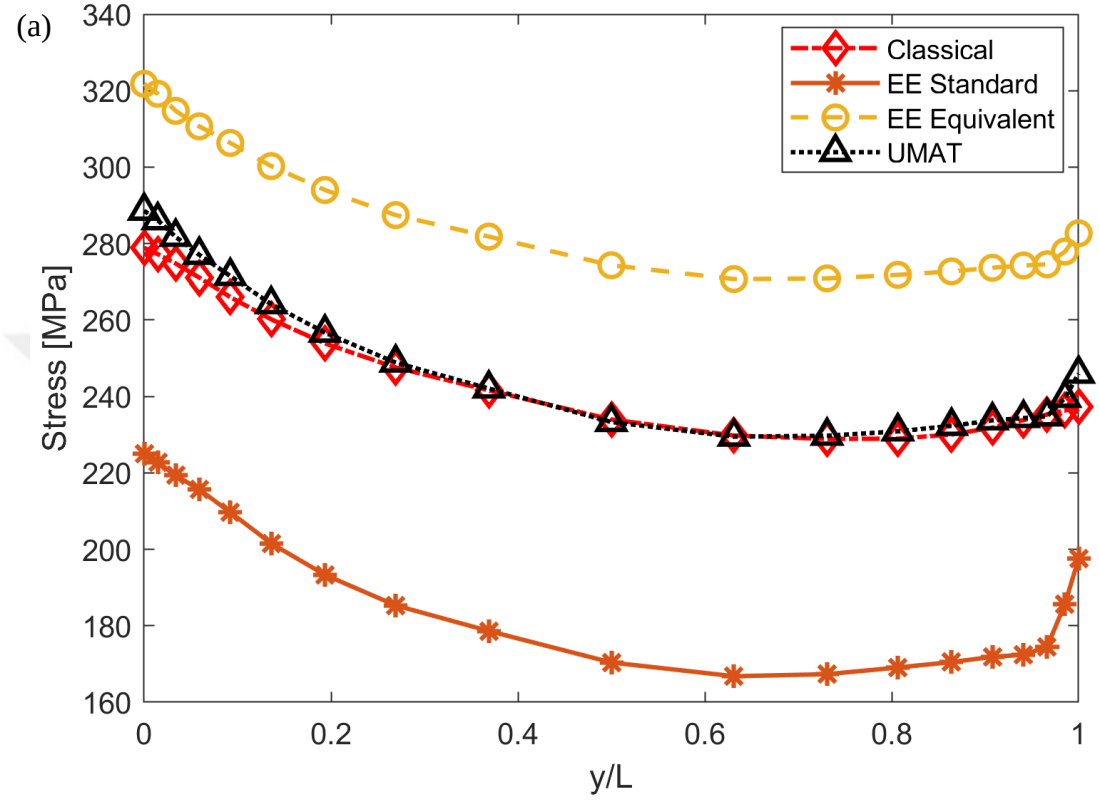

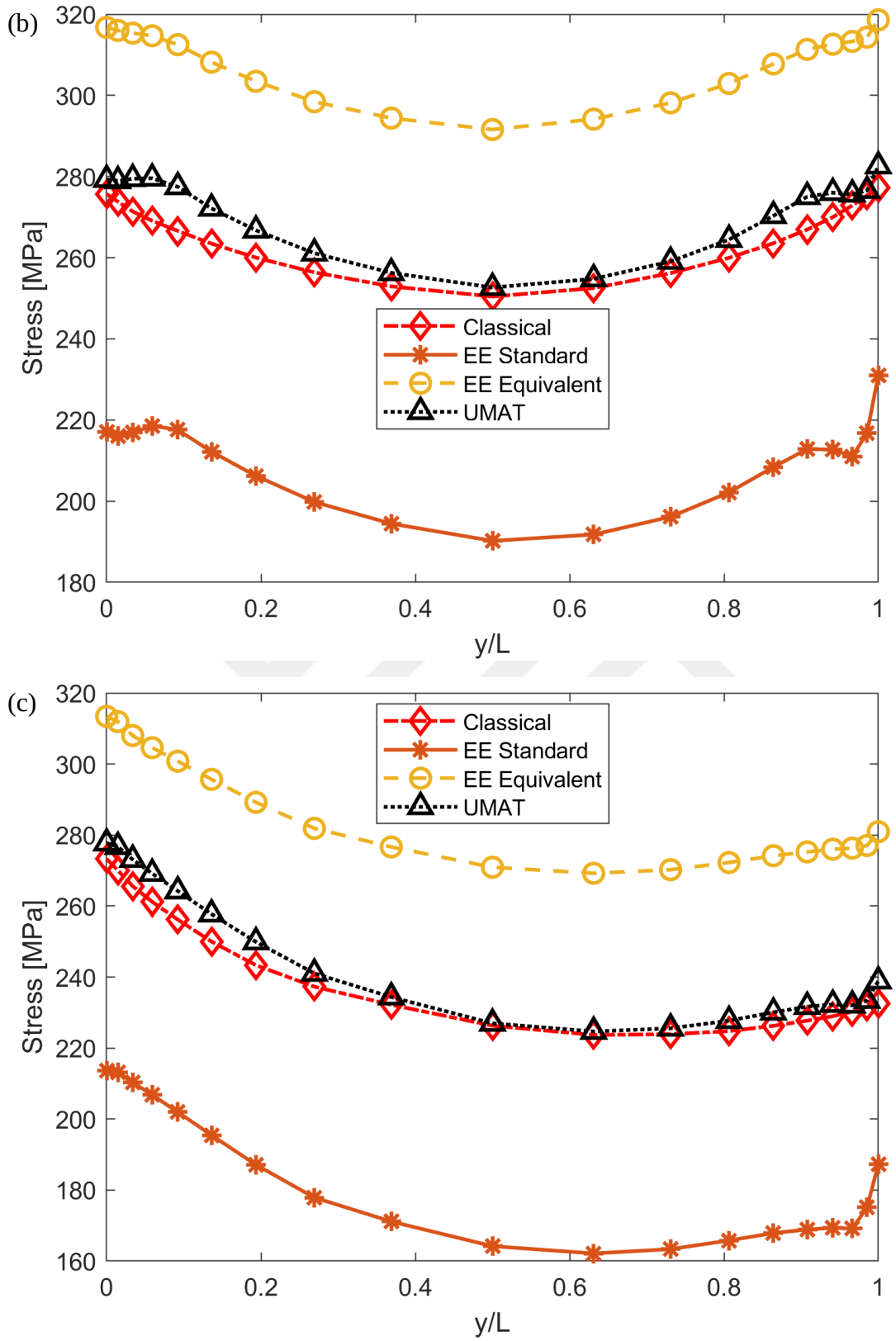

Figure 5.10. RDFM results for vf=0.4. a-b-c) represent S11 values for Fiber 1, Fiber 2 and Fiber 3, respectively.

Relation between different models tends to be as it is in vf=0.6 configuration, such as, S11 being the best performing direction to measure, S22 being not accurate and S12 shows good results for UMAT. However, with this configuration, the positive effect of smaller fiber volume fraction, on Embedded Element method can be observed, since UMAT results are almost identical to the Classical model for S11.

5.3.4. Effect of von Mises Plasticity

Von Mises plasticity (VM) is applied instead of Drucker-Prager plasticity (DP) to observe the results. Original VM does not take hydrostatic deformation into account. Thus, a modified formulation called "Elastic Volumetric Moduli" (EVM), which subtracts this hydrostatic part artificially in the subroutine is also considered. The details of this formulation are presented in the APPENDIX The results are shown for both UMAT variations in the original VM, given in Figure 5.11.

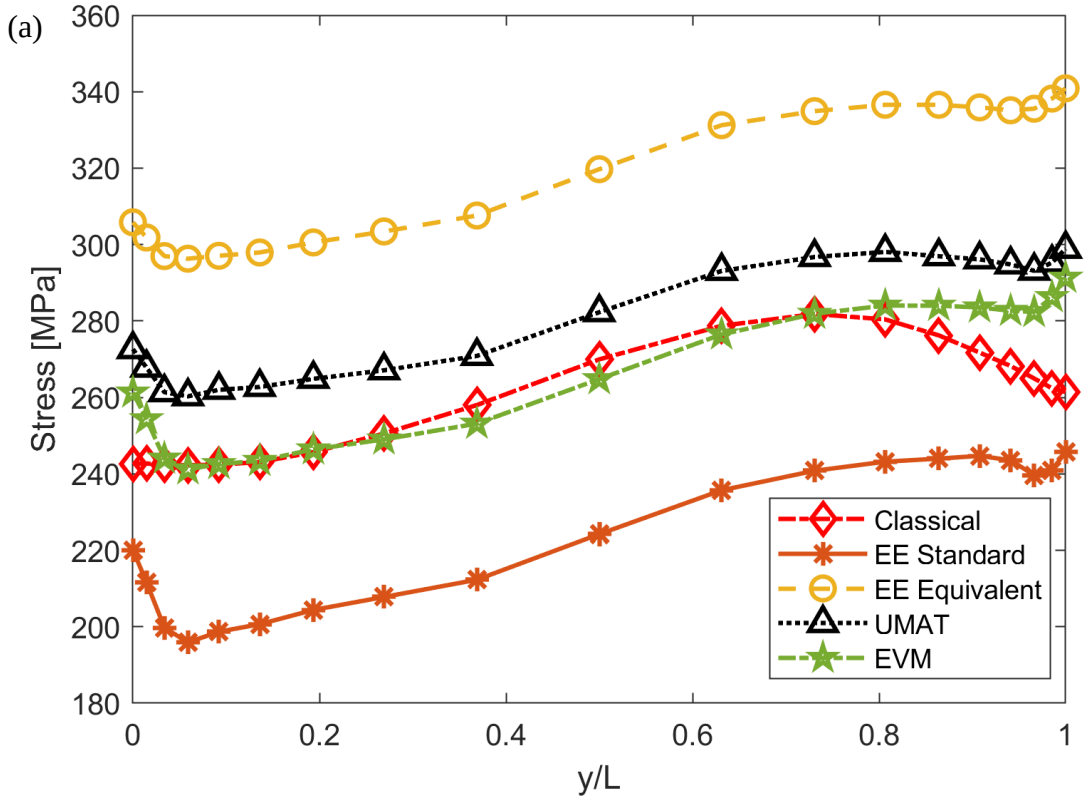

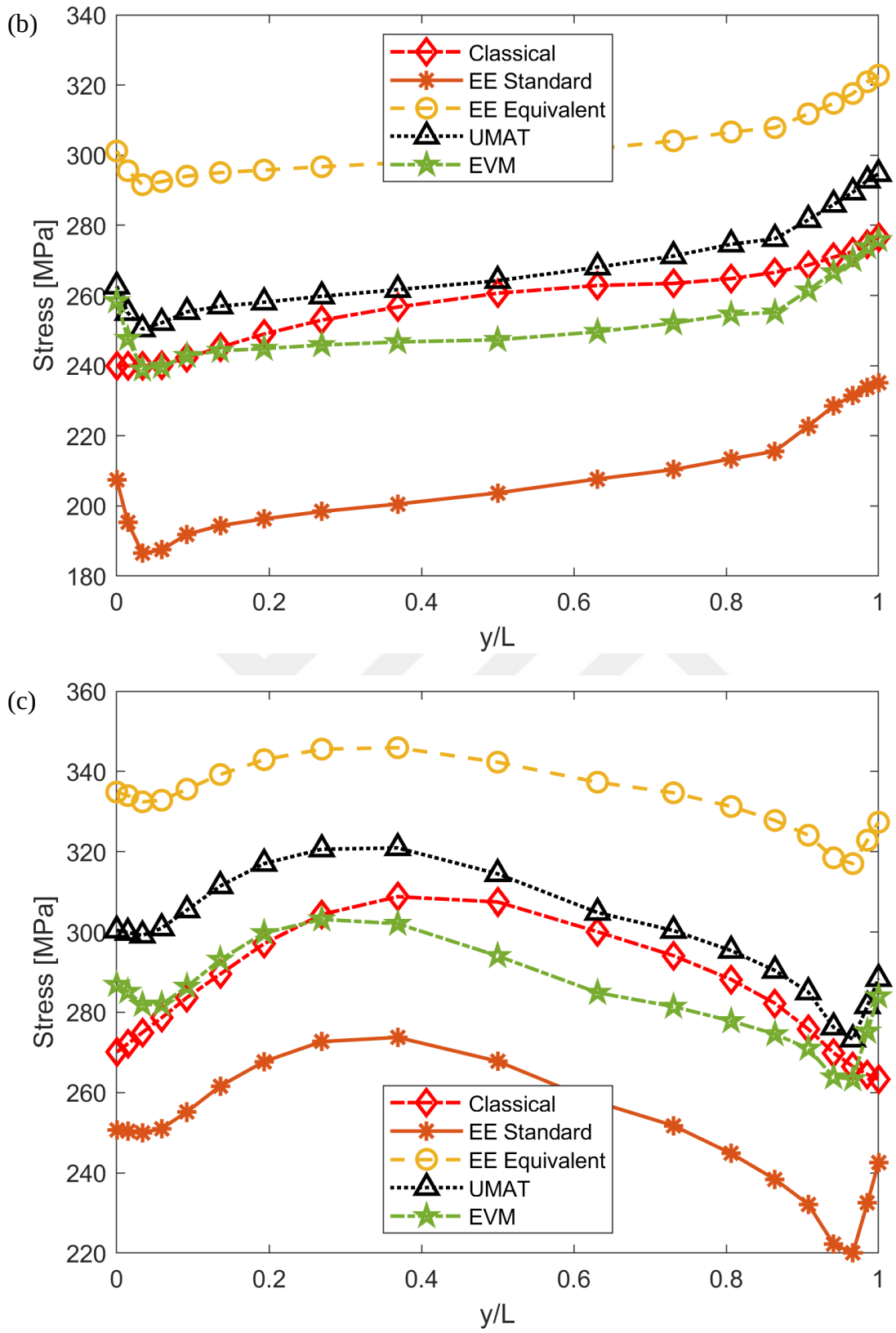

Figure 5.11. RDFM Results for von Mises plasticity. a-b-c) represent S11 values, for Fiber 1, Fiber 2 and Fiber 3, respectively.

In the S11 comparison, as seen in Figure 5.11a, b, c, both UMAT and EVM models provide similar results compared to the Classical model for all fibers.

5.3.5. Effect of IP_{cons}

As previously mentioned in the section 3.4.2, IP_{cons} is a limiting variable that limits the number of host nodes considered for the calculation of $C_i^{eq.m}$. Since performing the calculation based on all 6400 nodes would be costly, it is limited to 4 by default. Total analysis times of three different configurations, where IP_{cons} is equal to 4, 16 and 64 and represented by configuration numbers of 1,2 and 3 respectively. Three analyses are run under all configurations and their average are compared to each other. These analyses are performed in a workstation with 2.20 GHz, 20 core CPU and 32 GB of RAM. The results are given in Figure 5.12. Effect of IP_{cons} on the outcoming stress values are investigated with more IP_{cons} values, starting from 1 to 32. Stress values of 11-direction on Fiber 1 are compared and resulting plot is given in Figure 5.13.

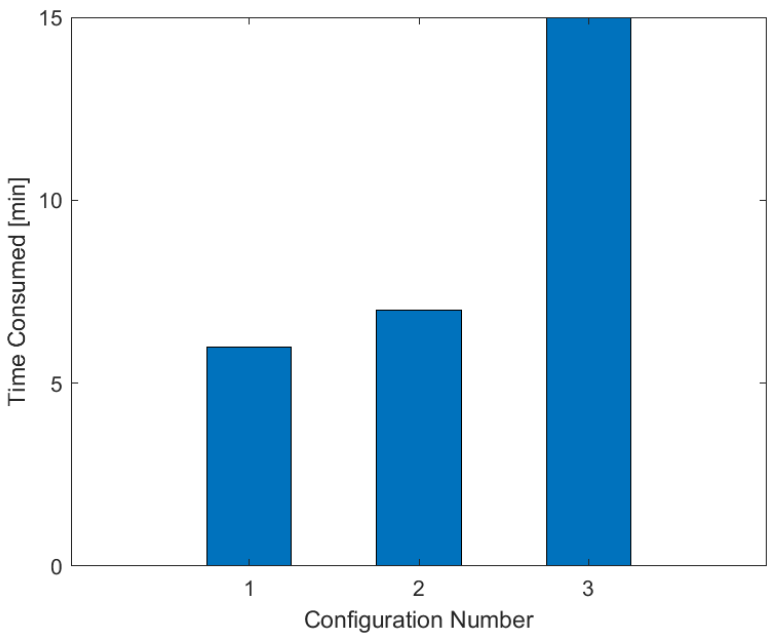

Figure 5.12. Effect of IPcons on processing time

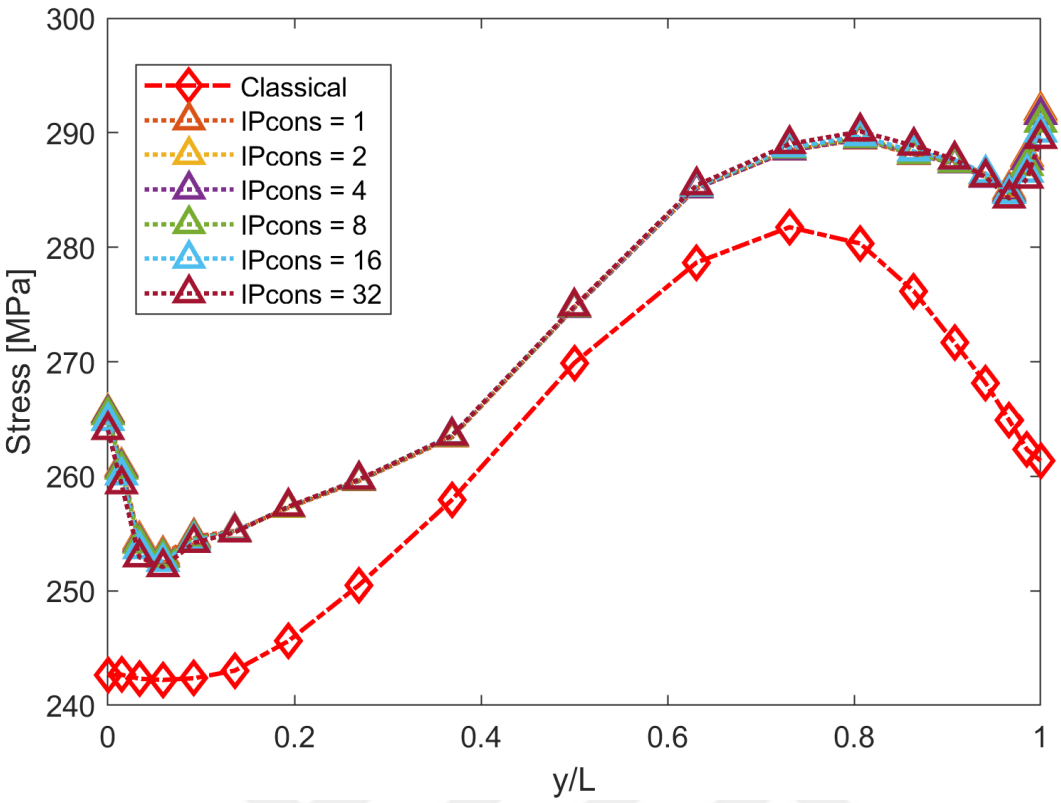

Figure 5.13. Effect of IPcons on stress values

In the first 2 configurations, multicore processing is used on all models. However, for the third configuration, EVM model could not be solved with multicore processing enabled. Hence, it is solved on a single processor, which caused a drastic time increase. For a better understanding of the effect of IP_{cons}, analysis times of only UMAT models can be compared. The result is 2, 2.5 and 2.83 minutes for configurations from 1 to 3, respectively. This data still provides an increase in processing time. It can be concluded that on higher numbers of IP_{cons}, models with subroutines may not be solved with a multicore processing option, which brings instability and long processing times into the equation. Limiting this number to 4 eliminates both of these problems.

In terms of results, there is negligible difference between different IP_{cons} numbers. This shows that the developed method can successfully predict the material behavior even under the involvement of fewer elements to use for calculations.

5.3.6. Performance of the Proposed Solution Under Shear Loading

As mentioned before in section 4.2.6, the model is tested under a shear loading for two different boundary condition cases. Since the load is a shear load, S12 results are compared and discussed in this section. Obtained results are given in Figure 5.14 and Figure 5.15.

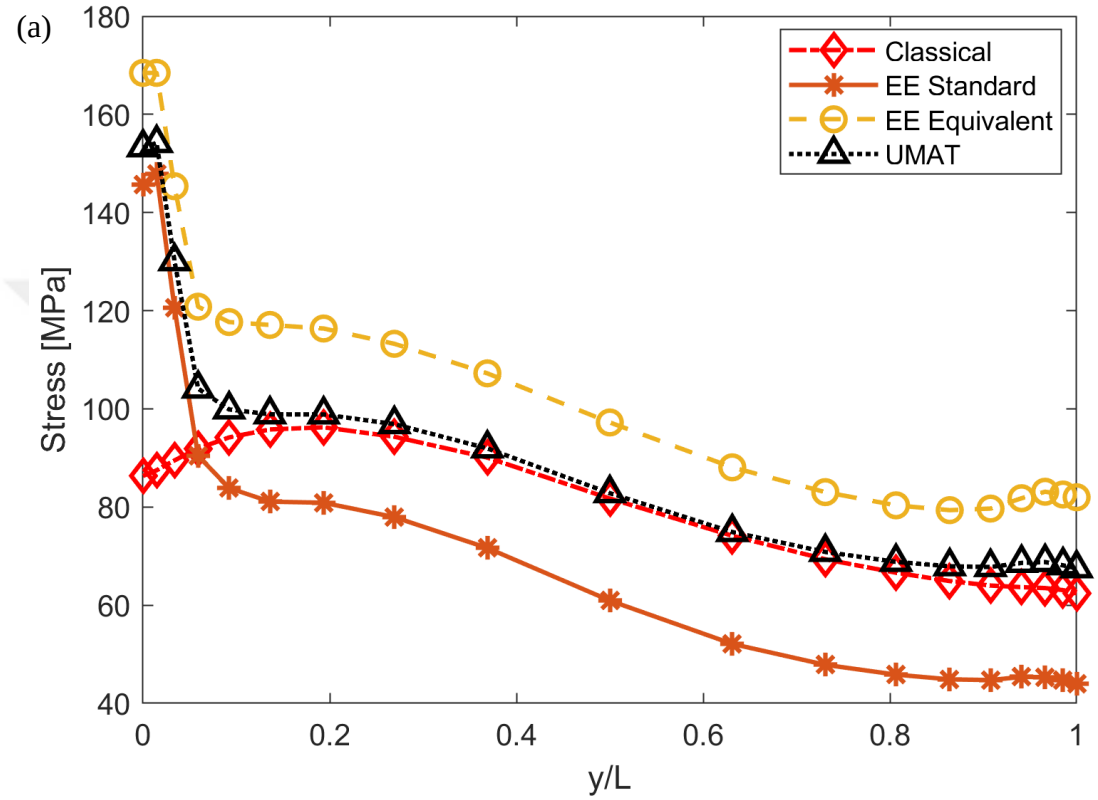

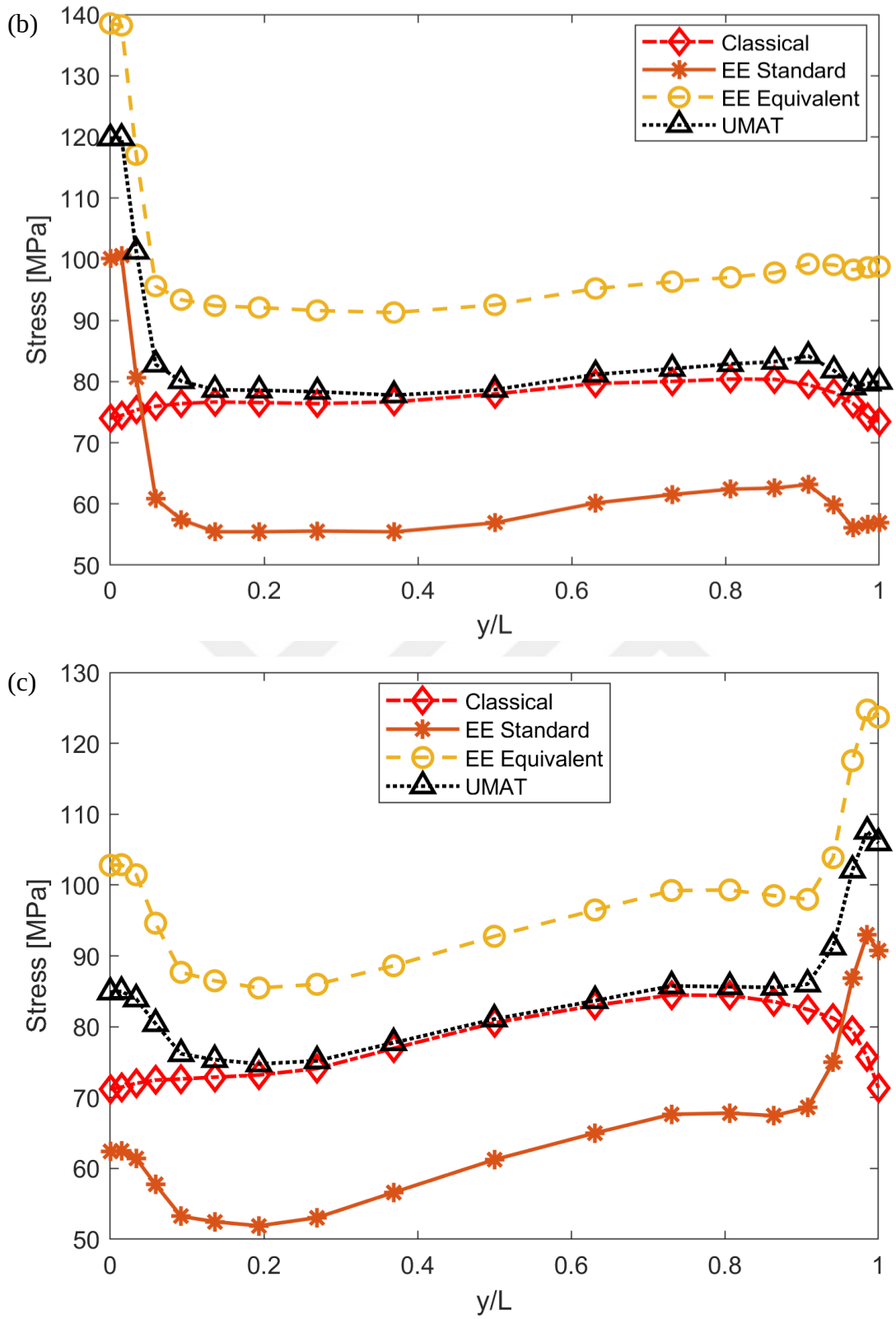

Figure 5.14. S12 results for the case without PBC application. Figures a, b and c represent Fiber 1, Fiber 2 and Fiber 3, respectively.

(a)

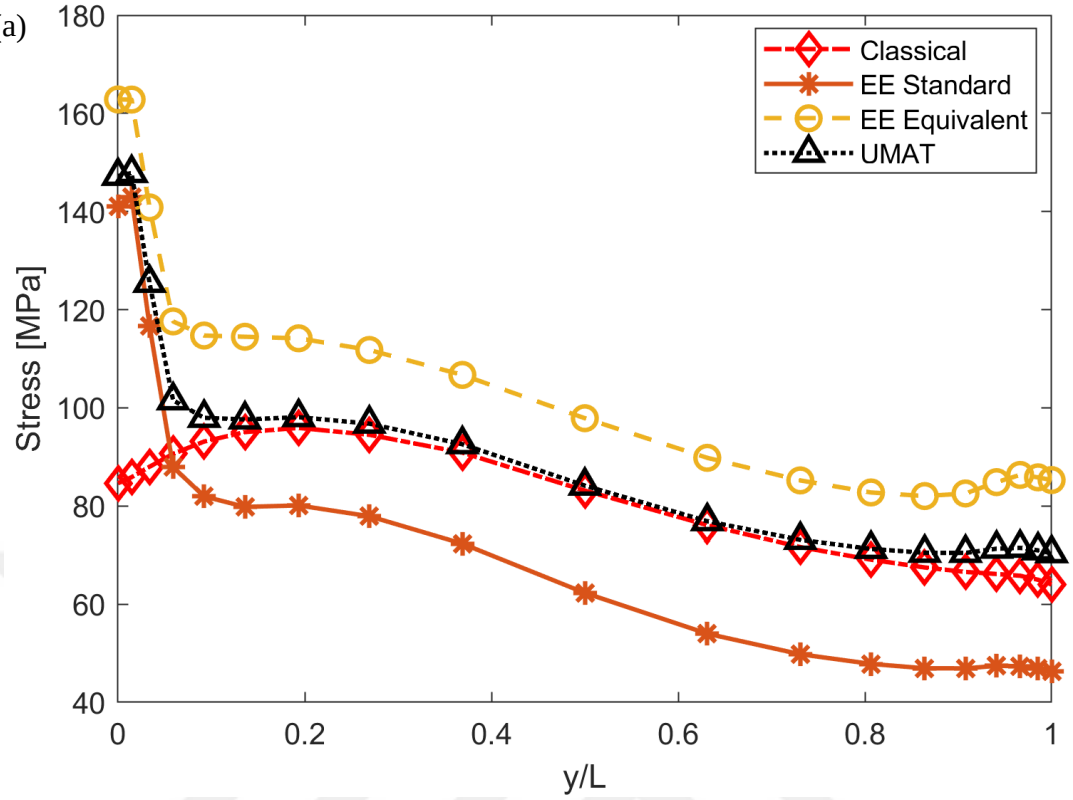
Classical
EE Standard
EE Equivalent
UMAT
Stress [MPa]
y/L
180
160
140
120
100
80
60
40
0
0.2
0.4
0.6
0.8
1

(b)

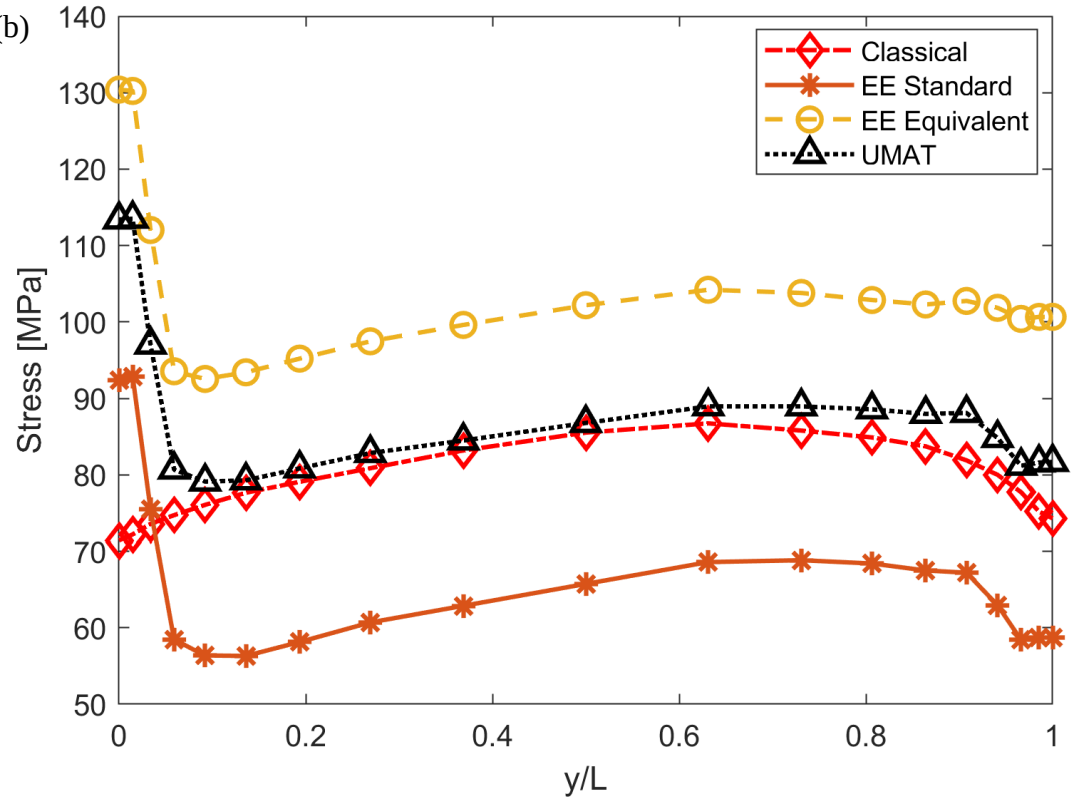
Classical
EE Standard
EE Equivalent
UMAT
Stress [MPa]
y/L
140
130
120
110
100
90
80
70
60
50
0
0.2
0.4
0.6
0.8
1

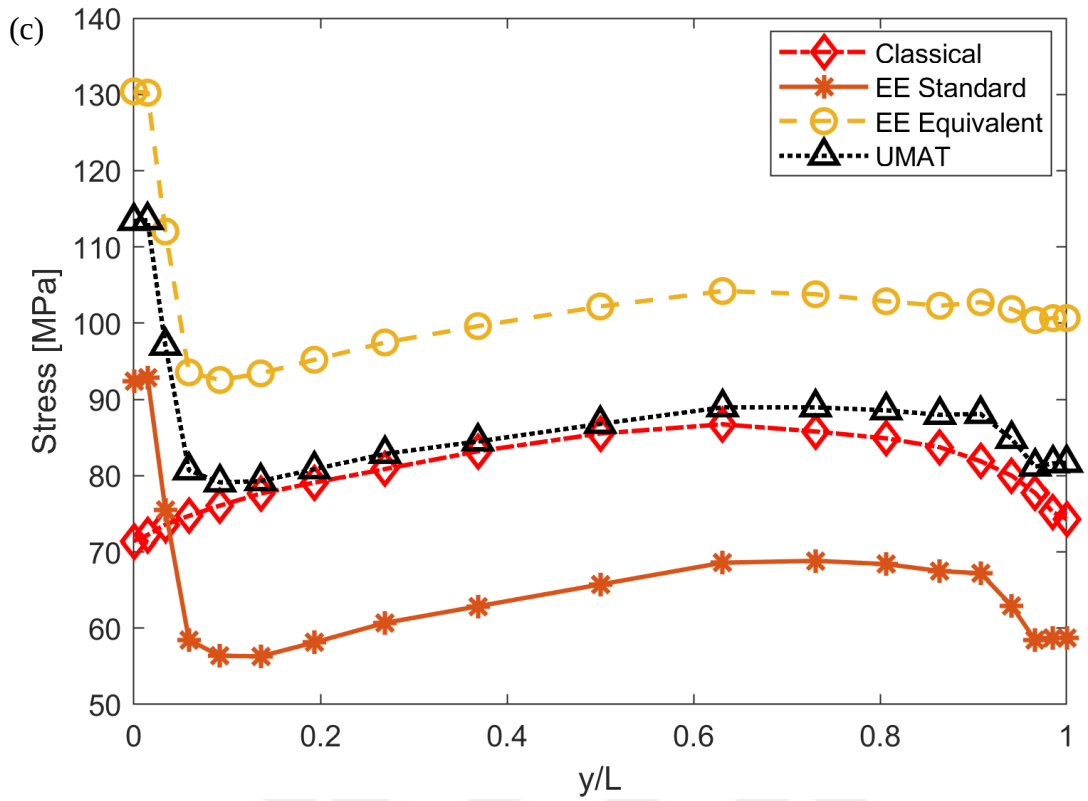

Figure 5.15. S12 results for the case with PBC application. Figures a, b and c represent Fiber 1, Fiber 2 and Fiber 3, respectively.

It can be clearly seen from the results of both models, the proposed method (UMAT) and the Classical model yields similar results to each other in S12 values. In both boundary condition cases, only discrepancies occur on the interface regions. As mentioned before in section 5.2, this is caused by the classical model having direct nodal connectivity between fiber and matrix elements, as opposed to the embedded element models. Thus, this discrepancy is expected. However, apart from the interface regions, the obtained results of UMAT model are nearly the same with the Classical model, which clearly indicates that the proposed method of solution can give reliable results under different loading conditions.

6. CONCLUSION

6.1. Summary of the Study

In order to design and manufacture composites in a reliable way, the mechanical behavior of them should be understood and studied upon extensively. In addition to that, investigation of the mechanical behavior of constituent materials adds great value to the design process. This information about matrix and fibers provides a better understanding of good sides and shortages of the subjected composite under certain circumstances. Embedded element method comes into play and provides analysis capability while modeling the constituents separately from each other. On the other hand, in the development of aerospace or biomechanics applications, constituents with non-linear elasto-plastic behavior or natural fibers, that their stiffnesses are close to the matrix material are being used. Embedded element method fails to predict the material behavior successfully by default on these types of materials. In this study, a new subroutine based approached is proposed to provide using of embedded element model for the case of high deformation. This study starts with the investigation of previous studies on embedded element method, that makes the method work under different conditions, given in Chapter 2. After that, a proposed method to achieve the analysis of non-linear materials with the embedded element method is described in Chapter 3. The proposed method is tested under various conditions. These conditions are explained in Chapter 4 and the results of the analyses under these conditions are given in Chapter 5.

6.2. Outcomes of the Study

Obtained results indicate that under the application of CPEG4 elements and Drucker-Prager plasticity, developed method gives realistic results for the stresses in the load application direction. In the other directions, the results are not accurate, which is not as important as the former one.

- Application of the method on the smaller fiber volume fractions yields much better results, as shown in Section 5.3.3.

- Usage of CPE4 elements instead of CPEG4 elements yield closer results between proposed model (UMAT) and the reference model (Classical). This element type can be a viable choice when it needed to be used.

- In the case of von Mises plasticity, EVM model provides a better solution than the UMAT model, as shown in Figure 5.11.

- Changing the IP_{cons} value does not have a significant effect on analysis results. Yet, as it increases, analyses become more and more unstable, causing the multiprocessing approach to become unusable. This issue increases the wasted time, especially after $IP_{cons} = 64$. This instability may be caused by the hardware limitations of the used workstation. Nevertheless, increasing this value will not have any positive effect on the analyses. Hence a number between 1 and 32 is suitable for usage.

- Overall, this developed method can be considered as a useful tool for solving problems that contain non-linearly behaving materials with the embedded element method.

6.3. Future Studies

With the help of the outcomes of this study, some studies can be performed for further development of this successful model in the future. The possible studies are listed below:

- The proposed solution method can be modified, such that it works for a 3D composite geometry, apart from a 2D geometry as the case in this study.
- Different types of materials for fiber and matrix can be implemented for a wider area of application.
- The subroutine can be adjusted for different, uncommon loading types which a novel application may require.
- An interface region between the fibers and the matrix can be introduced, which will have the mechanical properties between the matrix and the fiber values. This interface region can be used to eliminate the differences occur in the vicinity of

interface regions, between the reference model (Classical) and the proposed model (UMAT).

7. REFERENCES

Abdin, Y., Jain, A., Verpoest, I., Lomov, S.V., 2016. Mean-field based micro-mechanical modelling of short wavy fiber reinforced composites. Composites Part A: Applied Science and Manufacturing 91, 472-483.

Affdl, J.H., Kardos, J., 1976. The Halpin-Tsai equations: a review. Polymer Engineering & Science 16(5), 344-352.

Allen, P.A., 2002. Hydrostatic stress effects in low cycle fatigue. A Dissertation Presented for the Doctor of Philosophy Degree, Tennessee Technology University.

Baley, C., Perrot, Y., Busnel, F., Guezenoc, H., Davies, P., 2006. Transverse tensile behaviour of unidirectional plies reinforced with flax fibres. Materials Letters 60(24), 2984-2987.

Barbero, E.J., 2007. Finite element analysis of composite materials. CRC press.

Bedogni, E., Ivanov, D., Lomov, S.V., Pirondi, A., Vettori, M., Verpoest, I., 2012. Creating finite element models of 3D woven fabrics and composites: Semi-automated solution of interpenetration problem. 15th European Conference on Composite Materials (ECCM-15). Venice, Italy2012.

Bonfield, W., 1988. Composites for bone replacement. Journal of biomedical engineering 10(6), 522-526.

Chamis, C.C., 1989. Mechanics of composite materials: Past, present, and future. Journal of Composites Technology and Research 11(1), 3-14.

Chatzigeorgiou, G., Efendiev, Y., Lagoudas, D.C., 2011. Homogenization of aligned “fuzzy fiber” composites. International Journal of Solids and Structures 48(19), 2668-2680.

De Morais, A., Pereira, A., Teixeira, J., Cavaleiro, N., 2007. Strength of epoxy adhesive-bonded stainless-steel joints. International journal of adhesion and adhesives 27(8), 679-686.

Eshelby, J.D., 1957. The determination of the elastic field of an ellipsoidal inclusion, and related problems. Proceedings of the royal society of London. Series A. Mathematical and physical sciences 241(1226), 376-396.

Fagiano, C., Genet, M., Baranger, E., Ladevèze, P., 2014. Computational geometrical and mechanical modeling of woven ceramic composites at the mesoscale. Composite Structures 112, 146-156.

Fish, J., 1992. The s-version of the finite element method. Computers & Structures 43(3), 539-547.

Hill, R., 1965. A self-consistent mechanics of composite materials. Journal of the Mechanics and Physics of Solids 13(4), 213-222.

Holzapfel, G.A., 2001. Biomechanics of soft tissue. The handbook of materials behavior models 3, 1049-1063.

Honda, S., Zako, M., Kurashiki, T., Nakai, H., Lomov, S., Verpoest, I., 2008. A proposal of stress/strain analytical procedure of textile composites with stitch by M3 method. 13th European Conference on Composite Materials (ECCM-13).

Hua, Y., Crocombe, A., Wahab, M., Ashcroft, I., 2007. Continuum damage modelling of environmental degradation in joints bonded with E32 epoxy adhesive. Journal of adhesion science and technology 21(2), 179-195.

Iarve, E.V., Mollenhauer, D.H., Zhou, E.G., Breitzman, T., Whitney, T.J., 2009. Independent mesh method-based prediction of local and volume average fields in textile composites. Composites Part A: Applied Science and Manufacturing 40(12), 1880-1890.
Jain, A., Abdin, Y., Van Paepegem, W., Verpoest, I., Lomov, S.V., 2015. Effective anisotropic stiffness of inclusions with debonded interface for Eshelby-based models. Composite Structures 131, 692-706.
Jiang, W.-G., Hallett, S.R., Wisnom, M.R., 2008. Development of domain superposition technique for the modelling of woven fabric composites. Mechanical response of composites, pp. 281-291. Springer.
Joosten, M.W., Dingle, M., Mouritz, A., Khatibi, A.A., Agius, S., Wang, C.H., 2016. A hybrid embedded cohesive element method for predicting matrix cracking in composites. Composite Structures 136, 554-565.
Kundalwal, S.I., Ray, M.C., 2012. Effective properties of a novel composite reinforced with short carbon fibers and radially aligned carbon nanotubes. Mechanics of Materials 53, 47-60.
Kurashiki, T., Zako, M., Nakai, H., Imura, M., Hirosawa, S., 2007. Damage development of woven composites based on multi-scale analysis. Proceedings of 16th ICCM.
Li, C., Chou, T.-W., 2008. Modeling of damage sensing in fiber composites using carbon nanotube networks. Composites Science and Technology 68(15), 3373-3379.
Liu, H., Zeng, D., Li, Y., Jiang, L., 2016. Development of RVE-embedded solid elements model for predicting effective elastic constants of discontinuous fiber reinforced composites. Mechanics of Materials 93, 109-123.
Liu, Q., Gorbatikh, L., Lomov, S.V., 2019. A combined use of embedded and cohesive elements to model damage development in fibrous composites. Composite Structures 223, 110921.
Lomov, S.V., Ivanov, D.S., Verpoest, I., Zako, M., Kurashiki, T., Nakai, H., Hirosawa, S., 2007. Meso-FE modelling of textile composites: Road map, data flow and algorithms. Composites Science and Technology 67(9), 1870-1891.
Matveeva, A.Y., Böhm, H.J., Kravchenko, G., van Hattum, F.W., 2014. Investigation of the embedded element technique for modelling wavy CNT composites. Computers, Materials & Continua 42(1), 1-23.
Melro, A.R., Camanho, P.P., Pinho, S.T., 2008. Generation of random distribution of fibres in long-fibre reinforced composites. Composites Science and Technology 68(9), 2092-2102.
Mori, T., Tanaka, K., 1973. Average stress in matrix and average elastic energy of materials with misfitting inclusions. Acta Metallurgica 21(5), 571-574.
Muñoz, R., Martínez-Hergueta, F., Gálvez, F., González, C., Llorca, J., 2015. Ballistic performance of hybrid 3D woven composites: Experiments and simulations. Composite Structures 127, 141-151.
Nielsen, L.E., Landel, R.F., 1994. Mechanical properties of polymers and composites. M. Dekker, New York; Basel; Hong Kong.
Ohyama, D., Kurashiki, T., Watanabe, Y., Fujita, Y., Zako, M., 2011. Estimation of mechanical behavior of braided composites based on mesh superposition method. 18th Int. Conf. on Composite Materials, Jeju island, Korea.
Okabe, T., Ishii, K., Nishikawa, M., Takeda, N., 2010. Prediction of Tensile Strength of Unidirectional CFRP Composites. Advanced Composite Materials 19(3), 229-241.

Ren, X., Burton, J., Seidel, G.D., Lafdi, K., 2015. Computational multiscale modeling and characterization of piezoresistivity in fuzzy fiber reinforced polymer composites. International Journal of Solids and Structures 54, 121-134.
Romanov, V., 2015. Modeling Tools for Micro-scale Stress Analysis of Nano-engineered Fiber-reinforced Composites.
Sabuncuoglu, B., 2014. On the high stress concentrations in steel fiber composites under transverse loading. Journal of Reinforced Plastics and Composites 33(21), 1941-1953.
Sabuncuoglu, B., Gorbatikh, L., Lomov, S.V., 2018. Analysis of stress concentrations in transversely loaded steel-fiber composites with nano-reinforced interphases. International Journal of Solids and Structures 130-131, 248-257.
Savvas, D.N., Papadopoulos, V., Papadrakakis, M., 2012. The effect of interfacial shear strength on damping behavior of carbon nanotube reinforced composites. International Journal of Solids and Structures 49(26), 3823-3837.
Stolarski, T., Nakasone, Y., Yoshimoto, S., 2018. Engineering analysis with ANSYS software. Butterworth-Heinemann.
Tabatabaei, S.A., Lomov, S.V., 2015. Eliminating the volume redundancy of embedded elements and yarn interpenetrations in meso-finite element modelling of textile composites. Computers & Structures 152, 142-154.
Tabatabaei, S.A., Lomov, S.V., Verpoest, I., 2014. Assessment of embedded element technique in meso-FE modelling of fibre reinforced composites. Composite Structures 107, 436-446.
Vorobiov, O., Tabatabaei, S., Lomov, S.V., 2017. Mesh superposition applied to meso-FE modelling of fibre-reinforced composites: Cross-comparison of implementations. International Journal for Numerical Methods in Engineering 111(11), 1003-1024.
Zako, M., Kurashiki, T., Kubo, F., Imura, M., 2005. A multi-scale analysis for structural design of fibrous composites–M3 method. Proc. of 15th ICCM.
Zhang, M., Guan, Z., Wang, X., Du, S., 2017. Micro-mechanical analysis about kink band in carbon fiber/epoxy composites under longitudinal compression. Applied Composite Materials 24(5), 1011-1028.

APPENDIX

A. Introduction to the Plasticity Models

In this study, von Mises and Drucker-Prager (DP) plasticity models are tested. In the analysis of most materials, von Mises plasticity model is the most frequently used model. This model is assumed to be valid for metals generally. The model has two important properties, such that, yield stresses in tension and compression are equal and hydrostatic stress does not cause deformation. Deformation is only due to the deviatoric stress.

The principle of DP model is that, it takes hydrostatic stress into account for yield behavior. In order to define DP material properties into the proposed models, two different base models are employed, which is explained in the following subsections.

a. Original DP Approach

This approach is based on the model developed in the study of Allen (2002) and used for implementing the DP model to the proposed subroutine in the current study. This approach needs only one parameter to be defined. It defines the shape of the yield surface (conic shape parameters). Figure A. 1a show the von Mises plasticity yield surface. As observed, this is an infinite cylinder. This shows that even if the principle stress values, $\sigma_1 = \sigma_2 = \sigma_3 = 99999GPa$, no yield will be observed, which is not correct for polymeric materials. In DP model, there is a parameter that converts this infinite cylinder to a cone (Figure A. 1b). This parameter can be defined as "friction angle (θ)" or alpha (α). They are related with each other with the following equation:

$$\alpha = \frac{2sin\,\theta}{\sqrt{3}(3 - \sin\theta)} \tag{A.1}$$

So, either θ or α can be defined to determine the steepness of the cone in Figure A. 1b. There is another parameter called "dilation angle (α_v)" in the formulation but it is assumed to be equal to α in the original DP approach, which is a function of θ.

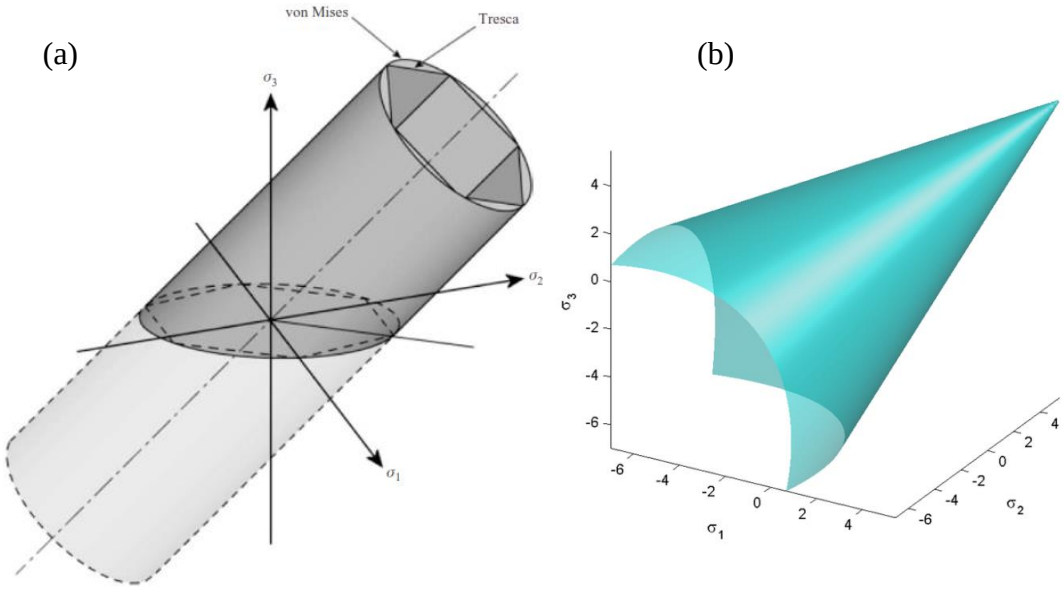

Figure A. 1 a) von Mises and Tresca yield surfaces; b) Drucker-Prager yield surface

b. Extended DP Approach

This approach can be readily found in the ABAQUS software. There are 3 parameters needed in this approach:

- θ (friction angle in ABAQUS): Same as it is in the original approach. α can be defined instead of this parameter.
- α_v (dilation angle): If this parameter is assigned equal to α, the model will be similar to the original approach. It can be assigned a different value if desired.
- K (flow stress ratio): This parameter is the result of $\frac{\sigma_{yt}}{\sigma_{yc}}$. If $\sigma_{yt} = \sigma_{yc}$, this value becomes 1 and the model becomes similar to the original approach.

Further explanation of these models with their equations are given in the following sections.

B. Drucker-Prager Plasticity Model Formulations

In this section, a pressure dependent plasticity model, the Drucker-Prager plasticity, is presented. Similar to the deviatoric von Mises plasticity, the strain tensor is assumed to decompose into an elastic part and a plastic part

$$\varepsilon_{ij} = \varepsilon_{ij}^{e} + \varepsilon_{ij}^{p} \tag{A.2}$$

where ε_{ij}^{e} and ε_{ij}^{p} are the components of the elastic and plastic parts, respectively. Assuming that the Drucker-Prager plasticity model is coupled with isotropic linear elasticity, one can compute the components of the stress tensor and the elastic modulus

$$\sigma_{ij} = \lambda\, \varepsilon_{kk}^{e}\delta_{ij} + 2\mu\varepsilon_{ij}^{e}, \qquad \mathbb{C}_{ijkl}^{e} = \lambda\delta_{ij}\delta_{kl} + 2\mu\mathbb{I}_{ijkl} \tag{A.3}$$

in terms of the Lame constant λ and the shear modulus μ, or

$$\sigma_{ij} = \kappa\, \varepsilon_{kk}^{e}\delta_{ij} + 2\mu\varepsilon_{ij}^{e\prime}, \qquad \mathbb{C}_{ijkl}^{e} = \kappa\delta_{ij}\delta_{kl} + 2\mu\mathbb{P}_{ijkl} \tag{A.4}$$

in terms of the bulk modulus κ and the shear modulus μ. In above equations δ_{ij} is the Kronecker delta, $\mathbb{I}_{ijkl} = \frac{1}{2}(\delta_{ik}\delta_{jl} + \delta_{il}\delta_{jk})$ is the fourth order identity tensor, $\mathbb{P}_{ijkl} = \mathbb{I}_{ijkl} - \frac{1}{3}\delta_{ij}\delta_{kl}$ is the fourth order deviatoric projection tensor and

$$(\cdot)_{ij}' = (\cdot)_{ij} + \frac{1}{3}(\cdot)_{kk}\delta_{ij} \tag{A.5}$$

represents the deviatoric part of a second order tensor.

The yield function is used to determine whether the response of the material would be elastic or plastic. To this end, the pressure-dependent Drucker-Prager yield function

$$\phi = \sqrt{3J_2} + \frac{1}{3}I_1\tan\theta - \sigma_{ys} = \sigma_{eff} - 3ap - \sigma_{ys}(\varepsilon_{eq}^{p}) \leq 0 \tag{A.6}$$

is used. In contrast to the von Mises yield function which depends only on the second basic invariant of the deviatoric part of the stress tensor

$$J_2 = \frac{\sigma_{eff}^2}{3} = \frac{1}{2}\sigma_{ij}'\sigma_{ij}' \tag{A.7}$$

the Drucker-Prager yield function depends also on the first principal invariant (volumetric stress)

$$I_1 = \sigma_{ii} \tag{A.8}$$

which makes the model pressure-dependent. In equation (A.6), p is the pressure

$$p = -\frac{1}{3} I_1 \tag{A.9}$$

a is a material constant related to the theoretical cohesive strength of the material and σ_{ys} is the actual yield strength of the material which is assumed to depend on the equivalent plastic strain ε_{eq}^{p}. The equivalent plastic strain is computed as

$$\varepsilon_{eq}^{p} = \int_0^t \dot{\varepsilon}_{eq}^{p} dt \qquad , \dot{\varepsilon}_{eq}^{p} = \sqrt{\frac{2}{3} \dot{\varepsilon}_{ij}^{p} \dot{\varepsilon}_{ij}^{p}} \tag{A.10}$$

Using a graphical representation of the yield surface in σ_{eff}-I_1 space, the material constant a can be computed as the slope of the graph of σ_{eff} versus I_1 as shown in Figure A. 2. In Figure A. 2, d is equal to the yield strength σ_{ys} at zero pressure, i.e., $I_1 = 0$. Furthermore, the value of I_1 for $\sigma_{eff} = 0$ corresponds to the theoretical cohesive strength σ_c of the material.

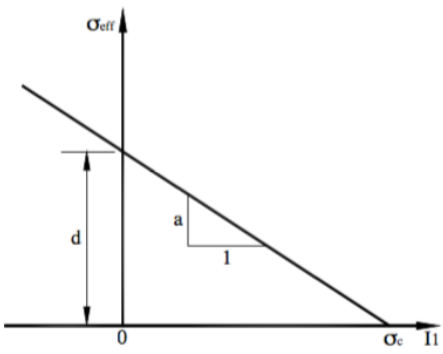

Figure A. 2. Visualization of the Drucker-Prager yield surface in σ_{eff}-I_1 plane.

The flow rule for the associated Drucker-Prager plasticity is computed form the yield function

$$\dot{\varepsilon}_{ij}^{p} = \dot{\gamma}\frac{\partial\phi}{\partial\sigma_{ij}} \tag{A.11}$$

in terms of the plastic slip rate $\dot{\gamma}$ and the plastic flow direction $\frac{\partial\phi}{\partial\sigma_{ij}}$. Considering the pressure-dependent structure of the Drucker-Prager yield function, the plastic flow $\dot{\varepsilon}_{ij}^{p}$ can be split into deviatoric and volumetric parts

$$\dot{\varepsilon}_{ij}^{p} = \dot{\varepsilon}_{q}^{p}\frac{3}{2}\frac{\sigma_{ij}'}{\sigma_{eff}} + \dot{\varepsilon}_{p}^{p}\frac{1}{3}\delta_{ij} \tag{A.12}$$

where $\dot{\varepsilon}_{q}^{p}$ and $\dot{\varepsilon}_{p}^{p}$ are the distortional and volumetric scalar plastic strain rates. Comparison of equations (A.11) and (A.12) with the help of the chain rule leads to the following identifications

$$\dot{\varepsilon}_{q}^{p} = \dot{\gamma}\frac{\partial\phi}{\partial\sigma_{eff}}, \qquad \dot{\varepsilon}_{p}^{p} = -\dot{\gamma}\frac{\partial\phi}{\partial p} \tag{A.13}$$

One can eliminate $\dot{\gamma}$ from (A.13) and write

$$\dot{\varepsilon}_{q}^{p}\frac{\partial\phi}{\partial\sigma_{p}} + \dot{\varepsilon}_{p}^{p}\frac{\partial\phi}{\partial\sigma_{eff}} = 0 \tag{A.14}$$

The partial derivatives of the Drucker-Prager yield function read

$$\frac{\partial\phi}{\partial\sigma_{eff}} = 1, \qquad \frac{\partial\phi}{\partial p} = 3a \tag{A.15}$$

Insertion of (A.15) into (A.14) then gives

$$3a\dot{\varepsilon}_{q}^{p} = \dot{\varepsilon}_{p}^{p} \tag{A.16}$$

The rate of plastic work $\dot{W}^{pl}$ can be defined in terms of the stress and the plastic strain rate or in terms of the effective yield stress and the equivalent plastic strain rate as follows

$$\dot{W}^{pl} = \sigma_{ij}\dot{\varepsilon}_{ij}^{p} = \sigma_{ys}(\varepsilon_{eq}^{p})\dot{\varepsilon}_{eq}^{p} \tag{A.17}$$

From equation (A.17) the equivalent plastic strain rate $\dot{\varepsilon}_{eq}^{p}$ can be obtained as

$$\dot{\varepsilon}_{eq}^{p} = \frac{\sigma_{ij}\dot{\varepsilon}_{ij}^{p}}{\sigma_{ys}(\varepsilon_{eq}^{p})} \tag{A.18}$$

The numerator can be expanded with the use of flow rule (A.12)

$$\sigma_{ij}\dot{\varepsilon}_{ij}^{p} = \dot{\varepsilon}_{q}^{p}\frac{3}{2}\frac{\sigma_{ij}\sigma_{ij}'}{\sigma_{eff}} + \dot{\varepsilon}_{p}^{p}\frac{1}{3}\sigma_{ij}\delta_{ij} \tag{A.19}$$

Using the relations $\sigma_{ij}\sigma_{ij}' = \sigma_{ij}'\sigma_{ij}' = \frac{2}{3}\sigma_{eff}^{2}$ and $\sigma_{ij}\delta_{ij} = \sigma_{ii}$, equation (A.19) can be simplified to

$$\sigma_{ij}\dot{\varepsilon}_{ij}^{p} = \sigma_{eff}\dot{\varepsilon}_{q}^{p} - p\dot{\varepsilon}_{p}^{p} \tag{A.20}$$

Finally, insertion of (A.20) into (A.*18*) gives

$$\dot{\varepsilon}_{eq}^{p} = \frac{\sigma_{eff}\dot{\varepsilon}_{q}^{p} - p\dot{\varepsilon}_{p}^{p}}{\sigma_{ys}(\varepsilon_{eq}^{p})} \tag{A.21}$$

The next step is the integration of the elastoplastic differential equations. The backward Euler integration scheme is selected since it is unconditionally stable. To this end, equations (A.3), (A.12), (A.16) and (A.21) are integrated using the backward Euler integration

$$\sigma_{ij}\big|_{n+1} = \sigma_{ij}^{*} - 2\mu\Delta\varepsilon_{q}^{p}n_{ij}\big|_{n+1} - \lambda\Delta\varepsilon_{p}^{p}\delta_{ij} \tag{A.22}$$

$$\Delta\varepsilon_{ij}^{p} = \Delta\varepsilon_{q}^{p}n_{ij}\big|_{n+1} + \frac{1}{3}\Delta\varepsilon_{p}^{p}\delta_{ij} \tag{A.23}$$

$$\Delta\varepsilon_{p}^{p} - 3a\Delta\varepsilon_{q}^{p} = 0 \tag{A.24}$$

$$\Delta\varepsilon_{eq}^{p} = \frac{\sigma_{eff}\Delta\varepsilon_{q}^{p} - p\Delta\varepsilon_{p}^{p}}{\sigma_{ys}(\varepsilon_{eq}^{p})} \tag{A.25}$$

In above equations $(\cdot)|_{n+1}$ means that the variable $(\cdot)$ is to be computed at time t_{n+1} and σ_{ij}^{*} is the elastic trial stress, i.e.,

$$\sigma_{ij}^{*} = \lambda\,(\varepsilon_{ij}\big|_{n+1} - \varepsilon_{ij}^{p}\big|_{n})\delta_{ij} + 2\mu(\varepsilon_{ij}\big|_{n+1} - \varepsilon_{ij}^{p}\big|_{n}) \tag{A.26}$$

The elastic trial stress can also be computed using the strain increment $\Delta\varepsilon_{ij} = \varepsilon_{ij}\big|_{n+1} - \varepsilon_{ij}\big|_{n}$, the elastic tangent and $\mathbb{C}_{ijkl}^{e}$ (A.3) and the stress form the previous time increment

$$\sigma_{ij}^{*} = \sigma_{ij}\big|_{n} + \mathbb{C}_{ijkl}^{e}\Delta\varepsilon_{ij} \tag{A.27}$$

In order to determine whether an increment is elastic or plastic, the yield function is evaluated with the elastic trial stress σ_{ij}^{*}, i.e.,

$$\phi^{*} = \sigma_{eff}^{*} - 3ap^{*} - \sigma_{ys}(\varepsilon_{eq}^{p}) \tag{A.28}$$

Here $\sigma_{eff}^{*} = \sqrt{\frac{3}{2}\sigma_{ij}^{*,\prime}\sigma_{ij}^{*,\prime}}$ is the effective elastic trial stress and $p^{*} = -\sigma_{ii}^{*}/3$ is the elastic trial pressure. Then the trial yield function $\phi^{*}$is checked

$$\phi^{*}\begin{cases} < 0 & \Longrightarrow \quad \text{elastic} \\ \geq 0 & \Longrightarrow \quad \text{plastic} \end{cases} \tag{A.29}$$

If the current increment is elastic ($\phi^{*} < 0$), then the stress at time t_{n+1} becomes equal to the trial elastic stress, the plastic strain at time t_{n+1} becomes equal to plastic strain at time t_n and tangent modulus becomes the elastic tangent.

$$\sigma_{ij}\big|_{n+1} = \sigma_{ij}^{*} \quad \varepsilon_{ij}^{p}\big|_{n+1} = \varepsilon_{ij}^{p}\big|_{n} \quad \mathbb{C}_{n+1}^{ep} = \mathbb{C}^{e} \tag{A.30}$$

If the current increment is plastic ($\phi^{*} > 0$), then the plastic increments, $\Delta\varepsilon_{p}^{p}, \Delta\varepsilon_{q}^{p}, \Delta\varepsilon_{eq}^{p}$ and $\Delta\varepsilon_{ij}^{p}$ need to be computed. The variable n_{ij} in (A.22) and (A.23) is the flow direction and can be computed as

$$n_{ij} = \frac{3}{2}\frac{\sigma_{ij}^{\prime}}{\sigma_{eff}} \tag{A.31}$$

It can be shown that the flow direction n_{ij} at time t_{n+1} and the trial flow direction n_{ij}^{*} are identical, i.e.,

$$n_{ij}\big|_{n+1} = \frac{3}{2}\frac{\sigma_{ij}^{\prime}\big|_{n+1}}{\sigma_{eff}\big|_{n+1}} = n_{ij}^{*} = \frac{3}{2}\frac{\sigma_{ij}^{\prime *}}{\sigma_{eff}^{*}} \tag{A.32}$$

Here $\sigma_{ij}^{\prime *}$ is the deviatoric part of the elastic trial stress. Note that following identities hold

$$n_{ij}n_{ij} = \frac{3}{2}, \quad \sigma_{ij}n_{ij} = \sigma_{eff} \tag{A.33}$$

Double contractions of equation (A.22) with $n_{ij}\big|_{n+1}$ and δ_{ij} with the help of identities in (A.33) give

$$\sigma_{eff}\big|_{n+1} = \sigma_{eff}^{*} - 3\mu\Delta\varepsilon_{q}^{p} \tag{A.34}$$

$$p|_{n+1} = p^{*} + \lambda\Delta\varepsilon_{p}^{p} \tag{A.35}$$

The system of equations to be solved is summarized below

$$\begin{gathered} \phi|_{n+1} = \sigma_{eff}\big|_{n+1} - 3ap|_{n+1} - \sigma_{ys}(\varepsilon_{eq}^{p}) = 0 \\ \Delta\varepsilon_{p}^{p} - 3a\Delta\varepsilon_{q}^{p} = 0 \end{gathered} \tag{A.36}$$

$$\sigma_{eff}\big|_{n+1} - \sigma_{eff}^{*} + 3\mu\Delta\varepsilon_{q}^{p} = 0$$

$$p|_{n+1} - p^{*} - \lambda\Delta\varepsilon_{p}^{p} = 0$$

$$\Delta\varepsilon_{eq}^{p} = \frac{\sigma_{eff}\big|_{n+1}\Delta\varepsilon_{q}^{p} - p|_{n+1}\Delta\varepsilon_{p}^{p}}{\sigma_{ys}(\varepsilon_{eq}^{p})}$$

The system (A.36) can be solved for the five unknowns $p|_{n+1}, \sigma_{eff}\big|_{n+1}, \Delta\varepsilon_{p}^{p}, \Delta\varepsilon_{q}^{p}$ and $\Delta\varepsilon_{eq}^{p}$

$$p|_{n+1} = \frac{p^{*}\mu + \lambda a\sigma_{eff}^{*} - \lambda a\sigma_{ys}(\varepsilon_{eq}^{p})}{3\lambda a^{2} + \mu} \tag{A.37}$$

$$\sigma_{eff}\big|_{n+1} = \frac{3ap^{*}\mu + 3\lambda a^{2}\sigma_{eff}^{*} + \mu\sigma_{ys}(\varepsilon_{eq}^{p})}{3\lambda a^{2} + \mu} \tag{A.38}$$

$$\Delta\varepsilon_{p}^{p} = \frac{a\left[\sigma_{eff}^{*} - \sigma_{ys}(\varepsilon_{eq}^{p}) - 3ap^{*}\right]}{3\lambda a^{2} + \mu} \tag{A.39}$$

$$\Delta\varepsilon_{q}^{p} = \frac{\sigma_{eff}^{*} - \sigma_{ys}(\varepsilon_{eq}^{p}) - 3ap^{*}}{9\lambda a^{2} + 3\mu} \tag{A.40}$$

$$\Delta\varepsilon_{eq}^{p} = \frac{\sigma_{eff}^{*} - \sigma_{ys}(\varepsilon_{eq}^{p}) - 3ap^{*}}{9\lambda a^{2} + 3\mu} \tag{A.41}$$

Having determined all the unknowns, the components of the plastic strain increment tensor are computed using (A.23) and the plastic strain tensor ε_{ij}^{p} and the stress tensor σ_{ij} at time t_{n+1} are obtained as

$$\varepsilon_{ij}^{p}\big|_{n+1} = \varepsilon_{ij}^{p}\big|_{n} + \Delta\varepsilon_{q}^{p}n_{ij}\big|_{n+1} + \frac{1}{3}\Delta\varepsilon_{p}^{p}\delta_{ij} \tag{A.42}$$

$$\sigma_{ij}\big|_{n+1} = -p|_{n+1}\delta_{ij} + \frac{2}{3}\sigma_{eff}\big|_{n+1}n_{ij}\big|_{n+1} \tag{A.43}$$

Finally, the tangent moduli

$$\mathbb{C}_{ijkl}\big|_{n+1} = \frac{d\sigma_{ij}\big|_{n+1}}{d\varepsilon_{ij}\big|_{n+1}} \tag{A.44}$$

need to be computed. From the stress expression given in (A.43) the tangent modulus is obtained as

$$\mathbb{C}_{ijkl}\big|_{n+1} = \lambda^{*}\delta_{ij}\delta_{kl} + 2\mu^{*}\mathbb{I}_{ijkl} + \left(\frac{3\mu\, h}{3\mu + h} - 3\mu^{*}\right)n_{ij}^{*}n_{kl}^{*} \tag{A.45}$$

where the variables μ^{*}, λ^{*} and h are defined as follows

$$\mu^* = \mu \frac{\sigma_{ys}}{\sigma^*_{eff}}, \quad \lambda^* = \kappa - \frac{2}{3}\mu^*, \quad h = \frac{d\sigma_{ys}(\varepsilon^p_{eq})}{d\varepsilon^p_{eq}} \tag{A.46}$$

Here h corresponds to the slope of the σ_{ys}-ε^p_{eq} curve which needs to be provided as a tabular data for the material model.

C. Von-Mises Plasticity Model Formulations

The Von-Mises plasticity model can be obtained by simplification of the previously explained pressure-dependent Drucker-Prager model. The decomposition of the strain into elastic and plastic parts given in equation (A.1) holds in Von-Mises plasticity as well. The key difference here is the deviatoric nature of the plastic flow. In other word, in the von Mises plasticity the plastic flow is entirely deviatoric and the volumetric response is purely elastic. To this end, the components of the stress tensor and the elastic modulus read

$$\sigma_{ij} = \lambda\, \varepsilon_{kk}\delta_{ij} + 2\mu\varepsilon^e_{ij}, \qquad \mathbb{C}^e_{ijkl} = \lambda\delta_{ij}\delta_{kl} + 2\mu\mathbb{I}_{ijkl} \tag{A.47}$$

The difference between (A.3) and (A.47) is that in the stress expression ε_{kk} appears in (A.47) instead of ε^e_{kk} in (A.3). This is due to the deviatoric nature of the plastic flow which leads to the following identities

$$\varepsilon^{p\prime}_{ij} = \varepsilon^p_{ij}, \qquad \varepsilon^p_{kk} = 0, \qquad \varepsilon_{kk} = \varepsilon^e_{kk} \tag{A.48}$$

Furthermore, the yield function of the von Mises plasticity is obtained by setting $a = 0$ in (A.6) as follows

$$\phi = \sqrt{3J_2} - \sigma_{ys} = \sigma_{eff} - \sigma_{ys}(\varepsilon^p_{eq}) \leq 0 \tag{A.49}$$

The flow rule (A.12) then simplifies to

$$\dot{\varepsilon}^p_{ij} = \dot{\varepsilon}^p_{eq}\frac{3}{2}\frac{\sigma'_{ij}}{\sigma_{eff}} \tag{A.50}$$

As can be seen from (A.50) the plastic flow is entirely deviatoric. For a plastic step the yield function should be equal to zero and the following has to hold

$$\phi|_{n+1} = \sigma_{eff}\big|_{n+1} - \sigma_{ys}(\varepsilon^p_{eq}) = 0 \tag{A.51}$$

Then equations (A.37) to (A.41) boil down to the following very simple form

$$\Delta\varepsilon_{eq}^{p} = \frac{\sigma_{eff}^{*} - \sigma_{ys}(\varepsilon_{eq}^{p})}{3\mu} \tag{A.52}$$

Having determined $\Delta\varepsilon_{eq}^{p}$, the components of the plastic strain tensor ε_{ij}^{p} and the stress tensor σ_{ij} at time t_{n+1} are obtained as

$$\varepsilon_{ij}^{p}\Big|_{n+1} = \varepsilon_{ij}^{p}\Big|_{n} + \Delta\varepsilon_{q}^{p} n_{ij}\Big|_{n+1} \tag{A.53}$$

$$\sigma_{ij}\Big|_{n+1} = \lambda\varepsilon_{kk}|_{n+1}\delta_{ij} + \frac{2}{3}\sigma_{eff}\Big|_{n+1} n_{ij}\Big|_{n+1} \tag{A.54}$$

where $\sigma_{eff}\Big|_{n+1} = \sigma_{eff}^{*} - 3\mu\Delta\varepsilon_{eq}^{p} = 0$ and $n_{ij}\Big|_{n+1} = n_{ij}^{*} = \frac{3}{2}\frac{\sigma_{ij}'^{*}}{\sigma_{eff}^{*}}$. Finally, the tangent moduli $\mathbb{C}_{ijkl}\Big|_{n+1} = \frac{d\sigma_{ij}|_{n+1}}{d\varepsilon_{ij}|_{n+1}}$ is computed similar to (A.45)

$$\mathbb{C}_{ijkl}\Big|_{n+1} = \lambda^{*}\delta_{ij}\delta_{kl} + 2\mu^{*}\mathbb{I}_{ijkl} + \left(\frac{3\mu\, h}{3\mu + h} - 3\mu^{*}\right) n_{ij}^{*} n_{kl}^{*} \tag{A.55}$$

where $\mu^{*} = \mu\frac{\sigma_{ys}}{\sigma_{eff}^{*}}$, $\lambda^{*} = \kappa - \frac{2}{3}\mu^{*}$ and $h = \frac{d\sigma_{ys}(\varepsilon_{eq}^{p})}{d\varepsilon_{eq}^{p}}$.

a. Elastic Volumetric Modulus

The von Mises plasticity is completely a deviatoric plasticity model. Therefore, when a deformation is entirely volumetric then the behavior of the model is linear elastic. Therefore, in embedded element model for those elements of the matrix that overlap with the inclusion, the volumetric part of the linear elastic modulus of (A.4), i.e. $\kappa\delta_{ij}\delta_{kl}$, is subtracted from the modulus expression obtained in (A.55). In this case, the modified modulus expression of elastoplastic matrix elements that overlap with the inclusion becomes

$$\mathbb{C}_{ijkl}\Big|_{n+1} = (\lambda^{*} - \kappa)\delta_{ij}\delta_{kl} + 2\mu^{*}\mathbb{I}_{ijkl} + \left(\frac{3\mu\, h}{3\mu + h} - 3\mu^{*}\right) n_{ij}^{*} n_{kl}^{*} \tag{A.56}$$

The results obtained with the modulus expression given in (A.56) is denoted as the Elastic Volumetric Modulus (EVM).

b. Consistent Tangent Modulus

In the last model, the consistent tangent modulus of a von Mises model with isotropic linear hardening is used. In a classical von Mises plasticity with isotropic linear hardening the stress and the elastic moduli read

$$\sigma_{ij} = \kappa\, \varepsilon_{kk}\delta_{ij} + 2\mu\varepsilon_{ij}^{e\prime}, \qquad \mathbb{C}_{ijkl}^{e} = \kappa\delta_{ij}\delta_{kl} + 2\mu\mathbb{P}_{ijkl} \tag{A.57}$$

The yield function can be written as

$$\phi = \sqrt{\sigma_{ij}'\sigma_{ij}'} - \sqrt{\frac{2}{3}}(\sigma_{y0} + \beta) \leq 0 \tag{A.58}$$

where σ_{y0} is the initial tensile yield strength, $\beta = H\alpha$, H is the isotropic linear hardening coefficient and α is the isotropic hardening variable. Following the principle of maximum dissipation, the evolution equations for the plastic strain tensor and the isotropic hardening variable read

$$\dot{\varepsilon}_{ij}^{p} = \dot{\gamma}\frac{\partial\phi}{\partial\sigma_{ij}} = \dot{\gamma}\frac{\sigma_{ij}'}{\sqrt{\sigma_{ij}'\sigma_{ij}'}}, \qquad \dot{\alpha} = -\dot{\gamma}\frac{\partial\phi}{\partial\beta} = \dot{\gamma}\sqrt{\frac{2}{3}} \tag{A.59}$$

The integration of (A.59) gives the following update formula for the components of the plastic strain tensor and the isotropic hardening variable

$$\varepsilon_{ij}^{p}\big|_{n+1} = \varepsilon_{ij}^{p}\big|_{n} + \gamma\, n_{ij}\big|_{n+1}, \qquad \alpha|_{n+1} = \alpha|_{n} + \gamma\sqrt{\frac{2}{3}} \tag{A.60}$$

where $n_{ij} = \frac{\sigma_{ij}'}{\sqrt{\sigma_{ij}'\sigma_{ij}'}}$ is the flow direction and $\Delta\gamma = \dot{\gamma}\Delta\mathrm{t}$ is incremental plastic parameter.

A trial yield function can be defined as

$$\phi^{*} = \sqrt{\sigma_{ij}'^{*}\sigma_{ij}'^{*}} - \sqrt{\frac{2}{3}}(\sigma_{y0} + \beta^{*}) \tag{A.61}$$

in terms of trial variables

$$\sigma_{ij}'^{*} = 2\mu(\varepsilon_{ij}\big|_{n+1} - \varepsilon_{ij}^{p}\big|_{n}), \qquad \beta^{*} = H\alpha|_{n} \tag{A.62}$$

Then, the trial yield function $\phi^{*}$is checked to determine whether an increment is elastic or plastic. If the current increment is elastic ($\phi^{*} < 0$), then the stress at time t_{n+1} becomes equal to the trial elastic stress, the plastic strain at time t_{n+1} becomes equal to plastic strain at time t_{n} and tangent modulus becomes the elastic tangent. If the current increment is plastic ($\phi^{*} > 0$), then the incremental plastic parameter $\Delta\gamma$ needs to be computed. Due to the fact that $n_{ij} = n_{ij}^{*}$ the yield condition can be written in the following form

$$\phi = \phi^* - \left(2\mu + \frac{2}{3}H\right)\Delta\gamma = 0 \tag{A.63}$$

which is known as the consistency condition. Then, the incremental plastic parameter can be obtained as

$$\Delta\gamma = \frac{\phi^*}{2\mu + \frac{2}{3}H} \tag{A.64}$$

Having determined $\Delta\gamma$, the plastic strain tensor can be obtained by using (59) and the stresses can be computed

$$\sigma_{ij} = \kappa\, \varepsilon_{kk}|_{n+1}\delta_{ij} + 2\mu\left(\varepsilon'_{ij}\big|_{n+1} - \varepsilon^p_{ij}\big|_{n+1}\right) \tag{A.65}$$

which can be further recast into the following form

$$\sigma_{ij}\big|_{n+1} = \kappa\varepsilon_{kk}|_{n+1}\delta_{ij} + \sigma'^*_{ij} - 2\mu\Delta\gamma n^*_{ij} \tag{A.66}$$

Finally, the consistent tangent moduli $\mathbb{C}_{ijkl}\big|_{n+1} = \frac{d\sigma_{ij}|_{n+1}}{d\varepsilon_{ij}|_{n+1}}$ need to be computed. The following derivatives are needed for the consistent tangent moduli

$$\frac{dn^*_{ij}}{d\varepsilon_{kl}} = \frac{2\mu}{\sqrt{\sigma'^*_{ij}\sigma'^*_{ij}}}\left(\mathbb{P}_{ijkl} - n^*_{ij}n^*_{kl}\right), \qquad \frac{d\Delta\gamma}{d\varepsilon_{ij}} = \frac{1}{1 + H/3\mu}n^*_{ij} \tag{A.67}$$

With the help of derivatives in (A.67) the moduli expression is obtained

$$\begin{aligned}\mathbb{C}_{ijkl}\big|_{n+1} = \kappa\delta_{ij}\delta_{kl} + 2\mu\mathbb{P}_{ijkl} - \left(\frac{2\mu}{1 + H/3\mu}\right)n^*_{ij}n^*_{kl} \\ - 2\mu\Delta\gamma\frac{2\mu}{\sqrt{\sigma'^*_{ij}\sigma'^*_{ij}}}\left(\mathbb{P}_{ijkl} - n^*_{ij}n^*_{kl}\right)\end{aligned} \tag{A.68}$$

For a general nonlinear isotropic hardening plasticity model, the σ_{ys}-ε^p_{eq} curve can be provided as a tabular data. However, between two data points the behavior can be assumed as linear and then this model is generally called as a multilinear hardening model. To this end, the slope of the σ_{ys}-ε^p_{eq} curve can be identified as the isotropic linear hardening coefficient H, i.e.,

$$H = h = \frac{d\sigma_{ys}\left(\varepsilon^p_{eq}\right)}{d\varepsilon^p_{eq}} \tag{A.69}$$

Then, the final form of the consistent tangent moduli become

$$\mathbb{C}_{ijkl}\Big|_{n+1} = \kappa\delta_{ij}\delta_{kl} + 2\mu\mathbb{P}_{ijkl} - \left(\frac{2\mu}{1+h/3\mu}\right) n_{ij}^{*} n_{kl}^{*} - 2\mu\Delta\gamma \frac{2\mu}{\sqrt{\sigma_{ij}'^{*}\sigma_{ij}'^{*}}}\left(\mathbb{P}_{ijkl} - n_{ij}^{*} n_{kl}^{*}\right) \tag{A.70}$$

The results obtained with the modulus expression given in (A.70) is denoted as the Consistent Tangent Modulus (CTM).

HACETTEPE UNIVERSITY
GRADUATE SCHOOL OF SCIENCE AND ENGINEERING
THESIS/~~DISSERTATION~~ ORIGINALITY REPORT

HACETTEPE UNIVERSITY
GRADUATE SCHOOL OF SCIENCE AND ENGINEERING
TO THE DEPARTMENT OF MECHANICAL ENGINEERING

Date: 24/06/2020

Thesis Title / Topic: MODELING OF THE MECHANICAL BEHAVIOR OF COMPOSITES SHOWING NONLINEAR MATERIAL BEHAVIOR USING THE EMBEDDED ELEMENT METHOD

According to the originality report obtained by ~~myself~~/my thesis advisor by using the *Turnitin* plagiarism detection software and by applying the filtering options stated below on 24/06/2020 for the total of 79 pages including the a) Title Page, b) Introduction, c) Main Chapters, d) Conclusion sections of my thesis entitled as above, the similarity index of my thesis is 4 %.

Filtering options applied:

1. Bibliography/Works Cited excluded
2. Quotes ~~excluded~~ / included
3. Match size up to 5 words excluded

I declare that I have carefully read Hacettepe University Graduate School of Sciene and Engineering Guidelines for Obtaining and Using Thesis Originality Reports; that according to the maximum similarity index values specified in the Guidelines, my thesis does not include any form of plagiarism; that in any future detection of possible infringement of the regulations I accept all legal responsibility; and that all the information I have provided is correct to the best of my knowledge.

I respectfully submit this for approval.

Date and Signature
24/06/2020

Name Surname: ALP ŞIK
Student No: N17121071
Department: MECHANICAL ENGINEERING
Program:
Status: ☒ Masters ☐ Ph.D. ☐ Integrated Ph.D.

ADVISOR APPROVAL

APPROVED.

Doç. Dr. Berrin SABUNCUOĞLU
(Title, Name Surname, Signature)

CURRICULUM VITAE

Credentials

Name, Surname	: Alp ŞIK
Place of Birth	: Zonguldak
E-mail	: alpsk555@gmail.com
Adress	: Yukarı Bahçelievler Mah. 69 Sok. 13/5 Çankaya/ANKARA

Education

B.Sc.	: Hacettepe University, Department of Automotive Engineering (2012-2017)
M.Sc.	: Hacettepe University, Department of Mechanical Engineering (2017-2020)

Foreign Languages

English – Advanced, German – Beginner

Work Experience

2019 - …	: Research Assistant, Hacettepe University Department of Mechanical Engineering